A Thesis

Submitted to the Graduate Faculty

in Partial Fulfillment of the Requirements

for the Degree of Master of Science

Department of Chemistry

Faculty of Science

University of Prince Edward Island

Donald John Alfred Cameron

Charlottetown, Prince Edward Island

April 2011

Your file Votre référence
ISBN: 978-0-494-82238-8
Our file Notre référence
ISBN: 978-0-494-82238-8

CONDITIONS FOR THE USE OF THE THESIS

The author has agreed that the Library, University of Prince Edward Island, may make this thesis freely available for inspection. Moreover, the author has agreed that permission for extensive copying of this thesis for scholarly purposes may be granted by the professor or professors who supervised the thesis work recorded herein or, in their absence, by the Chair of the Department or the Dean of the Faculty in which the thesis work was done. It is understood that due recognition will be given to the author of this thesis and to the University of Prince Edward Island in any use of the material in this thesis. Copying or publication or any other use of the thesis for financial gain without approval by the University of Prince Edward Island and the authors' written permission is prohibited.

Requests for permission to copy or to make any other use of material in this thesis in whole or in part should be addressed to:

Chair of the Department of Chemistry
Faculty of Science
University of Prince Edward Island
550 University Avenue, Charlottetown, PE
Canada C1A 4P3

SIGNATURE PAGES

iii-iv

REMOVED

Abstract

Poly(lactic acid) (PLA), a renewable, biodegradable, bioassimilable polymer derived from plant sources has become the focus of intensive research over the past 15 years. PLA technology has evolved greatly, with the development of metal catalysts that can control the insertion of lactide monomers to prepare stereoregular PLAs. The emergence of more complicated brush, dendrimer and star-like polymer architectures provide novel platforms to which this stereocontrol has not been applied. By combining the concepts of stereocontrol and star polymer architecture valuable information regarding the structure property relationships of these PLAs can be learned.

We have prepared the first series of stereoregular PLA polymer stars utilizing known aluminum catalysts and dipentaerythritol, a multi-functional initiator. Stars bearing atactic, heterotactic, isotactic-*rac* and isotactic-*L* microstructures have been prepared. The materials have been characterized by gel permeation chromatography, ^{1}H NMR spectroscopy, thermogravimetric analysis, differential scanning calorimetry and powder X-ray diffraction to elucidate the effect that stereocontrol has on the properties of these novel star polymers. The physical properties of these materials were found to be enhanced through the inclusion of stereoregularity. The isotactic samples are especially tunable by varying the percent tacticity. By changing the microstructure of the star PLAs, the glass transition temperatures (T_g) and melt temperatures (T_m) can be tuned by 10°C, while the thermal onset stability of the samples can be improved by 40°C through microstructure control. The dependence of observed properties on tacticity and molecular weight have been examined through the preparation of higher molecular weight isotactic stars, which exhibit 13°C and 25°C improvements in T_g and T_m respectively when accompanied by a 5 fold increase in molecular weight. These materials have also been

subjected to degradation studies to assess the quality of these materials in sustained release for drug delivery applications. Microstructure control has afforded these samples huge improvements in solution stability, with a 3-fold increase in lifetime observed between atactic and isotactic-*rac* stars.

Efforts to improve the stereocontrolled polymerization of lactide have been expanded to include the design and synthesis of novel aluminum anilido-aldimine catalysts incorporating diisopropylphenyl and cyclohexyl substituents on the anilido donors. These complexes have been screened in lactide polymerization to prepare PLA, and have been subjected to kinetic analyses.

Acknowledgement

The completion of this work is the culmination of long years of study and work. This point could not be reached without the influential contributions of many people who have not been properly thanked or recognized previously.

The most influential person during this time has been Dr. Michael Shaver. Your guidance throughout this process, both from a professional and personal standpoint has been very important and greatly appreciated. I have learned a lot from this opportunity and will take these lessons as I move forward into other avenues of study and development. You have succeeding in fostering a new research philosophy at UPEI, (the benefits of which I am a recipient of), and continue to do positive things for this university.

Similarily, I have been fortunate to work with very friendly and capable people over my time at UPEI. Dr. Laura Allan has provided in-lab guidance and mentoring to myself and fellow MSc candidates, while Mitchell Perry and Edward Cross have become valued colleagues and friends. The numerous Honours students that I have worked with have provided for entertaining times and a brightening of my days here. Michael Jones, Marieke Hutchison, Justin Belanger, Joshua Gallaway and Gayan Tennekone have all become good friends who I wish all the best to in the future. I would also like to thank the companionship of various other co-workers, especially Iskandar Saada and Simon Berger. These two have been friends of mine for what seems an eternity, and have been very supportive as we have taken this road together. I am sure that we will remain close friends as we move on to new and bigger experiences.

The faculty within the Department of Chemistry at UPEI are also deserving of thanks. I have taken courses from and learned from you all, including the late Dr. Robert Haines, who has truly been missed. I would like to specifically acknowledge Dr. Russell Kerr and Dr. Rabin Bissessur, my supervisory committee members. Dr. Kerr has been very helpful through the committee process, helping to direct and streamline the project towards the end goal. Dr. Bissessur deserves thanks for giving me an opportunity to work and research here at UPEI, both through a summer research assistant position and as an Honours undergraduate research student. Without those opportunities I would not have been able to achieve this most recent degree.

I have also been able to work with very supportive and helpful staff here in the Chemistry Department. Dawna Lund, Jill MacDonald, Janette Paquet and Sharon Martin have all been very helpful in a variety of ways throughout my time at UPEI.

Finally, I would like to thank my family for their support and understanding throughout this experience. They have always been supportive when my work was not progressing as I would have liked, and have also provided an audience (sometimes less than eager), when I have been successful in my work.

Dedication

For John and Donna

I may not be there yet, but I'm closer than I was yesterday -Unknown

Table of Contents

List of Figures

List of Schemes

List of Tables

Glossary of Abbreviations

ACN	acetonitrile
BDI	β-diiminate
BnOH	benzyl alcohol
bpy	bipyridine
^{n}Bu	*n*-butyl-
^{t}Bu	*t*-butyl-
^{n}BuLi	*n*-butyllithium
CD	cyclodextrin
Cy	cyclohexyl
CP	condensation polymerization
DCM	dichloromethane
dbm	dibenzoylmethane
diTMP	ditrimethylolpropane
DMAP	4-dimethylaminopyridine
DNA	deoxyribonucleic acid
DPE	dipentaerythritol
DSC	differential scanning calorimetry
EtOH	ethanol
GPC	gel permeation chromatography
La	Lanthanum
LA	lactic acid or lactide
L_n	ligand
M_{core}	molar mass of star core
M_i	mass of polymer sample
M_n	number average molecular weight
$M_{n,GPC}$	number average molecular weight determined by GPC
$M_{n,star}$	number average molecular weight of polymer star
$M_{n,th}$	theoretical number average molecular weight
M_w	weight average molecular weight
Me	methyl
MeOH	methanol
meso	*mesos*
N_i	number of molecules
NAS	N-acryloxy succinimide
NEt_3	triethylamine
NMR	nuclear magnetic resonance spectroscopy
Oct	octoate (2-ethylhexanoate)
P_m	probability of a *meso*-linkage
P_r	probability of a *racemic*-linkage
PCL	poly(ϵ-caprolactone)
PDI	polydispersity index
PDI_{arm}	polydispersity index of star polymer arm
PDI_{star}	polydispersity index of star polymer

PE	pentaerythritol
PET	polyethylene terephthalate
PHA	poly-3-hydroxy alkanoate
PLA	poly(lactic acid)
P*D*LA	poly(*D*-lactic acid)
P*DL*LA	poly (*D,L*-lactic acid)
P*L*LA	poly(*L*-lactic acid)
^{i}Pr	isopropyl
POX	poly-2-ethyl-2-oxazoline
PS	polystyrene
PTMC	poly(trimethylene carbonate)
PVLO	poly(δ-valerolactone)
pXRD	powder X-ray diffraction
rac	*racemic*
ROP	ring opening polymerization
S°	Standard entropy
Sm	Samarium
salan	salicylaldehyde and ethylenediamine (saturated)
salen	salicylaldehyde and ethylenediamine
T_c	crystallization temperature
T_g	glass transition temperature
T_m	melt temperature
T_{max}	maximum decomposition temperature
T_{onset}	onset temperature
TBD	1,5,7-triazabicyclo[4.4.0]dec-5-ene
TGA	thermogravimetric analysis
THF	tetrahydrofuran
TMA	trimethylaluminum
TMP	trimethylolpropane
TPE	tripentaeryithritol
X_c	percent crystallinity
Y	Yttrium
Yb	Ytterbium
$\Delta H_f°$	Standard enthalpy of formation
$\Delta H_m°$	Standard enthalpy of melting
ΔH_m	heat of melting
ΔT_{decomp}	thermal decomposition window

Chapter One

Introduction

1.1 Oil and the world polymer market

Current and future growth of the world economy will place additional stresses on our resource-based energy and manufacturing sectors. Economic growth models for the BRIC countries, (Brazil, Russia, India and China) project that together they will possess an economy greater than the United States and the developed European nations by 2050.[1] By 2025, another 200 million people with incomes in excess of $15,000/year will be incorporated into the world economy, a number greater than the current combined populations of Germany, France and the United Kingdom.[1] These projections have already been manifesting in auto sales, as American auto giant General Motors saw double digit increases in sales in Russia, Brazil and China in the 2010 fiscal year. Additionally, for the first time in its 102 year history GM sold more vehicles in China than in its domestic market.[2] Unfortunately, this growth is largely dependent on petroleum resources.

The price of this expanded oil dependency is steep, as increased consumption will further hasten the depletion of global oil reserves, and expose pristine natural environments to contamination. The oncoming arrival of peak oil (the maximum achievable rate of global petroleum extraction), and swiftly declining discoveries of future reserves necessitates an adaptation to drilling and extracting from less conventional sources.[3] Unconventional oil sources include oil shales or sands, coal or biomass-based liquid supplies, as well as those liquids arising from the chemical processing of natural gas.[4]

The expansion of the Athabasca oil sands and the recent Gulf of Mexico spill illustrate the inherent dangers of increasing production of so-called unconventional oils.[4] The largest of these challenges being the supremely large risks of terrestrial and water contamination from surface mining megaprojects,[5] and the difficulty of handling catastrophic blowouts at extreme depths or unpredictable environments.[6] With respect to the Gulf of Mexico spill, the total costs of this disaster are practically incalculable when both economic and environmental factors are considered. Forgotten amongst the the scale of this disaster is the ponderous volumes of chemical dispersant used to eliminate the surface slicks. In many cases the environmental impacts of these dispersants are not known, and may only be revealed many years from now. Ultimately, increased land, water and atmospheric pollution are all to be expected from increases in drilling and refinery activity, as well as the associated accidents and spills.

The oil industry is not limited strictly to fuels. The enormity of the petrochemical plastics industry is less well known but nearly equal in potential impact. Over 11% of a typical barrel of US oil is converted to petrochemicals, which may then be used in the production of a wide variety of polymer, elastomer or fibrous materials.[7] These materials are extremely successful, both in terms of utility and economics. They are observed in all facets of modern

living including, but not limited to, textiles, food packaging, electronics, toys and auto parts.[8] Estimates for worldwide plastics production suggest over 200 billion pounds is produced annually, and that Americans alone discard 100 billion plastic bags per year, or roughly 1.5 billion pounds.[9] The widespread application of plastics hinges on an ability to maintain mechanical integrity, while remaining lightweight and cost-efficient. It may be argued that plastics perform their function too well, as they have become largely disposable. This post-life phase, where products made from petro-based materials are discarded to landfill is particularly damaging to the environment. Possessing extremely long lifetimes, these materials may take hundreds of years to degrade, leaving residual waste with no reusable benefits. This residual waste can cause harm to animal life, including numerous species of birds, fish and other marine life, both directly and indirectly.[10]

Additionally, new evidence has come to light concerning the safety for human consumption and use of products containing phthalates,[11-13] a common plasticizer that adds flexibility and longevity to plastic materials. Recent research has shown that these materials can have serious health effects, including increased risks of autism in children, the onset of precocious puberty, and has even been linked to the obesity epidemic.[13] With all of these factors considered, it is clear that cost-efficient, natural and non-toxic alternatives to petrochemical plastics would be a great boon to this industry.

1.2 Biodegradable plastics

In seeking out solutions to these problems, macromolecular research has invested heavily in the growing field of biodegradable materials. If biodegradable substitutes with similar properties to oil-based polymers can be found, then total waste can be decreased and the reliance on non-renewable feedstocks will be lessened. Traditional research in biodegradable materials has focused on materials such as collagen and chitin, biomaterials that are derived from plant and animal life.[14] These beginnings have evolved to allow for research in the area of synthetic biodegradable polymers to utilize a more directed chemical approach.

The ability of some polymers to degrade via natural pathways is not a new phenomenon, as poly(ϵ-caprolactone) (PCL), a polyester derived from petrochemicals, was known to decompose into eco-friendly byproducts in bioactive environments such as soil as early as 1973.[15] Various other polyesters, such as poly(δ-valerolactone) (PVLO),[16] and poly(trimethylene carbonate) (PTMC),[17] have also displayed biodegradability, making them suitable 'green material' substitutes in many applications currently utilizing non-biodegradable polymers such as polystyrenes (PS) and poly(ethylene) terephthalates (PET).

Although an improvement with respect to waste handling, these materials do not fully adhere to the principles of green chemistry (a set of protocols associated with eco-friendly processes), as they are not derived from natural and renewable sources. The greatest step in the development of truly 'green' bioplastics is the development of polymers from plant materials or microbial sources. The two largest classes of these green synthetic biodegradable polymers are poly(hydroxyl) alkanoates (PHA)s, of which poly(3-hydroxybutyrate) is the most common,[18] and various natural polyesters. The most commercially relevant, and of greatest interest to our

research group is poly(lactic acid).[19,20] PLA technology is far from new, but changing industrial interests have made it one of the fastest growing fields of synthetic compostable materials. In addition to being biodegradable, PLA is also a bioassimilable material safe for use in the medical and food sectors. Originally focused in the biomedical field, PLA has long been utilized in the production of sutures,[21] stents[22] and tissue scaffolds.[23] These sutures, the first biomedical devices derived from PLA and poly(glycolic acid) block copolymers need not be removed from the body,[24] and are degraded through biological pathways to benign materials; water and carbon dioxide. Screws and bone pins derived from PLA have eliminated the need for an invasive secondary surgery, as they degrade in conjunction with the healing process.[25] The lactide monomer, various other cyclic esters and the resulting polyester polymers are shown in Figure 1.1.

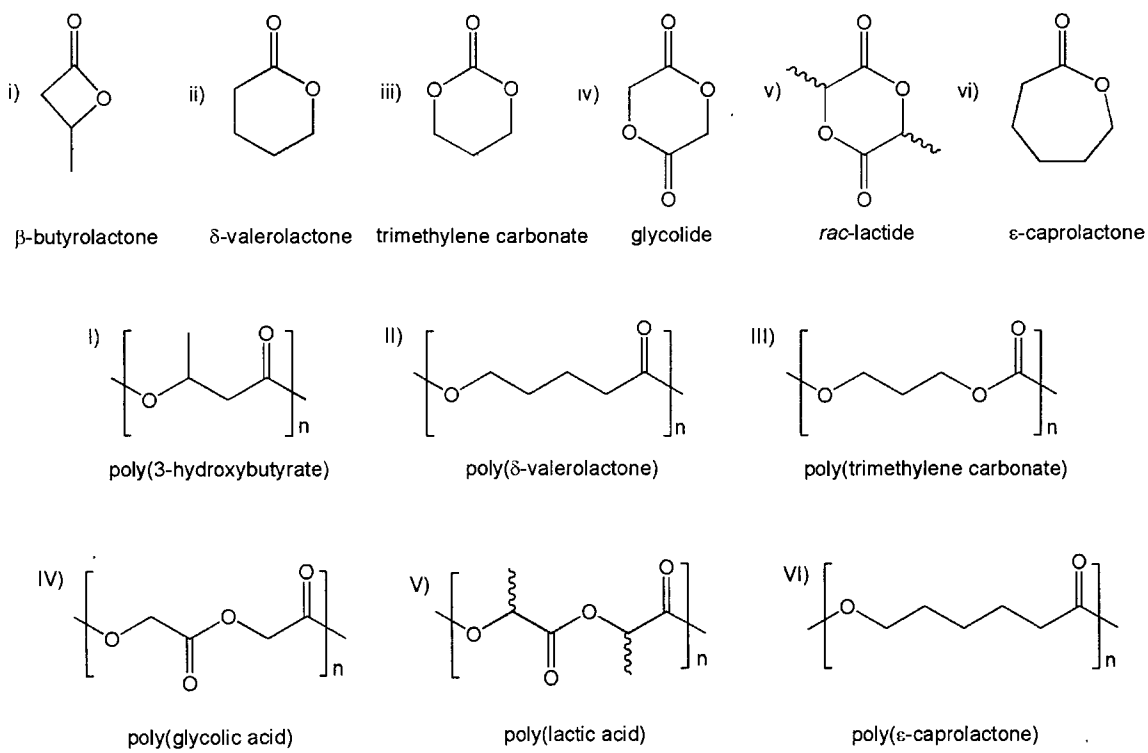

Figure 1.1. Various polyesters that possess desirable biodegradability properties.

Reductions in the production costs of PLA materials have opened up new avenues in packaging and textiles. The food packaging sector now consists of over 70% of the lactic acid market,[26] and is continuing to trend upwards, with annual growth rates exceeding 15%. These applications include dinnerware, food wraps, packaging, shrink wrap, bottles, cups and trays. The most visual representation of PLA materials is in use as bags for Sun Chips™ brand multigrain chips. Expansion in the medical field includes the manufacturing of operative field sheets, surgical masks, blouses, dressing and compresses, in addition to those materials mentioned earlier. The additional benefits of these materials include their ability to avoid contamination and prevent secondary skin reactions.

A novel role for PLA materials is focused on their use as controlled drug delivery vectors. A drug or bioactive agent is encapsulated within the polymer matrix and implanted subcutaneously or particlized and delivered by injection. As the polymer material degrades the agent is delivered to the bloodstream over an extended period of time. Oral or nasal administration of drug-loaded PLA nanoparticles is viewed as a method for more specific targeting of a biological target site.[27]

1.3 Poly(lactic acid): Synthesis, mechanism and degradation

Fuelling the growth in PLA research is its decreased environmental footprint, as the polymerizable monomer 3,6-dimethyl-1,4-dioxan-2,5-dione, (lactide or LA) is derived from lactic acid, a product that may be fermented from the sugars of various cultivable plants. With improvements to the necessary infrastructure for the manufacturing and processing of PLA, the cost of PLA materials has drastically decreased, opening up new avenues of use (*vide supra*).

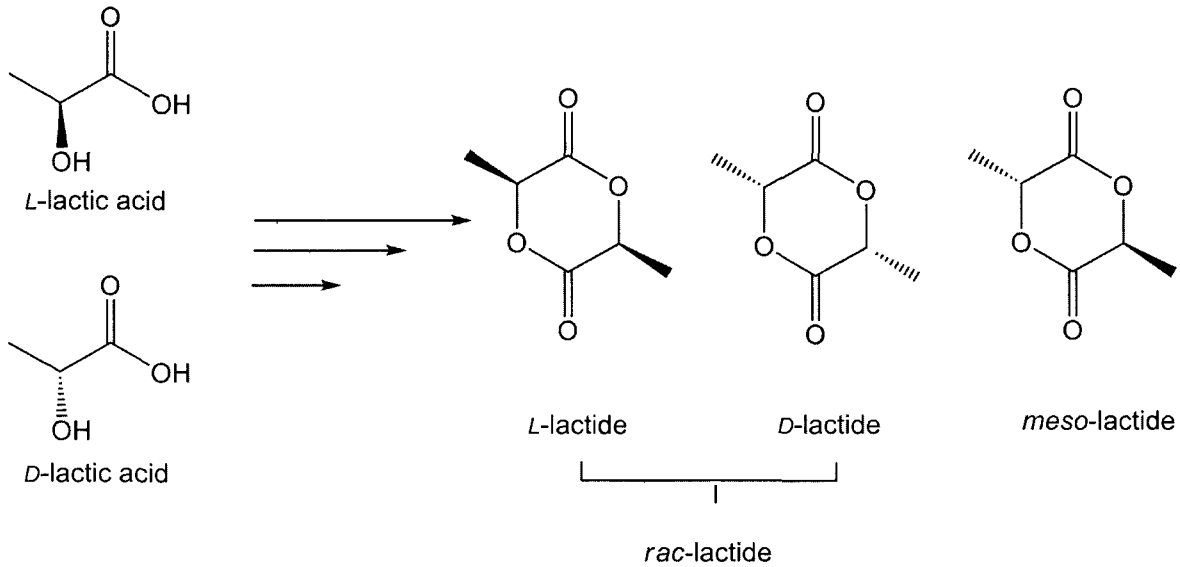

Scheme 1.1. Lactic acid and the stereoisomers of lactide.[28]

Currently, the world's largest producer of PLA is NatureWorks LLC, a subsidiary of Cargill Dow Polymers LLC, based in Blair, NE. Boasting a 300 million ton capacity, NatureWorks PLA, sold under the branded name Ingeo™, is derived from the dextrose (*D*-glucose) extracted from corn, which is then fermented to produce lactic acid. This lactic acid may then be used to form lactide. NatureWorks claims that their materials are the first greenhouse-gas neutral polymers ever produced, and that the process utilizes 68% less fossil fuel energy than traditional plastics.[28]

Poly(lactic acid) (PLA) is typically synthesized via a condensation polymerization of lactic acid, or a ring-opening polymerization of lactide (ROP) (Scheme 1.2). The condensation process utilizes an azeotropic dehydrative route to produce PLA,[29] requiring lactic acid, high temperatures and high boiling point solvents to produce high molecular weight PLA through the elimination of water. This method is an uncontrolled process, yielding polymers of inconsistent properties, namely variable molecular weights, (M_n & M_w) (Figure 1.2) and a broad distribution of these molecular weights (polydispersity, PDI).[30]

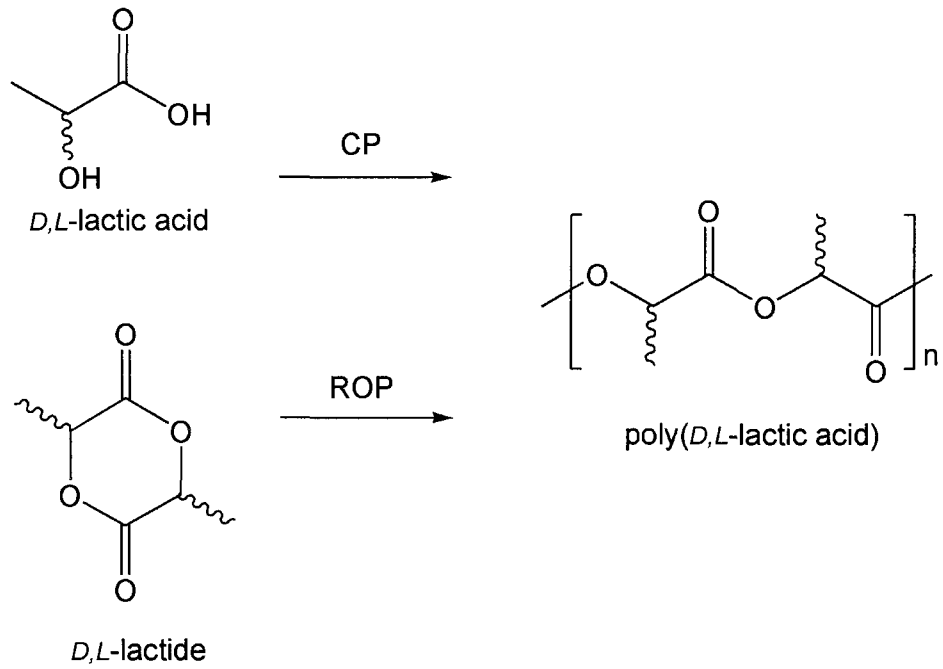

Scheme 1.2. Transformation of lactide to PLA via condensation polymerization (CP) or ring-opening polymerization (ROP) mechanisms.

$$M_n = \frac{\sum_i N_i M_i}{\sum_i N_i} \qquad M_w = \frac{\sum_i N_i M_i^2}{\sum_i N_i M_i} \qquad PDI = \frac{M_w}{M_n}$$

Figure 1.2. Mathematical representation of M_n, M_w and PDI, where N_i is the number of polymer molecules with mass M_i.

The other widely used method involves the use of catalysts to perform ROP.[31] As the driving force for this process is the elimination of ring strain it requires less harsh conditions than the condensation method. Although a six-membered ring, lactide possesses greater ring strain than analogous six-membered rings (cyclohexane possesses no total strain) due to its unusual geometry imposed by the two ester linkages.[32] The ester groups are nearly planar, which forces the ring into an atypical skew-boat conformation whereby the methine protons are found at axial positions and the methyl groups are located at equatorial positions. The standard enthalpy (ΔH_f°)

of the ring-opening polymerization is -23 KJ mol^{-1}, with a standard entropy (S°) of -40 J K^{-1} mol^{-1} [33].

Industrially prepared lactide is derived from lactic acid, which first undergoes a condensation to form a low molecular weight prepolymer, which is subsequently depolymerized to form lactide.[34] (Scheme 1.3) Upon purification, the lactide may undergo the catalyzed ROP process to form PLA of high molecular weight. Tin(II) 2-ethylhexanoate is the catalyst that is typically employed to synthesize industrial PLA. The advantages of this method are the absence of solvents, as all processes may be carried out in the melt (melting point of *rac*-lactide 116-119°C), and the enhanced polymer properties that metal-mediated ROP affords, controlled M_n and narrower PDI.[35]

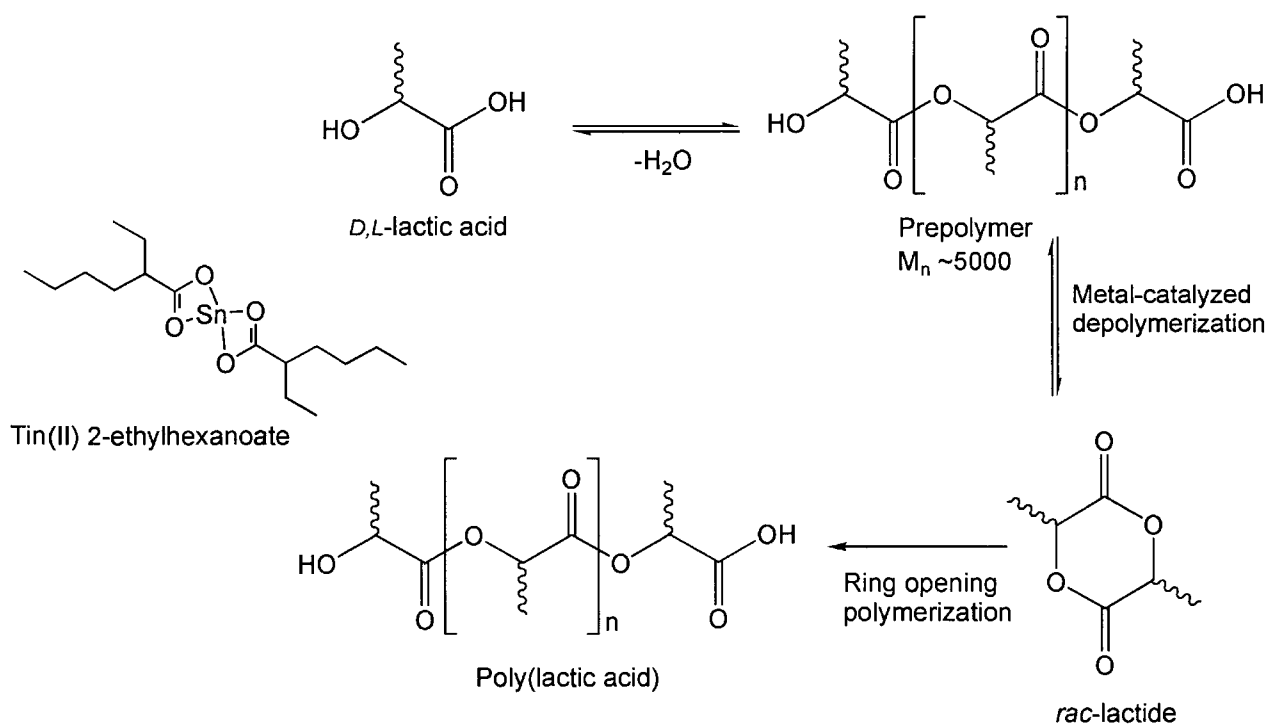

Scheme 1.3. Industrial preparation of PLA through tin catalyzed synthesis of prepolymer and ring-opening polymerization.

Although these organometallic tin catalysts are highly successful at the ROP of lactide, they are not the only methods. Enzymatic,[36-38] anionic,[39,40] cationic[41-45] and organocatalytic[46-50] processes have all been employed in the synthesis of PLA. All of these methods and catalysts have been utilized to form PLA with more consistent polymeric properties when compared to the condensation polymerization method. The ultimate goal of these ROP processes being the realization of a living polymerization.

Living polymerizations may be concisely defined as "a chain polymerization from which chain transfer and [early] chain termination are absent. In many cases, the rate of chain initiation is fast compared with the rate of chain propagation, so that the number of kinetic-chain carriers is essentially constant throughout the polymerization."[51] It then follows that if a polymerization is truly living, and follows these criteria, that the molecular weight distribution (PDI) is uniform, and that the rate of consumption of monomer is constant. This will produce a linear increase in molecular weight with conversion. In addition, the absence of terminating events should allow for the restarting of the polymerization upon addition of more monomer after it has proceeded to 100 percent completion.

Deviation from these theoretical constraints in PLA synthesis is mainly due to the process of transesterification, which is the predominant chain transfer mechanism in the polymerization of lactide.[39] Transesterification may occur via an intermolecular or an intramolecular mechanism. Intramolecular transesterification occurs via a back-biting mechanism which results in the formation of a shortened linear chain and a cyclic polymer. This occurs through a carbonyl oxygen reacting with the metal-alkoxide bond. In intermolecular transesterification, the polymer ends of two closely associated chains undergo a random exchange that produces two new chains with lengths $n_1 = \frac{1}{2}n_o$ and $n_2 = (n_o + \frac{1}{2})$, where n_o is the original chain length, and n_1, n_2 are the

chain lengths after transesterification has occurred. Both of these mechanisms will lead to a broadening of PDI. This concept is illustrated in Figure 1.3.

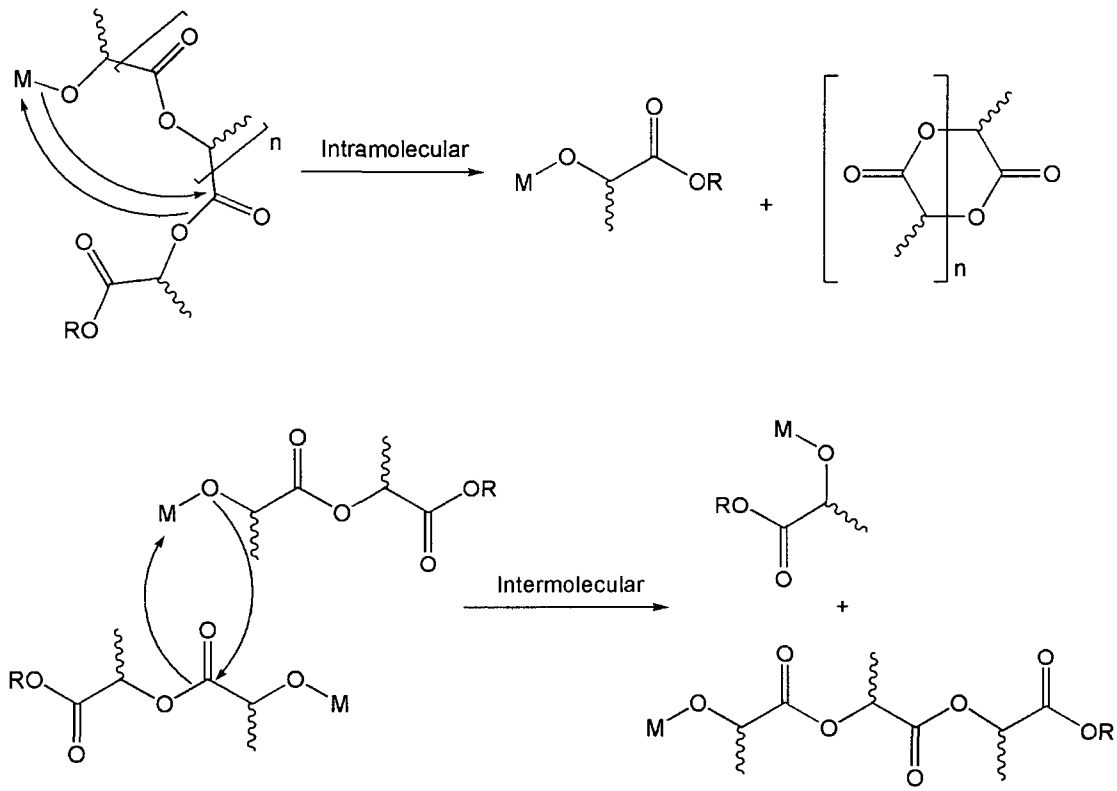

Figure 1.3. Intramolecular and intermolecular transesterification mechanisms that may occur during the polymerization of lactide.

Another process which causes deviation from true living behaviour is termination. This process usually results from the decomposition of the catalyst or the introduction of a proton source (H_2O or ROH) into the polymerization mixture. Avoidance of these mechanisms will promote living behaviour which is desirable for the precise control of molecular weights via catalyst, monomer and initiator loadings that it offers, as well as reaction times that are pseudo-living with respect to conversion.

The living mechanism of PLA formation (for metal mediated ROP processes) is most often thought to proceed through the co-ordination insertion mechanism (Scheme 1.4). As the

name implies, the first step of this mechanism is the co-ordination of a lactide monomer to the metal centre through a Lewis Acid-Base bond between metal centre (M) and the carbonyl oxygen (Scheme 1.4). This is followed by an insertion of the monomer into the metal-alkoxide bond (M-OR) via nucleophilic attack at the carbonyl carbon adjacent to the alkoxy initiating group, to prepare a secondary alkoxide. The ring is then opened by cleavage of the acyl bond. When alkoxide initiators are employed, this leads to an ester linkage on one end of the polymer chain and an alcohol end group on the other end, assuming hydrolysis of the catalyst occurs. The evidence supporting this mechanism was first reported by Kricheldorf and Teyssie.[52-53]

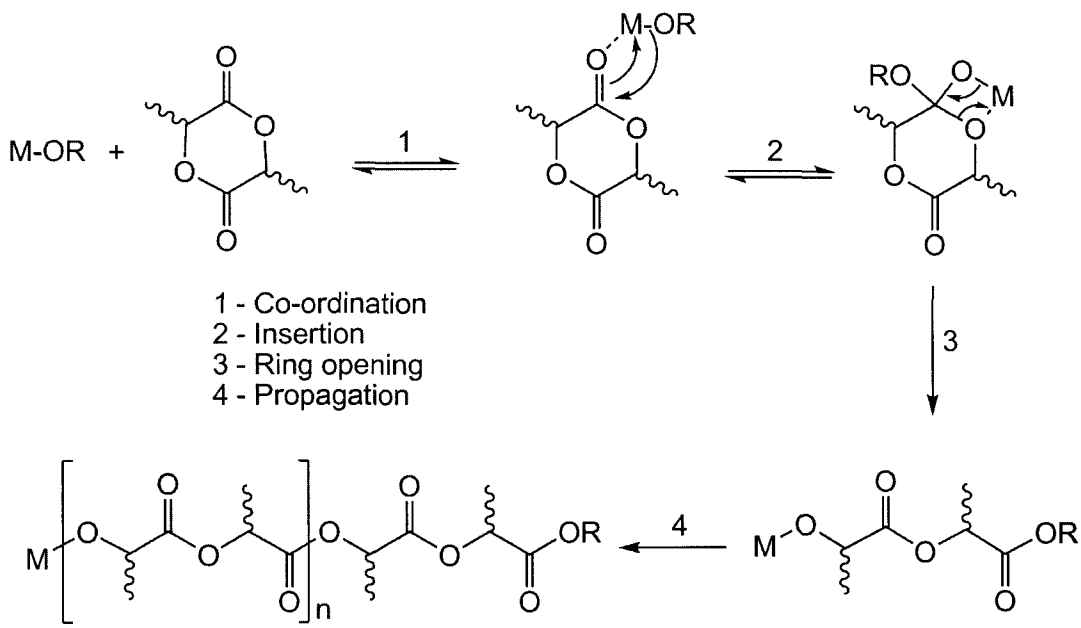

Scheme 1.4. Co-ordination-insertion mechanism of lactide polymerization facilitated by metal catalysts.

The degradation of PLA may occur through one of two mechanisms: hydrolysis of the polyester chain or enzymatic degradation. Hydrolysis may be achieved under both acidic[54] and basic conditions,[55] and an increase in temperature and humidity is shown to increase the rate of degradation. The rate of hydrolysis is dependent upon several factors, including the molecular weight and the crystallinity of the polymer chain. Increases in crystallinity retard the permeation

of the solution through the polymer domains.[54] Once the chain has been hydrolyzed into smaller chains (< 40 000 g mol^{-1}), micro-organisms can further degrade the polymer to carbon dioxide and water via the Kreb's cycle to produce usable energy.[56] With the ever increasing production of PLA, appropriate infrastructure to handle the large-scale degradation of PLA must be developed. Current figures place the number of locations capable of composting PLA in the United States at 113.[57] NatureWorks claims that their PLA can be degraded in fewer than 90 days in such an environment, where the temperature meets or exceeds 140°C for 10 days. However, the composting industry has concerns over an expansion of PLA technology, as the release of lactic acid makes the compost wetter and more acidic, while its breakdown necessitates increased oxygen demand for microbes, resulting in a proliferation of undesirable odors. Promising advances in this area focus on the use of enzymes for such tasks, typically derived from yeasts like *Candida antarctica* and *Rhizomur miehei*.[58]

Lipases such as proteinase K have shown activity in the biodegradation of PLA. Very efficient in this process, proteinase K loses its effectiveness when confronting high molecular weight PLA. This necessitates the use of a two-step degradation pathway that combines both hydrolysis and enzymatic digestion.[34]

More recently enzymes from the yeast *Cryptococcus* have been used to degrade high molecular weight PLA, as well as other biodegradable polymers based on poly(ϵ-caprolactone).[59] These enzymes typically have a strong preference for degrading P*L*LA versus P*D*LA, and the highest observed rates are for the amorphous, (atactic), regions of the polymer chain.[60] With the very real possibility of stereocontrolled PLA products hitting the consumer market, degradation technology will have to adapt and expand.

While acknowledging that PLA waste handling infrastructure must improve, the long-term benefits of providing biodegradable materials as alternatives to petroleum-based products far outstrips these initial costs.

1.4 Stereocontrol in PLA

Polymeric microstructures can have wide ranging effects on the macroscopic properties of a material, and this is readily illustrated in PLA.[61] Investigations into the stereoregularity of polymers date back to Natta's work in controlling the microstructure of polyolefins by utilizing metal catalysts.[62] While some polymers can possess differences in the linking arrangements, the symmetry of the lactic acid subunit limits PLA to exhibiting different microstructures arising solely from the stereochemical configuration. The structure of the lactide monomer, possessing two chiral centres, allows for the synthesis of several stereoregular forms. The relative configuration of these chiral centres dictates the microstructure of the polymer backbone. A polymer chain possessing sequences of stereocentres that are of the same relative stereochemistry is isotactic, while an alternation of the sequences is labelled syndiotactic. No apparent regularity in the chain indicates that it is atactic.

The assignment of the relative stereochemistry of polymer chains is accomplished via NMR spectroscopy, typically utilizing the ^{1}H and ^{13}C nuclei, where short polymer sequence (triads and tetrads) may be assigned to various stereosequences based on the distinct chemical shifts they possess.[63] A triad is a sequence of three monomer units, a tetrad of four, etc. The assignment of these short sequences is labelled according to the linkages that the sequence possesses. These linkages may be either meso or racemic in nature. A meso linkage indicates that

the two adjacent monomers have equivalent absolute stereochemistry, while a racemic linkage indicates that the two adjacent monomers possess opposite stereochemistry.

The mechanisms employed by catalysts in stereoselective polymerizations are twofold: enantiomorphic site control and chain-end control.[64] In the enantiomorphic site control method, a chiral catalyst will preferentially and selectively polymerize a specific stereoisomer of the monomer over its opposing enantiomer. The chain-end control method utilizes the chirality of the last incorporated monomer in the growing polymer chain. Determination of the exact mechanism at work can be quite difficult, and both mechanisms may be working in tandem to achieve an enhancement of stereocontrol, or in a deleterious fashion to lower the observed stereoselective bias of the polymer chain.[65]

The key in determining which of the control mechanisms is operating is the way in which the stereoerrors are propagated. In non-ideal systems, insertion errors will occur. For catalysts that employ the enantiomorphic site control mechanism, an insertion error is corrected by the selectivity of the catalyst. As the insertion is directed solely by the ligand set, a new monomer will be correctly inserted following the error. In catalysts that employ chain-end control, an error will switch the entry of the following monomer, causing the error to be propagated throughout the chain. This type of insertion fault will create stereoblocks, the length of which is determined by the selectivity of the catalyst as seen in Figure 1.4.

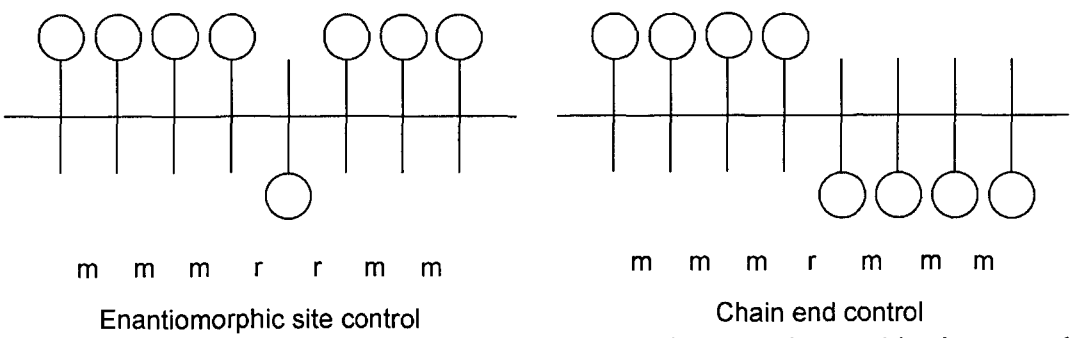

Figure 1.4. Propagation of stereoerrors in catalysts employing enantiomorphic site control and chain-end control.

The probability of different stereosequences occurring has been modelled mathematically with the two most common models being the Bernoulli trial and first-order Markov steps.[66-67] In mathematical terms a Bernoullian system presents two possible events each with a given probability of occurring. In the case of propagation of a polymer chain, the two events are either the meso or racemic linkage formed between two monomers. The probability of these two events occurring may be represented as P_m and P_r. In this case the probabilities are independent of the previous event. This closely models the actions in a system employing enantiomorphic site control, as the chirality of the next monomer is independent of the previous one.

The alternative statistical method is the Markov model of probability, where the next event is influenced by the current state of the system. In a case involving two events (meso or racemic linkage), there are then four different probabilities represented: $P_{m/m}$, $P_{m/r}$, $P_{r/r}$, $P_{r/m}$. These outcomes resemble those occurring in a chain-end control mechanism. Higher order Markov models may be used to account for the stereochemistry of additional chain units. Both the Bernouilli trial and Markov steps are modelled in Figure 1.5.

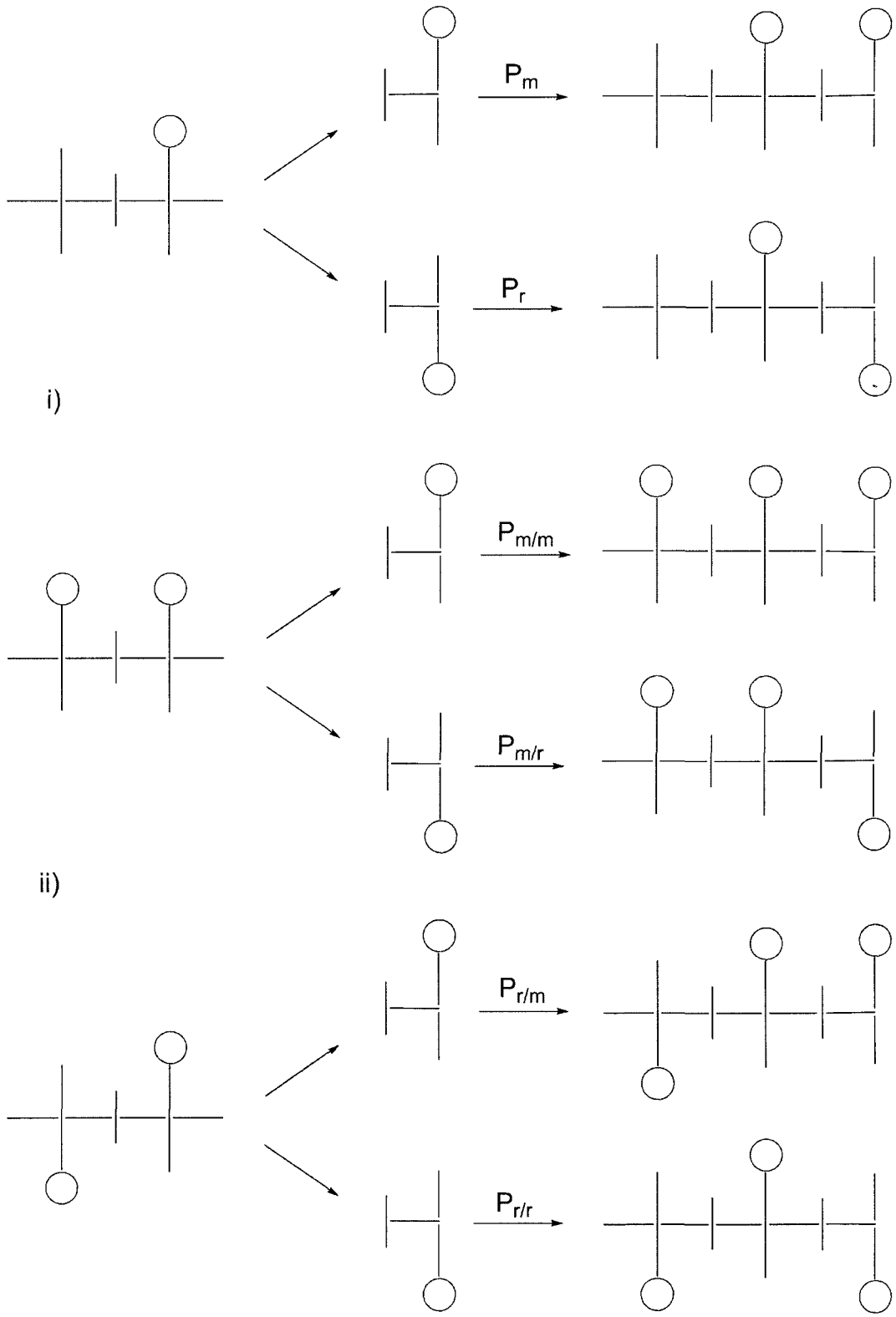

Figure 1.5. Representation of i) Bernoullian and ii) Markov statistical modelling of enantiomorphic site and chain end contol enchainment processes.

As lactide possesses two stereocentres, a large number of microstructures are observable in PLA. Isotactic, syndiotactic and atactic microstructures that are possible with many other stereoregular polymers are joined by heterotactic, stereoblock and stereocomplex microstructures of PLA (Figure 1.6).[68] Stereocomplex PLA results from P*L*LA and P*D*LA polymer chains cocrystallizing to form closer associations through intermolecular attractions. *Rac*-lactide, the racemic mixture of *D*- and *L*-lactide is capable of producing isotactic, heterotactic, stereoblock and stereocomplex PLA upon polymerization.

Heterotactic PLA can be formed through the selective alternation of enantiomer insertion upon each monomer insertion event. Syndiotactic PLA can only be prepared from *meso*-LA, as the only way to achieve alternating stereocentres in the backbone is if the monomer contains both an R- and an S-centre. The catalyst utilized must then preferentially ring-open at one stereocentre of *meso*-lactide to obtain a syndiotactic polymer.[69] If an alternation of the position of acyl bond cleavage occurs, the result is the heterotactic microstructure.[70] Isotactic PLA may be synthesized by polymerizing the enantiopure forms of *D*- or *L*-lactide or by the chiral resolution of *rac*-lactide using an enantioselective catalyst. It has been shown that *rac*-salen ([O,N,N,O] chelating ligand derived from a salicylaldehyde and ethylenediamine), aluminum catalysts are successful in the production of stereocomplex P*L*LA/P*D*LA from *rac*-lactide. In this study the R-catalyst preferentially polymerizes *D*-lactide while the S-catalyst polymerizes *L*-lactide to form P*L*LA.[71-74.]

The preparation of stereoblock PLA can be achieved through three distinct methods.[35] Control of the polymer, first though the complete polymerization of an enantiopure form (*D*-lactide), followed by addition of *L*-lactide will produce stereoblock isotactic PLA. When utilizing *rac*-lactide, an enantiopure catalyst can be used to prepare isotactic stereoblock PLA, however a

tapered stereoblock with a changing percent composition of the two monomers throughout the chain length is likely to result. Finally, stereoblock PLA has been proposed to form from a chain transfer events when *rac*-lactide is polymerized with a *rac*-catalyst. Coates proposed that rapid chain transfer occurred between two enantiomers of the catalyst, utilizing the relative ratios of different stereosequences in the polymer chain to justify the mechanism.[75]

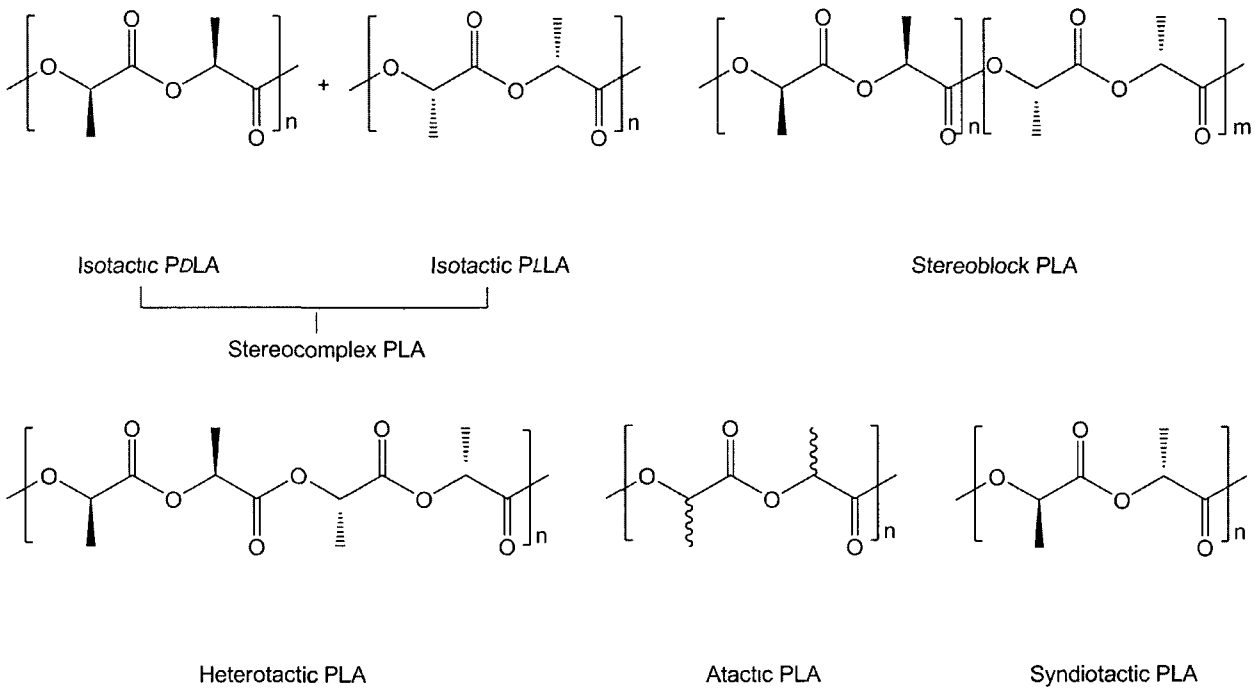

Figure 1.6. Possible stereoregular forms of PLA.

Simple ^{1}H NMR spectra of PLA reveal two sets of peaks corresponding to the methine and methyl protons of the chain. The methine protons, coupled only to the adjacent methyl protons, are observed as a number of overlapping quartets. The methyl region is similarly viewed as an overlapping of doublets. Homonuclear decoupling of these signals simplifies the ^{1}H NMR of PLA samples. Constant irradiation of the methyl region saturates the excited state of the methyl protons, eliminating spin-spin coupling relaxation processes with the methine protons. Without this coupling the overlapping quartets of the methine region are reduced to a series of singlets.[76] These singlets then correspond to the eight different tetrad sequences: rrr, mmm, mrm,

rmr, mmr, rmm, rrm and mrr (Figure 1.7). For those samples prepared from *rac*-lactide, only five of the eight tetrads are observed: mmm, mrm, rmr, mmr and rmm. The two peaks for the mmr and rmm tetrads are coincident, thus these two stereosequences are indistinguishable by ^{1}H NMR. The three other tetrads, rrr, rrm and mrr are only observable when *meso*-lactide is polymerized, or if a scrambling of the stereocentres occurs. This may happen through racemization of the monomer or by an exchange of the chains during transesterification. From a visual standpoint, the ^{1}H NMR of heterotactic PLA contains two peaks of relative intensity, (rmr and mrm sequences), while purely isotactic PLA contains only 1 sequence (mmm). For PLA chains that are isotactic enriched, the rmr, mmr and rmm sequences are also present, as they are in atactic samples. Syndiotactic PLA exhibits only one stereosequence corresponding to rrr.

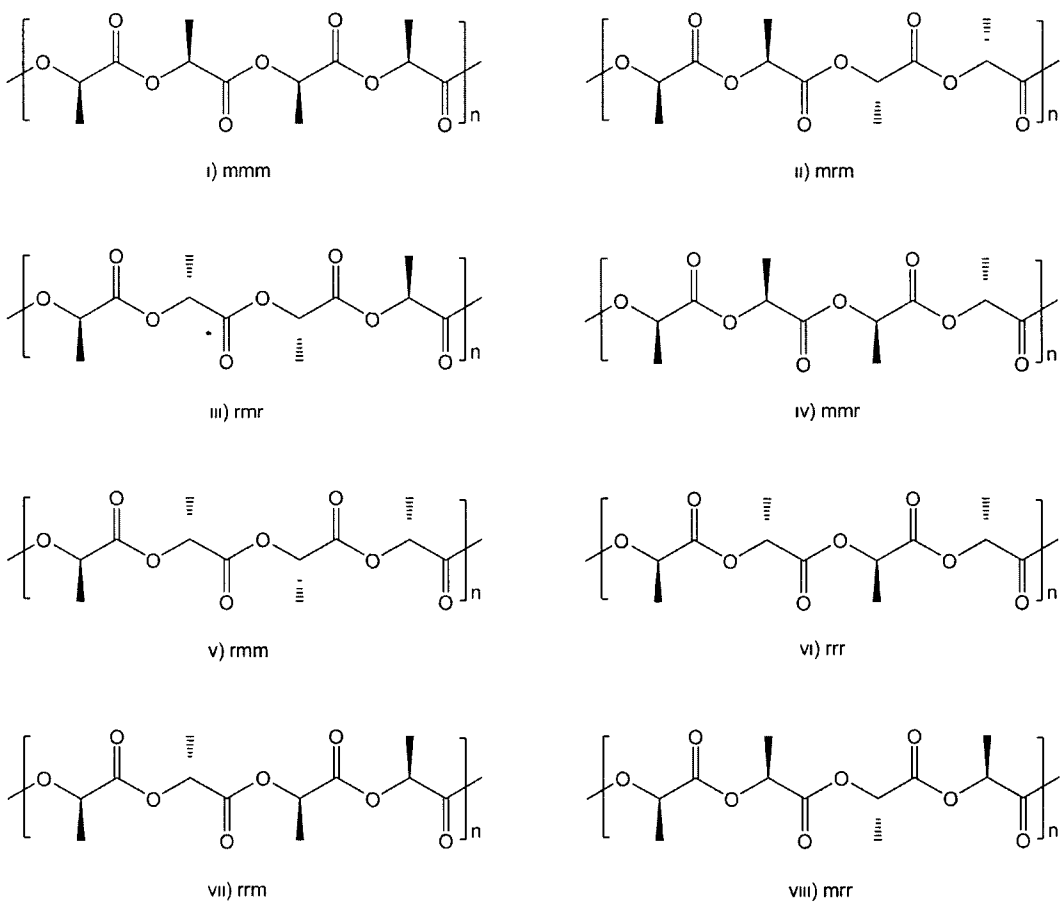

Figure 1.7. Illustration of the possible tetrads of PLA. Tetrads i-v are possible from *rac*-lactide, vi-viii arise from *meso*-lactide.

The presence of stereoerrors in heterotactic and syndiotactic PLA will lead to observation of the rrm and mrr tetrads. Examination of the relative integration of these tetrad sequences allows for a determination of the tacticity bias of the polymer chain, as well as revealing critical information in determining the mechanism of stereocontrol that the catalyst employs. As previously alluded to, the mechanism of stereocontrol can be determined through the way in which stereoerrors propagate. In the case of catalysts employing enantiomorphic site control, the resultant PLA will possess a decoupled ^{1}H NMR integration ratio of 1:2:1:1 for mmr, mrm, rmr and rmm tetrads. A catalyst that utilizes the chain end control mechanism will possess a ratio of 1:1:1 for mmr, mrm and rmm tetrads, as isotactic stereoblocks will be formed and the rmr tetrad will be absent.[63,75]

The relative integration of these different stereosequences can then be used to determine the probability of meso (P_m) or racemic (P_r) linkages in the polymer chain. When correlated to the known microstructures, a P_m value ~1 is isotactic, and P_r ~1 is syndiotactic. This P_r value close to 1 will also be found for heterotactic PLA, as the linkages formed when *rac*-lactide monomers are opened contribute to the value. It is noteworthy that the designation of m and r for linkages is based on the connections between lactic acid subunits, and not simply those found between lactide units.

Table 1.1. Mathematical representation of the probabilites of different tetrads with *rac*- and *meso*-lactide.

	Probability	
Tetrad	***rac*-lactide**	***meso*-lactide**
mmm	$P_m^2 + P_rP_m/2$	0
mmr	$P_rP_m/2$	0
rmm	$P_rP_m/2$	0
rmr	$P_r^2/2$	$(P_m^2 + P_rP_m)/2$
rrr	0	$P_r^2 + P_rP_m/2$
rrm	0	$P_rP_m/2$
mrr	0	$P_rP_m/2$
mrm	$(Pr^2 + P_rP_m)/2$	$P_m^2/2$

Analysis by ^{13}C NMR can also be used to confirm the results found in decoupled ^1H NMR. Hexads, (a stereosequence with 6 subunits) may be resolved in the carbonyl region, the assignment of which is attributed to Kaspercyzk.[40] Methine region resolution is lower but assignment at the tetrad level may be achieved. The corresponding P_r and P_m values can be calculated from the intensity of the peaks, in an analogous method to decoupled ^1H NMR.

1.5 Catalysts for ring-opening polymerization of lactide

As mentioned earlier, the driving force for the ROP of lactide is the release of ring strain. Although studies have shown that LA can be polymerized by enzymatic,[36-38] anionic,[39,40] cationic[41-45] and organocatalytic[46-50] means, the most widely studied area is metal-mediated ROP.[77,78] The initial successes of aluminum alkoxides such as $Al(O^iPr)_3$[79] led to further investigations with these types of systems. Zinc lactate[80] and other simple alkoxides (La- and $Y(OR)_3$, where R = ^{i}Pr and ^{n}Bu)[81-82] showed improved activity when compared to aluminum systems. No induction period was observed and the propagation rate constant showed a great increase in activity, (0.6 L mol^{-1} min^{-1} for $Al(O^iPr)_3$ at 70°C vs 1.9×10^3 L mol^{-1} min^{-1}for $Y(O^iPr)_3$ at room temperature). Closely related oxoalkoxide clusters of La, Sm, Y, and Yb have also been

investigated, with the greatest activity observed for lanthanum derivatives.[83-88] Unfortunately, the molecular weight distributions of these systems were broad as ester exchange was occurring during the induction period.

Tin based systems, namely tin(II) butoxide, have been utilized in the ROP of lactide and compared with analogous tin alkoxides prepared from $Sn(Oct)_2$.[89-90] Evidence supports that these alkoxides are the true active species in $Sn(Oct)_2$ polymerizations of lactide. This is demonstrated in Scheme 1.5. As expected, two chains propagate from the metal centre, and $Sn(OBu)_2$ had a polymerization rate 100 times greater than tin alkoxides generated from $Sn(Oct)_2$.[89] Unfortunately, these tin systems continue to be plagued by transesterification reactions leading to broad PDIs (1.2-1.8).

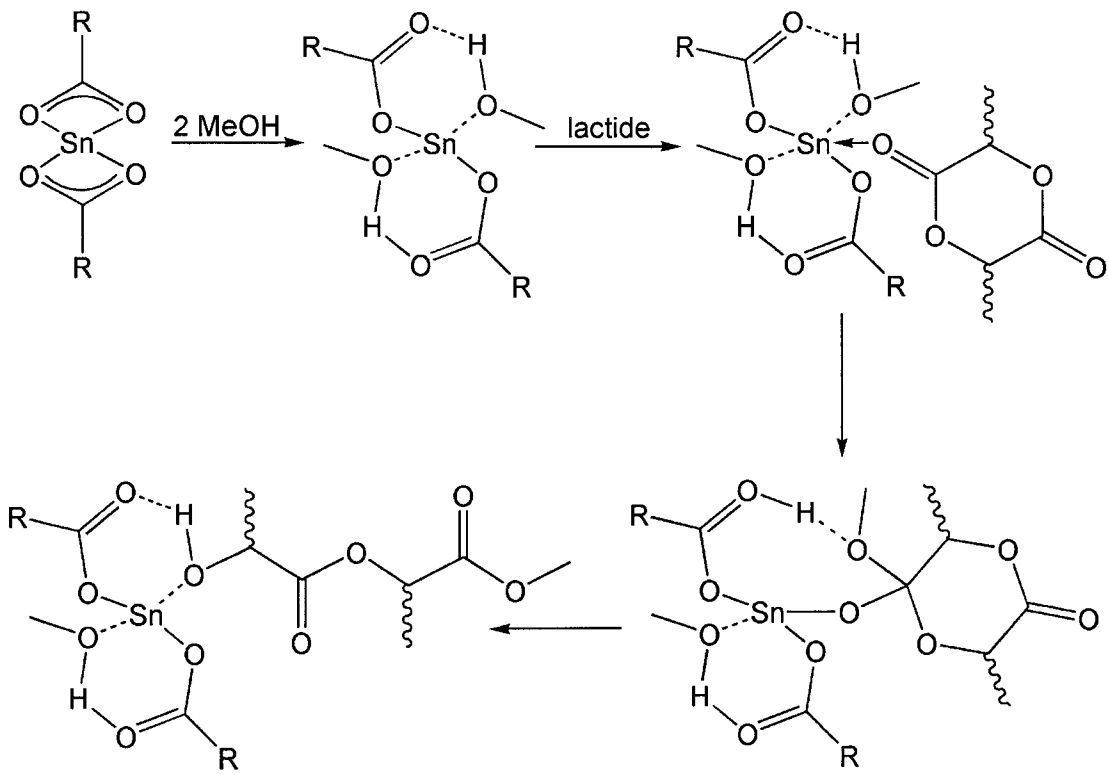

Scheme 1.5. Initiation mechanism of $Sn(Oct)_2$ catalyzed polymerization of lactide.

Remedies to these problems were hoped to be found from bis- and trisaryl tin(IV) alkoxides ($Ph_2Sn(OR)_2$ and $Ph_3Sn(OR)$),[91-92] tin(IV) amides ($Ph_2Sn(NMe_2)_2$)[93] and cyclic tin(IV) bisalkoxides ($Bu_2Sn(-OCH_2CH_2O-)$.[94-96] These systems have yielded mixed results, where the tin(IV) alkoxides and amides exhibited resistance to hydrolysis but extremely slow polymerization rates, and the spirocyclic tin initiators exhibited improved PDI (1.05-1.22), but slow reaction rates as well. This catalytic geometry has also been extended to germanium.[97]

To promote improved biocompatibility, calcium and iron, two metals that actively participate in human metabolism, were investigated for the ROP of lactide. Calcium dialkoxides of the form $Ca(OR)_2$, where R = ^{i}Pr and Me, were found to be highly successful ROP catalysts, exhibiting no induction period and achieving complete conversion in 30 minutes at room temperature.[98] Treatment of the same calcium precursor ($Ca[N(SiMe_3)_2]_2$), with a β-diketone allowed for the preparation of a dinuclear complex as seen in Figure 1.8.[99]

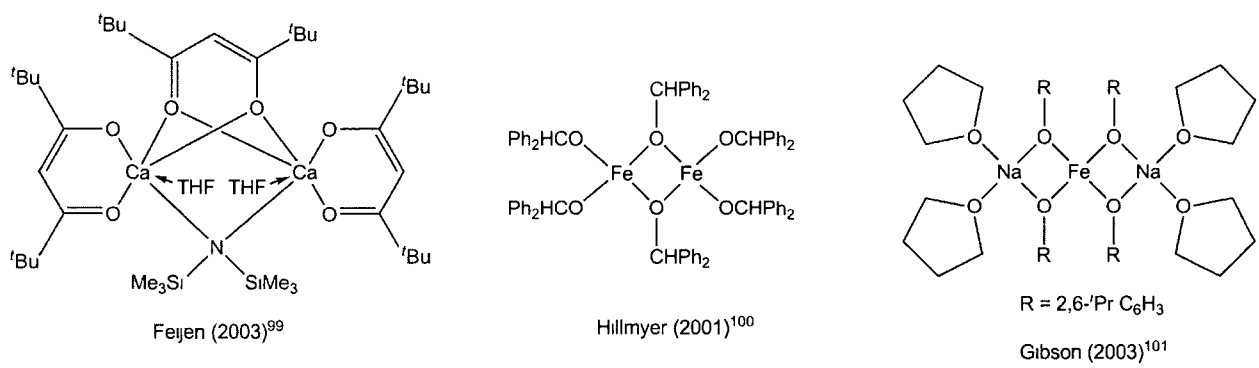

Figure 1.8. Bimetallic calcium, iron and heterobimetallic iron and sodium complexes.

Iron clusters, similar to the lanthanide oxoalkoxide examples have been prepared from $Fe(OEt)_3$ and yielded PLA with narrow PDI (1.1-1.2) via the co-ordination insertion mechanism.[100-101] Similarly, an iron dimer ($Fe_2(OCHPh_2)_6$ has shown activity,[100] as well as some heterobimetallic Fe-Na alkoxides developed by Gibson and co-workers.[102]

The deficiencies of these metal alkoxides, broad PDI, low conversion, slow rates, aggregation and transesterification, led to investigations which focused on metal catalysts possessing non-labile ancillary ligands. This was viewed as a method of moving steric bulk closer to the metal centre and hopefully minimizing or eliminating the transesterification reactions that plagued the simple alkoxides.

These catalysts for ROP of lactide typically take the form L_nMR, where L_n is the set of ancillary ligands which, although not actively involved in the polymerization mechanism, strongly influence the sterics and electronics encountered at the metal centre. M is typically a Lewis acidic metal centre, while R is the initiating group. The most effective initiators reported have been alkoxides, but alkyls,[103] halides[103] and amides[104] have all been shown to successfully initiate the polymerization of lactide. Some debate remains concerning the ability of protic impurities, i.e. lactic acid, alcohols or water, to initiate ROP in these instances.

The evolution of ancillary ligand systems for the ROP of lactide originated with metalloporphyrins synthesised by Inoue in the late 1980s.[71-74] While these catalysts gave low PDI values with high conversions, the reaction rates were slow (96 h for 100 equivalents of lactide). Study of the mechanism using γ-valerolactone revealed the role of two metal centres in the polymerization. In this case, the initiating group of one catalyst performs a nucleophilic attack on the carbonyl group of the monomer, which is activated by the Lewis acidity of another equivalent of catalyst.

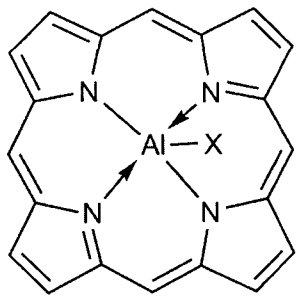

Metalloporphyrin
X = $^{-}CH_2CH_3$, $^{-}OCH_3$

Figure 1.9. Aluminum porphyrin, the first homogenous lactide polymerization catalyst.[71]

In attempting to achieve a monometallic mechanistic pathway, more flexible ligand frameworks were employed. This was carried out to impart a less constrained geometry at the metal centre, as the incoming monomer and initiator must possess a *cis*-geometry for the mechanism to be viable. In the porphyrin examples the metal is encompassed by a rigid ligand system leaving only two *trans* axial sites open for the co-ordination of the initiator and monomer.

The second motif developed was built around a diamidoamino system co-ordinated to aluminum, samarium, tin, zinc and group 3 elements (Figure 1.10).[105-108] Monometallic trigonal monopyramidal geometries were observed for the aluminum and tin species, of which the tin was found to be most active. The samarium and zinc analogues were found to possess a dimeric form that was attributed to the enforced geometry of the diamidoamino ligand, which is adapted to a bent arrangement vs. a linear, allenic-type geometry expected for monomeric zinc complexes. Bulk copolymerizations with glycolide reached high conversions (>95%) however the PDI of such reactions were broad (2-3).

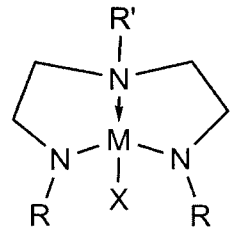

Diamidoamino
M = Al, Sm, Sn, Zn
R = SiMe, R' = Me, $SiMe_3$
X = Me, H

Figure 1.10. Diamidoamino complexes, the second generation of homogenous lactide catalysts.[105-108]

Further work to prevent transesterification reactions involved the incorporation of bulkier tridentate ligands. To this end, trispyrazolyl-hydroborate ligands were used in the preparation of complexes of calcium, magnesium and zinc for lactide polymerization.[109-112] Calcium analogues were the most active, capable of polymerizing 100 equivalents of lactide in one minute at room temperature, whilst Zn was the least active, requiring 6 days to achieve 90% conversion.[109] This order of reactivity was attributed to the polarity of the metal-initiator bonds. Magnesium and zinc trisindazolyl-hydroborate analogues were prepared and an increase in activity was observed when compared to the diamidoamino systems. While first order dependence on the catalyst concentration was observed, PDI values, although improved, remained high for controlled living polymerizations (1.6-1.7).

Oxygen based bisphenolates and methylenebisphenolates complexed with aluminum have shown ability in the ROP of lactide,[113,114] as have chalcogen-bridged bisphenolates with titanium.[115,116] This framework has been expanded to include dichalcogen-bridged biphenolates complexed to rare-earth metals such as lanthanum and lutetium.[117] Thiophenolate derivatives of these ligands have been prepared and complexed with aluminum,[103] however these systems

exhibited poor capacity for the ROP of lactide, with the thiophenolate ligands initiating the polymerization and failing to maintain the integrity of the metal complex.

Bidentate N-donor ligands have shown promise in the ROP of lactide, with diamido zinc,[118] amidinate yttrium,[119] tin[120] and iron,[121] and β-diiminate zinc,[70,122-128] tin,[127] magnesium,[123-126] calcium[110] and iron[128,129] systems all being investigated for lactide polymerization (Figure 1.11). The most successful of this group are the β-diiminate catalysts, which generally display the characteristics of living systems.[70,110,122-129] These ligands have been used widely in the stabilization of low-valent species and their sterics are believed to have greater influence because the nitrogen substituents point in the direction of the bonded centre.[130] In all cases of β-diiminate complexes, lactide polymerization was observed in dichloromethane at room temperature, with the reactivity following the trend: Mg>Zn~Fe~Ca>Sn, which roughly parallels the electropositive character of the metals.[129] The activity of these complexes was also highly dependent upon the initiating group. For zinc complexes, silylamido, silylalkoxy, acetate and ethyl initiating groups were all significantly slower than alkoxy co-ligands. The magnesium catalysts continue to be amongst the most active catalysts for the metal-mediated ROP of lactide, while the zinc analogues of Coates possess high activity and exhibit stereoselectivity in the polymerization. The success of these systems has led to phosphorous-containing analogues, namely methylene-bis(phosphinimino) ligands, of which some preliminary investigation has occurred.[131]

Combination-type chelating ligands, containing both N and O-donors remain a pillar of ROP catalyst technology, with the greatest number of reports focusing on salen ligand systems (Figure 1.11). Inspired by Inoue's porphyrinato ligands, these frameworks are derived from salicylaldehydes and ethylenediamines (N,N'-bis-(salicylidene)ethylenediamine) and have been

complexed to aluminum,[68,69,72,73,132-143] tin,[144] yttrium[75] and zinc.[145,146] These zinc complexes made use of the half-salen ligand with various imine substitutions.

Intensive study of the aluminum complexes has revealed that changes made to the ligand backbone play a key role in the activity of the catalyst. Chlorine substitution at the *para* position of the phenol ring led to higher polymerization rates and less transesterification.[137] These phenomena have been attributed to enhanced aluminum electrophilicity and/or an increase in the polarization of the Al-X initiating bond.

Increasing the steric influence at the metal centre, through *ortho* substitution of bulky groups on the phenol ring, led to a dramatic decrease in both inter and intramolecular transesterification reactions.[138-140] While decreased rates were observed for those catalysts possessing the bulky R1 substituent, the stereoselectivity was enhanced. Those aluminum-salen catalysts possessing a flexible backbone (C_2, C_3 or Cy) have been shown to possess a higher rate of polymerization than more rigid systems, such as those bearing an aromatic linker.[138-139] The presence of sp^3 hybridized carbons in this linker seems to promote improved polymerization rates. End-group analysis of the resultant PLA revealed the presence of ester linkages, indicating the operation of the co-ordination insertion mechanism in these catalysts. PLA produced with these catalysts possesses a narrow molecular weight distribution and the living character is demonstrated through a linear relationship between conversion and molecular weight.

Salan analogues of these aluminum complexes, where the imine linkage has been reduced to a secondary amine, or reductively aminated to give tertiary amines, are also active in the polymerization of LA.[147] These catalysts have been shown to be highly effective in the heterotactic polymerization of *rac*-lactide.

The half-salan zinc complexes have shown impressive reaction rates, became the most active PLA catalyst at the time of their report.[146] Developed by Hillmyer and Tolman, the activity of these systems was attributed to the facile co-ordination of lactide to a less co-ordinatively saturated metal centre. Other types of mixed N,O donor ligands have been employed in the ROP of lactide, with reports focusing on titanium and tantalum atrane type complexes, (Figure 1.11)[148-150] yttrium and lanthanum complexes bearing alkoxy-amino-bisphenolate ligands,[151] 1,4,7-triazacyclononane frameworks bound to yttrium,[152,153] as well as zinc complexes bearing phenolate-based ligands with ethylene-diamine arms (Figure 1.11).[146,154]

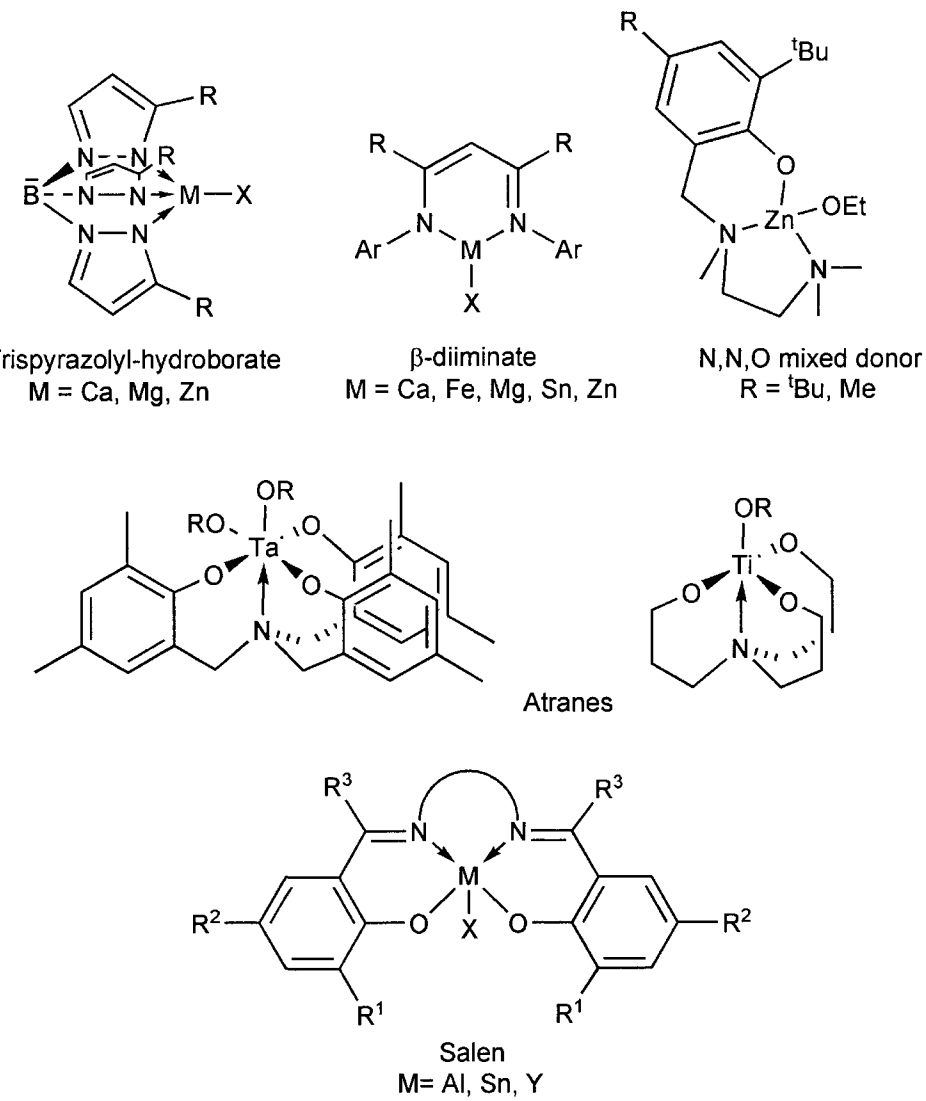

Figure 1.11. Common catalyst motifs in the ROP of lactide.

While the aforementioned catalysts have focused on activity and molecular weight control, a great number of reports have focused on the area of stereoselective lactide polymerization, with catalyst design being paramount in the study of isotactic, heterotactic and syndiotactic poly(lactic acid)s. These systems utilize numerous metals including aluminum,[155-160] germanium,[161] hafnium,[162,163] indium,[164,165] magnesium,[166] zinc,[166,167] zirconium[162] and various lanthanides.[168,169]

Isotactic polymerization of lactide was first investigated with aluminum salen catalysts derived from (R,R)-binaphthyldiamine.[68,141] These chiral catalysts have been demonstrated to exhibit enantiomorphic site control (through ^{1}H NMR analysis of the resulting PLA) in the polymerization of *D*-lactide to form isotactic PLA. Achiral salen complexes have been shown to polymerize lactide via the chain-end control method, with the greatest tacticity bias for the catalyst bearing ^{t}Bu substituents at the *ortho* and *para* positions of the phenol ring and an n-propylene linker.[155] This catalyst is reported to yield isotactic PLA from *rac*-lactide with a P_m value of 0.88 and PDI of 1.07 at moderate reaction times with >90% conversion.

The heterotactic polymerization of *rac*-lactide has been achieved most effectively with aluminum salan derivatives[147] (Figure 1.12) and zinc β-diiminate complexes.[70,123] The salan complexes of Gibson, possessing dichloro substitution at the *ortho* and *para* positions of the phenol ring and an n-propylene linker provided PLA with a P_r value of 0.88 at 70°C in toluene, while the zinc complexes provide heterotactic PLA with tacticity bias upwards of 0.90 at room temperature. In all of these complexes, a stable ligand set is sought, but thiol containing scandium salen complexes developed by Okuda show chain-end control through fluxionality of the ancillary ligand.[170] Representing a new type of dynamic monomer recognition, these scandium complexes were able to achieve P_r values of up to 0.96.

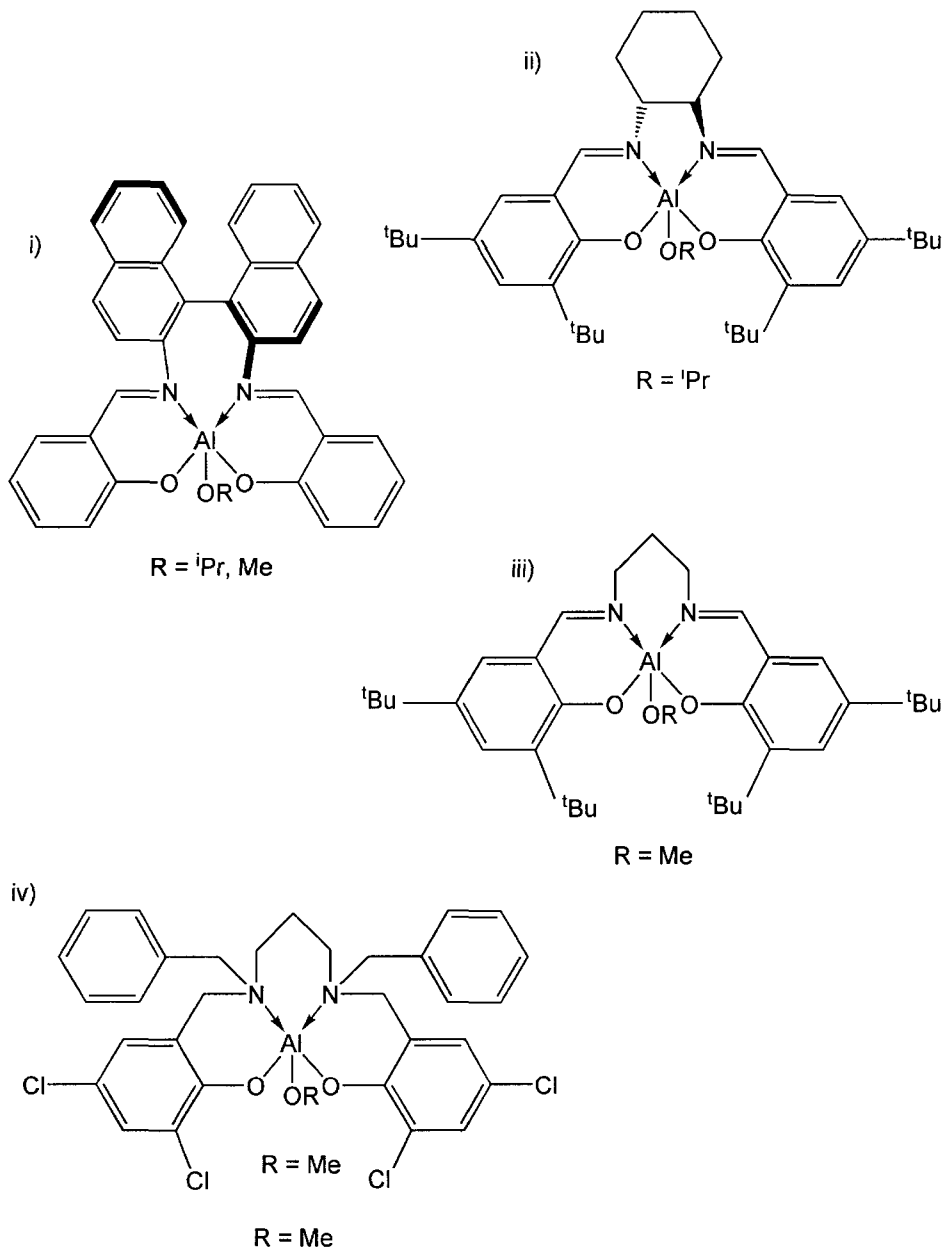

Figure 1.12. Stereoselective aluminum catalysts for the ROP of lactide, i,ii) operate by enantiomorphic site control, iii, iv) operate by chain end control.

1.6 Polymer stars

To this point the discussion has focused solely on linear polymers, however PLA has been synthesized in a variety of macromolecular architectures. These take the form of brushes, dendrimers or stars. Star polymers can be defined as multi-armed polymeric materials in which arms radiate from a central core. These systems were developed through the pioneering work of Flory, who synthesized four- and eight-arm star polymers of ε-caprolactam.[171] Possessing rheological, mechanical and biomedical properties that are not accessible in traditional linear polymers, these star polymers have attracted attention from multiple disciplines within chemistry, biochemistry and materials engineering, particularly as controlled drug delivery release systems and in nanotechnology applications.[172,173]

From a chemical standpoint, star polymers possess increased concentrations of terminal functional groups, improved solubility and different hydrodynamic volumes when compared to linear analogues with comparable molecular weights. Polymer stars often will possess lower melt viscosities, different thermal properties and improved physical processing when compared to linear polymers, as physical properties are influenced more by the molecular weight of the star arms more so than the total molecular weight of the star.[174] The synthesis of star polymers is typically achieved through one of two methods, arm-first or core-first, illustrated in Scheme 1.6.[173]

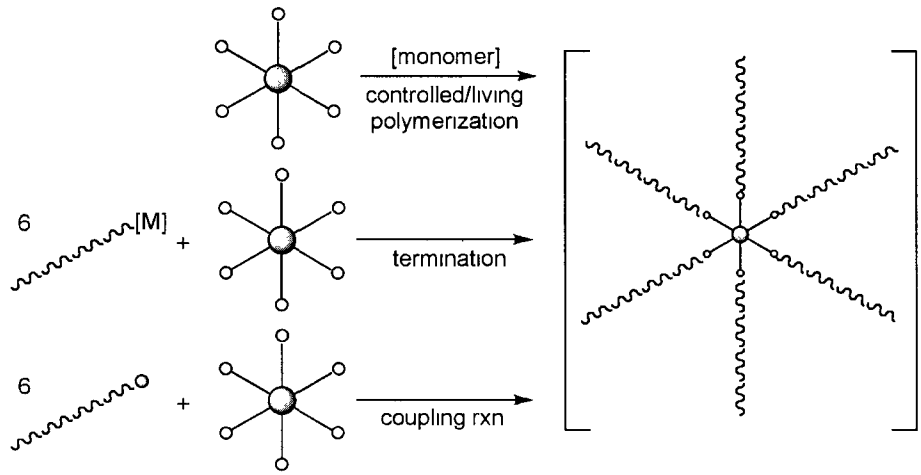

Scheme 1.6. Synthetic routes to star polymers.

In the core-first method a multi-functional core initiates the living polymerization of a reactive monomer. The polymer chains will grow from a fixed position directly on the core. Alternatively, the arm-first method couples linear polymer chains with a multi-functional core bearing reactive terminal groups. The 'fixing' of the arms can be achieved through a termination of the linear living polymer chains by the core, or through a coupling reaction between reactive polymer end-groups and core functionalities. While both methods are viable for the creation of polymer stars, the core-first method is more versatile for synthesizing PLA homopolymers.

Although the polymer star architecture can be built with a wide range of monomers and polymers,[175-177] much work has focused on aliphatic polyesters. The abundance of these aliphatic star polymers is partially derived from the convenience that multi-functional alcohols provide in acting as initiators in the ROP of cyclic esters via the core-first approach. This approach has been highly successful in preparing star polymers of lactide, ϵ-caprolactone, glycolide, β-butyrolactone and trimethylene carbonate, cyclic lactones whose benefits have been mentioned earlier. Similarly to linear polymers, synthesis of these stars is initiated by an alcohol group and

catalyzed by a metal complex to form active metal alkoxides, which may then participate in the co-ordination insertion mechanism, (Scheme 1.4).[178,179]

Despite the long history of star polymers (1948),[171] the first report of PLA star macromolecules dates to 1989,[180] and research in the area has coincided with the boom in PLA interest over the last decade. The rise in popularity is attributed to the unique properties that star-shaped PLAs possess when compared to linear homopolymers. These stars exhibit lower melting temperatures (T_m), glass transition temperatures (T_g) and crystallization temperatures (T_c).[179,181] In addition to these thermal considerations, star polymers of PLA exhibit coiling, possess lower hydrodynamic volumes, have higher viscosity and can form micelles in aqueous solution.[181] A greater correlation between the viscosity and temperature is also observed with star PLA, as the entanglement of the arms suppresses longitudinal motion.[182]

Many types of cores have been employed in the synthesis of PLA polymer stars.[183] They can be generally summarized as discrete, polymeric, miktoarm and dendritic/hyperbranched cores. For our purposes, only discrete cores will be analyzed in detail. Discrete cores can be simply regarded as small molecules bearing multiple hydroxy functionalities that may be used in initiating ROP. They are often termed polyols if derived from sugar alcohols, but may be other organic molecules that possess no repeat units or branch points. In almost all literature reports the PLA arms possess atactic stereochemistry, and are synthesized utilizing the $Sn(Oct)_2$ catalyst.[183]

The simple polyols pentaerythritol (PE)[181,184-194] and dipentaerythritol (DPE)[19,187,189,190,195-198] are the most commonly used cores in PLA star synthesis and produce four- and six-armed stars respectively. Additionally, 3-armed stars based on trimethylolpropane

(TMP) and glycerol, [185,187,192-195,199,200] 4-armed stars based on diTMP and erythritol,[187,199] 5-armed stars based on xylitol,[199] 6-armed stars based on inositol and sorbitol,[192,199] and 8-armed stars based on tripentaerythritol (TPE) and modified diTMP[187,201] have also been synthesized. These polyol cores can be seen in Figure 1.13.

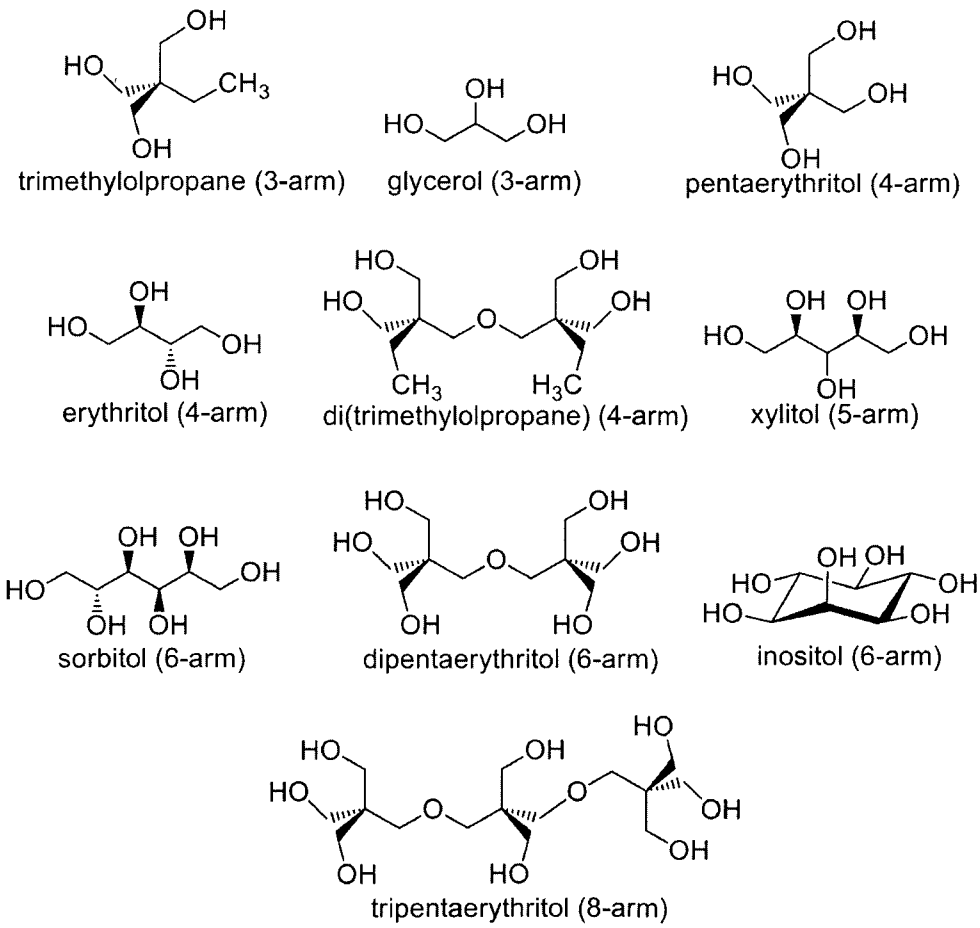

Figure 1.13. Simple polyols utilized as star polymer cores.

The reports that contain polymer and thermal characterization of star PLA polymers are summarized in Table 1.2. From the data we can see that reported molecular weight distributions are typically very good, evidence of concurrent initiation of ROP at all core OH functional groups, as well as the efficiency of $Sn(Oct)_2$ in these systems. Strong correlations are also observed between the catalyst loading ratios, with both low and high catalyst:initiator ratios

resulting in anomalously high PDIs.[181,202] Confirmation that all alcohol functionalities have initiated is verified by ^{1}H NMR spectroscopy in most cases.[197]

Table 1.2. Thermal data for P*L*LA polymer stars prepared with $Sn(Oct)_2$ catalyst.

Core	M_n	PDI	T_g (°C)	T_c (°C)	T_m (°C)	X_c (%)	Ref
Glycerol	17400	1.78	55.9	109.5	160.2	-	195
Glycerol	21200	1.56	53.7	100.8	157.2	38.7	185
Glycerol	8600	1.19	-	-	126.6	-	199
PE	1940	1.97	60.6	107.3	179.1	51.9	181
PE	20200	1.94	50.5	115.2	160.2	-	195
PE	31700	1.75	58.2	98.0	162.1	44.4	185
PE	165000	1.90	53.0	93.0	172.0	-	181
PE	13250	1.05	51.4	105.4	153.2	48.3	191
Erythritol	8300	1.12	-	-	112.5	-	199
Xylitol	8300	1.10	-	-	113.1	-	199
DPE	29800	1.43	55.3	118.3	152.4	-	195
DPE	12700	1.10	49.3	100.5	147.7	41.0	191,196
Sorbitol	8500	1.09	-	-	114.8	-	199
TPE	52800	1.81	57.6	101.4	166.3	-	195

With respect to the thermal properties, there are also clear trends. The T_g of the star more closely relates to the molecular weight of the star, rather than the specific core or the number of arms it possesses. For P*L*LA stars that are prepared under similar conditions, the T_g values range from 49°C (M_n = 12700) to 58°C (M_n = 31700) and significantly lower temperatures would be expected for *rac*-lactide stars when correlating to the behaviour of linear PLA systems.[179] In addition, an increase in the control of the ROP (lower PDI) results in lower T_g values, indicating that uniformity of the star structure plays an important role in the observed thermal properties.

Crystallization behaviour of some PLA polymer stars has been investigated. Here the core has a much larger effect on the values of T_c. PE-based P*L*LA stars have lower T_c values than DPE-based P*L*LAs, even when the PE stars have greater molecular weights.[185,195] When samples possess the same core, an increase in molecular weight leads to an enhancement of the T_c value. This phenomenon is also observed for melting temperatures. An increase in M_n of star P*L*LAs will lead to enhanced melt properties of that material.

The number of arms is also shown to have little effect on the melting temperature of the PLA stars. A report that details the preparation of 3-, 4-, 5- and 6-armed P*L*LA star polymers provides evidence to support this assertion.[199] It is notable that the number of arms impacted the crystallization rates significantly. Beyond this little work has been completed regarding the crystallinity of polyol star P*L*LAs.

Clearly evident from analysis of the data is that little batch-to-batch consistency exists amongst star P*L*LAs. Predominantly due to wide-ranging differences in experimental design, catalyst loadings and monomer:initiator ratios, a more systematic approach would greatly enhance understanding of the impact of core, catalyst and molecular weight on the observed properties of PLA polymer stars.

Nearly all published reports of PLA stars utilize $Sn(Oct)_2$ to catalyze ROP, although alternatives do exist. Enzyme catalyzed synthesis of four- and six-armed stars based on PE and inositol has been achieved using lipases derived from *Pseudomonas fluorescens*.[192] Spirocyclic tin initiators based on tin-substituted polyethylene ethoxylate[203,204] and cyclic stannoxanes[205] have been used in the preparation of PLA star polymers as well as the linear analogues mentioned previously. Organocatalytic systems, namely dimethylaminopyridine

(DMAP)[206] have been utilized to successfully prepare 6-armed stars from a luminescent ruthenium complex.

The scope of metal-based catalysts has been expanded to include zinc amino- and thio-phenolate[207,208] and bis(calcium)pentaerythritol[209] systems tthat can be used for the preparation of PLA star polymers. Stereocontrolled stars have been reported only once, where the aluminum salan complex, (where salan = N,N'-ethylenebis(benzyl)bis(3,5-di-chlorosalicylamine)), mentioned earlier was used to prepare 6-armed stars based on dipentaerythritol.[210]

We have seen that the nature of the core and catalyst play an important role in the properties of PLA polymer stars, but the significance of the polymer star arm end-group cannot be understated. The nature of this group plays a key role in the hydrolytic degradation stability of the polymer stars. As this is an important feature in assessing the quality of these materials for drug delivery systems, PLA polymer stars were studied by analyzing the solution stability and resistance to hydrolytic degradation of stars possessing OH, Cl, NH_2 and COOH terminated arms.[185] The cold crystallization temperatures of the Cl, NH_2 and COOH terminated PLAs were higher than OH terminated samples. These samples also possessed enhanced thermal stability when compared to the hydroxyl terminated stars, and those with Cl and NH_2 end-groups were the most resistant to hydrolytic degradation. An increase in the number of end-groups, moving from few armed discrete cores to hyperbranched and dendritic systems led to an enhancement of the end-group effects, a characteristic of polymer stars. This work is summarized in Table 1.3.

Table 1.3. Terminating end-group effect on PLA polymer star properties.[a]

Term.	Core	M_n	PDI	T_g (°C)	T_c (°C)	T_m (°C)	ΔH_m[b]
OH	Glycerol	21200	1.56	53.7	100.8	157.2	40.9
Cl	Glycerol	21300	1.56	57.1	126.8	159.1	33.9
NH_2	Glycerol	20200	1.56	52.3	111.5	156.9	42.0
COOH	Glycerol	18800	1.76	53.2	121.9	155.3	32.9
OH	PE	31700	1.75	58.2	98.0	162.1	47.4
Cl	PE	32400	1.73	58.3	128.5	163.5	39.4
NH_2	PE	33700	1.61	55.2	123.2	161.7	40.3
COOH	PE	33200	2.14	53.7	125.0	159.4	34.6

[a]$Sn(Oct)_2$ catalyst, *L*-lactide. [b]Enthalpy of melting (J g^{-1}).

This method of end-group functionalization has been used to generate PE-based PLA stars with succinic acid end-groups.[194] These succinic acid groups can be cross-linked with succinic anhydride post synthesis to form complex polymer networks. These networks were capable of maintaining thermal properties (similar T_g and T_m) while exhibiting greatly reduced crystallinity.

Beyond simple polyols, more complex cores have been utilized to prepare PLA stars while maintaining a lack of branch points. Cholic acid, a natural crystalline bile acid, has been used to prepare 4-armed star-PLAs.[211-216] PLA stars based on this core have been investigated for applications in substrate mediated gene delivery and cell transfection. The PLA stars can act as a support for DNA co-precipitate complexes as well as functioning as *in vitro* drug delivery vectors. These versatile stars can also be linked through the condensation of multiple cholic acid oligo-PLA macromolecules to form PLA-co-cholate chains.[216] These PLA stars were found to have relatively fast degradation times and their chemically benign and bioassimilable nature were key requirements for success in transfection systems.

Another class of multi-functional initiators used in the ROP of LA are tosylated β-cyclodextrins.[217] Adaptation of these systems to prepare PLA-β-CD-POX block copolymers through the copolymerization of LA and 2-ethyl-2-oxazoline, allowed for the testing of these

materials as supramolecular carriers. The PLA-containing stars were loaded with Congo Red dye, and the maximum loading capacity, degradation and release profiles were monitored by UV-visible spectroscopy, further confirming the capacity of these materials for drug deliversy systems.

Alternatively, six-armed PLA stars were prepared from a hexahydroxy triphenylene core (2,3,6,7,10,11-hexa(10′-hydroxy decanoxyl triphenylene) (Figure 1.11). This system was expanded to prepare copolymers with styrene and N-acryloxysuccinimde (NAS) as well.[218] First, the hydroxyl terminated PLA stars were reacted with with α-bromo-isobutyric chloride to generate bromine terminated stars. These materials were then employed as macroinitiators for the atom transfer radical polymerization (ATRP) of styrene and NAS. Cross-linking and the formation of micelles afforded nanospheres, which could be hollowed out by hydrolysis of the PLA core. This example, as well as others we have seen, illustrates the versatility of PLA polymer stars, the synthetic flexibility they possess and their capacity for drug delivery systems.

The inclusion of novel tetra- and hexa-hydroxy functionalized perylene chromophores into PLA star technology has introduced rigidity to the star architecture (Figure 1.14).[219] The implementation of this more rigid core has resulted in an improvement in the thermal stability compared to flexible polyol cores, minimizing the destabilizing effects observed in the switch from linear to star architectures. These stars have also been investigated for their potential in the encapsulation of small molecules, with results indicating that loading capacity is heavily dependent upon the length of the star arms.

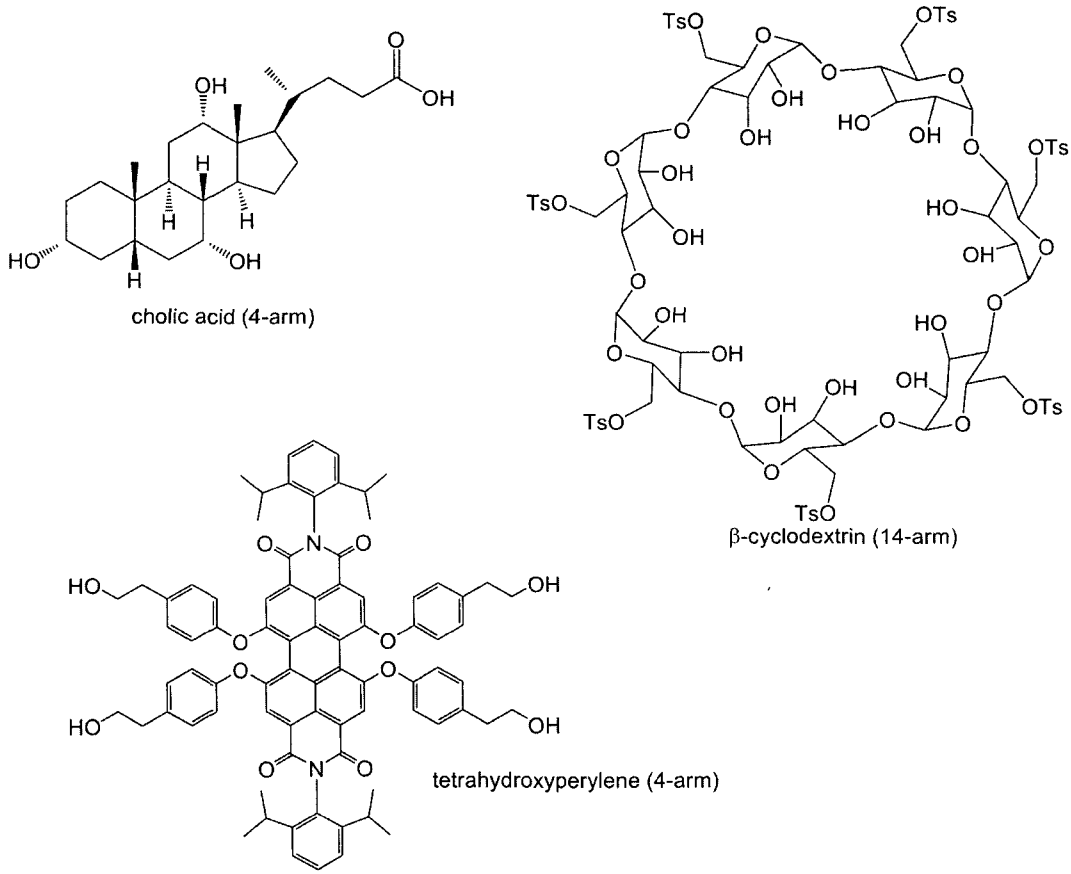

Figure 1.14. More complex cores utilized in PLA polymer stars.

Recently the effects of rigid cores has been analyzed on atactic PLA stars.[20] The thermal properties of PE and DPE centred stars were compared to stars prepared from 1,3,5-tris(hydroxyl)methylbenzene (THMB) and hexa-hydroxymethylbenzene (HHMB). The enhanced rigidity of the core was found to have a substantial influence on the observed T_m.

Finally, discrete transition metal complexes have been employed as cores for PLA nanoparticles (Figure 1.15). Discrete cores based on iron, ruthenium and europium with hydroxyl-substituted dibenzoylmethane (dbm) and bipyridine (bpy) ligands have been utilized as PLA ROP initiators. For dbmOH, ROP of LA was followed by complexation to the metal centre,[220,221] while the bpyOH ligands must first be complexed with the metal to create transition metal macroinitiator cores. The presence of a metal during the ROP process led to an increase in the observed PDIs, but was counteracted by increased activities and

conversions, especially in the instances of iron-based cores. These materials were designed for specialist applications, including use as stimuli-response materials, luminescent materials for drug delivery and imaging or responsive chromophores.

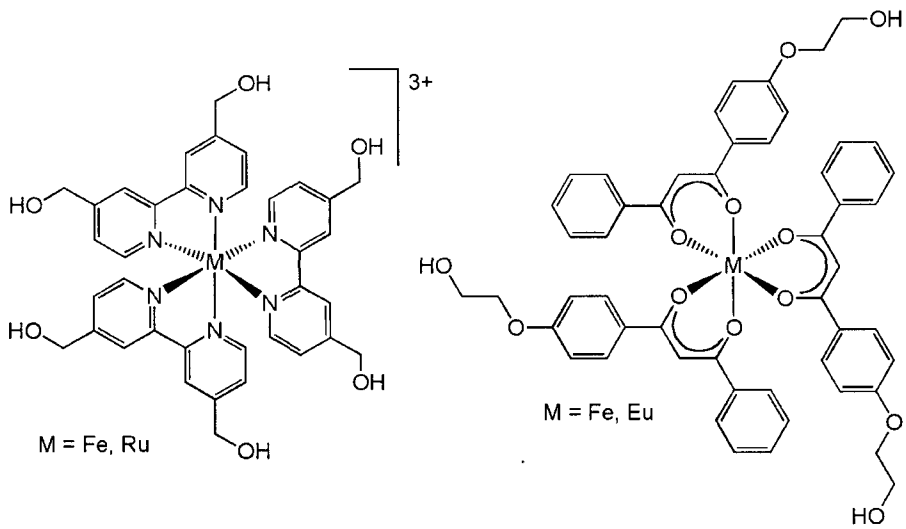

Figure 1.15. Metal complexes utilized as cores in PLA polymer stars.

1.7 Mandate of Research

This thesis was developed with the intentions of examining the effects of introducing tacticity control into the synthesis of PLA polymer stars. Polymer stars, while being a versatile and unique macromolecular scaffold with important applications, are plagued by lowered physical, thermal and solution properties.[183] It was expected that by promoting stereoregularity in the polymer arms of the star architecture, the properties of this unique polymer microstructure could be enhanced to those associated with linear PLAs of comparable molecular weights. By utilizing a combination of *rac* and *L*-lactide in conjunction with a series of previously reported catalysts (^{tBu}[salen]AlMe (**1**), ^{Cl}[salan]AlMe (**2**) and $Sn(Oct)_2$ (**3**)), that have been shown to promote isotactic-*rac* (**1**), heterotactic (**2**), atactic (**3**) and isotactic-*L* (**3**) the properties of the resultant stars would be improved. This concept, of combining control over polymer macrostructure with metal catalysts capable of controlling PLA microstructure to tune properties was hitherto unreported in the published literature.

This concept was thought to be especially significant with respect to the physical, thermal and degradation properties of these materials. Star PLAs suffer from decreased crystallinity, a result of their less regular packing arrangements, depressed thermal properties (especially melt properties and temperature stability), and degrade much more quickly in solution. By promoting regularity in the observed tetrads for the PLA star arms, it was envisaged that the crystallinity, thermal properties and solution lifetimes would be enhanced, improving the quality of these macromolecules for a variety of applications. The potential for determining the degradation kinetics of these star-shaped PLAs in solution was of particular interest with respect to their utility as drug delivery vectors, capable of delivering bioactives upon degradation.

The extent of control capable of being exterted over the properties of stereocontrolled PLA stars was further examined through the preparation of isotactic stars with a variety of tacticity biases. By combining the *rac* and *L*-lactide monomers at various ratios, and utilizing the $Sn(Oct)_2$ catalyst, which is well known to produce PLA with controlled molecular weight properties, a series of isotactically-biased PLA stars will be produced. The tacticity of these stars is hypothesized to correlate to to the observed physical (crystallinity), thermal (glass transition and melt temperatures) and solution (lifetime) properties.

Additionally, novel anilido-aldimine aluminum catalysts were to be prepared. Bearing much bulkier substitution patterns adjacent to the metal centre, these systems were envisaged to possess improved control over the stereocontrolled polymerization of *rac*-lactide. As steric influence of the co-ordination sphere is known to promote the isotactic insertion of *rac*-lactide monomers, these catalysts were hoped to possess high P_m values, nearing or surpassing those in the known literature. This involved the synthesis of novel cyclohexyl substituted anilido-ligands and the complexation of these ligands, in addition to diisopropylphenyl substituted analogues, with aluminum to prepare ^{R}[N,N,N,N]AlMe complexes in which the anilido-aldimine ligands are co-ordinating in a tetradentate fashion, a previously unreported phenomenon. The quality of these catalysts in the polymerization of lactide was to be investigated, including a kinetic analysis.

Chapter Two

Stereocontrolled PLA polymer stars based on dipentaerythritol

2.1 DPE-PLA stars with oligomeric arm lengths

2.1.1 Synthesis and polymer characterization

As discussed in Chapter 1, star polymers can be synthesized in a variety of ways. For this study the core-first approach was chosen. Core-first star synthesis is known for its success in one-pot reactions, and has precedence in lactide star preparation.[197] The employed reaction parameters are shown in Scheme 2.1, while the employed catalysts are shown in Figure 2.1.

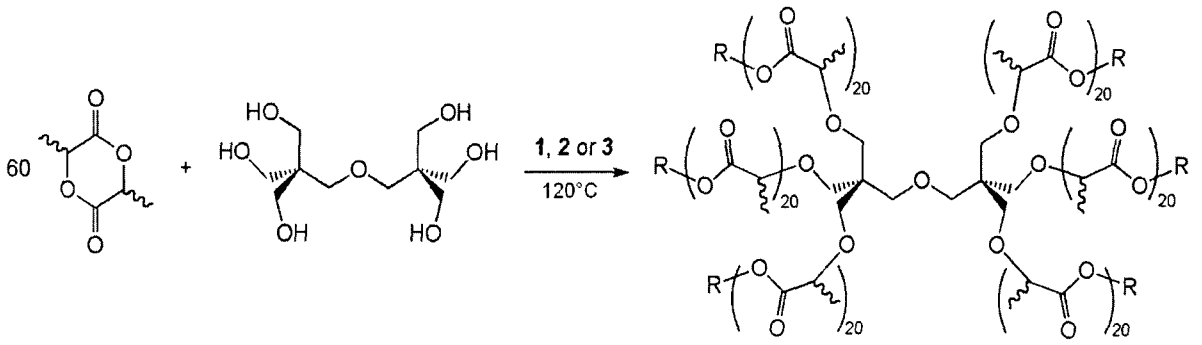

Scheme 2.1. Reaction scheme for the synthesis of DPE-centred PLA stars.

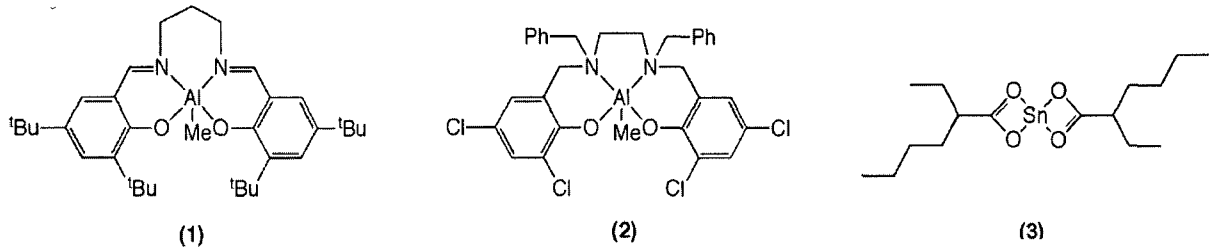

Figure 2.1. Catalysts utilized in the stereocontrolled synthesis of PLA stars. (**1**) ^{tBu}[salen]AlMe, (**2**) ^{Cl}[salan]AlMe and (**3**) $Sn(Oct)_2$.

The core chosen for this work was dipentaerythritol (DPE) to allow comparisons to be made with previous work.[197] Additionally, DPE was thought to impart features that would be desirable in the synthesis of PLA stars: a flexibility that would lend itself to unique opportunities for coiling and stereocomplex behaviour, and a significantly large number of arms (6), to allow for a meaningful comparative analysis of the stereocontrolled star polymer properties vs. linear systems.

Literature catalysts exhibiting excellent M_n, PDI and monomer insertion control were selected for the synthesis of stereocontrolled stars from *rac*-lactide. Aluminum catalysts ^{tBu}[salen]AlMe (**1**), (where ^{tBu}[salen] is *N,N'*-propylenebis(3,5-di(*tert*-butyl)salicylimine), and ^{Cl}[salan]AlMe (**2**), (where ^{Cl}[salan] is *N,N'*-ethylenebis(benzyl)(bis(3,5-dichlorosalicylamine), were selected for their efficiency in lactide polymerization with respect to reaction times, living

characteristics and high conversions, coupled with low PDI and high tacticity biases.[147,155] These catalysts yield isotactic and heterotactic PLA from *rac*-lactide respectively, with a P_m value of 0.88 and a P_r value of 0.96. $Sn(Oct)_2$ (**3**), is well-known to be highly efficient in the production of atactic PLA from *rac*-lactide, as well as the polymerization of optically pure *L*-lactide to form poly(*L*-lactic acid) (P*L*LA).

Monomer to initiator ratios of 60:1 were used to prepare 6-armed stars with 10 monomer units per arm, to obtain a system that would achieve high conversion with small variance between arm length, as opposed to stars with a higher molecular weight but greater variances in arm length. Consistency in the length of the arms was of great importance for comparisons between samples of different tacticities. Elimination of the known effects of M_n on thermal properties and solution stability would reveal the true effect of tacticity control. To achieve the polymer stars with the desired monomer:initiator ratios, higher than typical catalyst loadings had to be employed for monomer:catalyst:initiator ratios of 60:6:1. This was necessary as each initiating group on DPE required a catalyst.

Initial experimentation with the traditional polymerization methodology gave undesirable results. Attempts to adapt the ^{tBu}[salen]AlMe and ^{Cl}[salan]AlMe catalysts to star PLA synthesis proved difficult; at 70°C in toluene bimodal molecular weight distributions were repeatedly observed when analyzed by GPC. Accompanying this broadening of the observed PDI was a severe reduction of conversion and an undesirable induction period which resulted in very slow reaction rates (24 h for 20%). This problem was attributed to the low solubility of DPE in non-polar organic solvents, a phenomenon that is known in the literature.[55]

This problem was overcome through the use of molten lactide as the reaction medium. Improved solubility of DPE was countered by concerns regarding the suitability of the Al

catalysts for the more rigorous reaction conditions (120°C). While catalysts (**1**) and (**2**) were shown to be efficient ROP initiators in solution, they had not been reported as capable initiators dissolved in molten lactide. Preliminary studies revealed the capacity of these catalysts to retain structural integrity at the necessary higher temperatures; however, the effect on the tacticity control mechanisms was unknown. Removal of the solvent also aligned with 'greener' reactions by utilizing the capacity of the monomer to act as a reaction medium.

A typical synthetic procedure involved the loading of monomer (*rac* or *L*-lactide), initiator (DPE) and catalyst (**1**, **2**, or **3**) at the required ratios into a glass ampoule equipped with a magnetic stirring bar under inert atmosphere (N_2). This sample was heated at 120°C for a predetermined period of time, at which point it was removed from the heat and quenched with a 10:1 v/v solution of dichloromethane (DCM) and methanol (MeOH). The polymer was dissolved by vigorous shaking and allowed to stir for 30 minutes to ensure complete termination of the polymer chains. The sample was then dried by rotary evaporation and dissolved in a minimal amount of DCM (2-3 mL) and precipitated dropwise into cold (-15°C), stirring MeOH. The opaque supernatant was decanted and the resulting PLA was dried *in vacuo*. Reprecipitation was completed, as necessary, by repeating the aforementioned procedure. Requirement of a reprecipitation was typically assessed through the presence of catalyst/monomer in the ^{1}H NMR spectrum or thermogravimetric (TGA) analyses. The conversion of the polymerizations was determined gravimetrically through comparison to a theoretical yield. The polymer properties are summarized in Table 2.1.

Table 2.1. Polymerization data for DPE-centred stars.[a]

Sample	Catalyst	Monomer	Tacticity[a]	% Conv.	$M_{n,GPC}$[b]	$M_{n,th}$[c]	PDI	PDI_{arm}[d]
A-I	**3**	*rac*-LA	At	94	8873	9464	1.14	2.51
A-II	**3**	*rac*-LA	At	92	9058	9833	1.18	2.14
H-I	**2**	*rac*-LA	Ht	95	8755	8923	1.26	2.21
H-II	**2**	*rac*-LA	Ht	95	8240	8497	1.19	2.65
IR-I	**1**	*rac*-LA	Iso-(*rac*)	92	8501	8639	1.22	2.40
IR-II	**1**	*rac*-LA	Iso-(*rac*)	94	8688	8781	1.22	2.40
IL-I	**3**	*L*-LA	Iso-(*L*)	99	8771	8781	1.18	2.24
IL-II	**3**	*L*-LA	Iso-(*L*)	99	8691	8781	1.08	2.14

[a] Polymerization conditions: 60:6:1 monomer:catalyst:iniator @ 120°C [b] At-Atactic, Ht-Heterotactic, Iso-(*rac*)-Isotactic-*rac*, Iso-(*L*)-Isotactic-*L* [c] theoretical M_n [d] Calculated from the Szymanski method[222] [e] Conditions: 1 mL min^{-1} in THF, 2 mg mL^{-1} sample PS standards 6 point calibration 0.58 conversion factor.

From the data, it is shown that samples of four tacticity types have been synthesized and characterized. By judicious choice of catalyst (**1**, **2** or **3**) and monomer (*rac*- or *L*-lactide), a series of polymer stars have been synthesized with the varying tacticities possible for *rac*- and *L*-lactide. The four tacticities are the aforementioned atactic (At), heterotactic (Ht), isotactic derived from *rac*-lactide (Iso-*rac*) and isotactic derived from *L*-lactide (Iso-*L*).

The conversion of these PLA samples was calculated from weighing the resultant PLA and comparing to a theoretical yield. While the chemistry of $Sn(Oct)_2$ in polymer star synthesis is known, the high conversions indicate all catalysts are retaining high ROP efficiency in a solvent-free environment. GPC analysis of the samples indicates an excellent correlation between experimental molecular weights (M_n) and the theoretical values. This is a strong indication of the controlled character of the polymerization and demonstrates that these systems are working effectively, with minimal undesirable transesterification reactions which would result in lower molecular weights and broadened PDIs. The excellent polydispersities support a true Gaussian distribution of molecular weights for these star PLA systems. Following an emerging trend in polymer star analysis, the polydispersities of the arms (PDI_{arm}) has been calculated by the following equation (Figure 2.2).

$$PDI_{star} = 1 + \left(\frac{PDI_{arm} - 1}{f}\right) \times \left(\frac{M_{nstar} - M_{core}}{M_{nstar}}\right)^2$$

Figure 2.2. Formula for PDI of arm of star polymer (PDI_{arm}) from PDI of star (PDI_{star}), number of arms (f), molecular weight of star ($M_{n,star}$) and molar mass of core (M_{core}).

Typically employed in the analysis of dendritic and hyperbranched polymers, this measure of arm uniformity will be recognized as being broader than traditional PDI values. These DPE-based polymer star systems show PDI_{arm} values of < 2.7, indicating good control over the distribution of arm lengths, as typically values less than four are considered to be controlled.[223]

Further confirmation of the validity of the synthetic methodology and the accuracy of the molecular weight data was achieved by ^{1}H NMR. The presence of the polyolic core peaks of DPE (4.15 (m) ($OCH_2C(CH_2)_3$ and 3.34 (s) (OCH_2)) are diagnostic for DPE-centred stars and are observed in Figure 2.3.

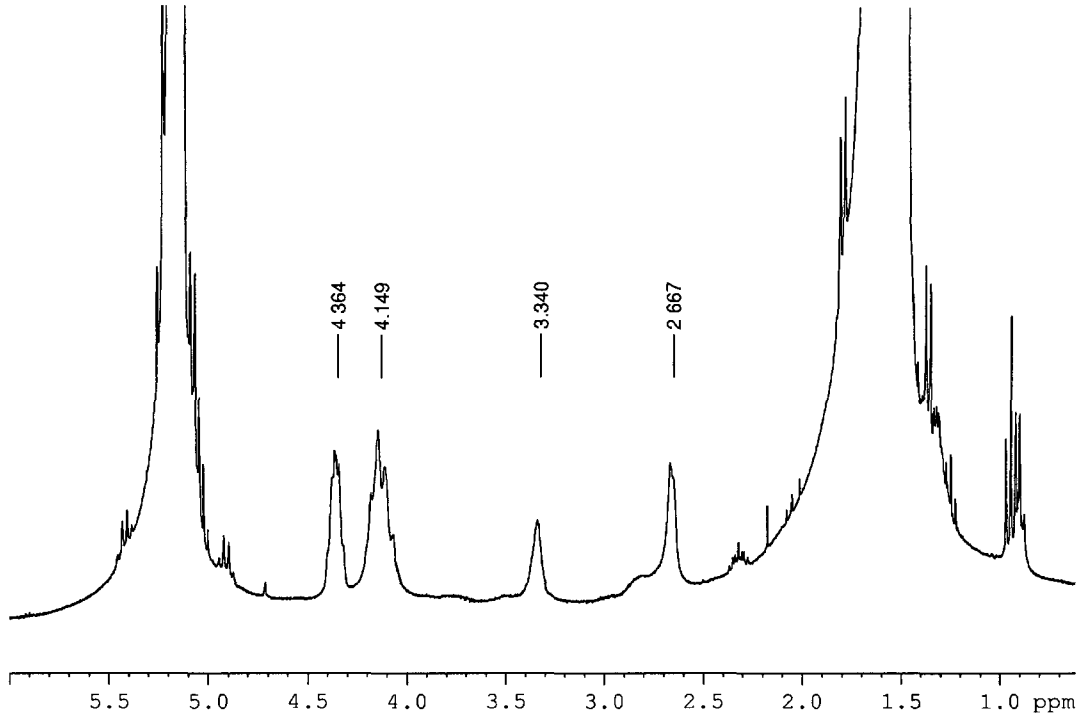

Figure 2.3. ^{1}H NMR of DPE-PLA star showing the major peaks derived from DPE core.

Integration of the methyl and methine protons of the PLA chains versus the signals derived from the DPE core reveal good M_n control exhibited by these systems and illustrate the accuracy of molecular weights determined by GPC. Typically M_n determination by NMR is fairly accurate, but the presence of small impurities in the sample can distort the integrations, especially for low molecular weight polymers, which maximize the effects of these impurities. Additionally the end-group of high M_n polymers can be washed out in the spectral background noise. These results are summarized in Table 2.2.

Table 2.2. ^{1}H NMR data for DPE-centred stars.

Sample	Catalyst	Monomer	Tacticity	Tact. %[a]	$M_{n,NMR}$[b]	Tetrads[c]
A-I	**3**	*rac*-LA	At	-	9488	mmm, mrm, rmr, mmr, and rmm
A-II	**3**	*rac*-LA	At	-	9862	mmm, mrm, rmr, mmr, and rmm
H-I	**2**	*rac*-LA	Ht	86	8982	**rmr, mrm,** mmm, mmr and rmm
H-II	**2**	*rac*-LA	Ht	86	8451	**rmr, mrm,** mmm, mmr and rmm
IR-I	**1**	*rac*-LA	Iso-(*rac*)	82	8704	**mmm**, mrm, rmr, mmr, and rmm
IR-II	**1**	*rac*-LA	Iso-(*rac*)	82	8846	**mmm**, mrm, rmr, mmr, and rmm
IL-I	**3**	*L*-LA	Iso-(*L*)	100	8852	**mmm**
IL-II	**3**	*L*-LA	Iso-(*L*)	100	8839	**mmm**

[a] Tacticity bias calculated from integration of decoupled methine (C*H*) signals from ^{1}H NMR
[b] $M_{n,NMR}$ calculated from integration of PLA (CH_3) vs DPE (CH_2) peaks from ^{1}H NMR
[c] Observed tetrads for PLA stars in decoupled ^{1}H NMR with dominant tetrad highlighted

As previously discussed, decoupling of the ^{1}H signals of PLA allows for greater clarity in assessing the polymer microstructure. This technique allows the identity assignment of the PLA tetrads of various stereocontrolled stars to be determined through comparison with widely accepted literature assignments.[76] A decoupled ^{1}H NMR spectrum for all of the synthesized stereoregular forms may be observed in Figures 2.4-2.7 below.

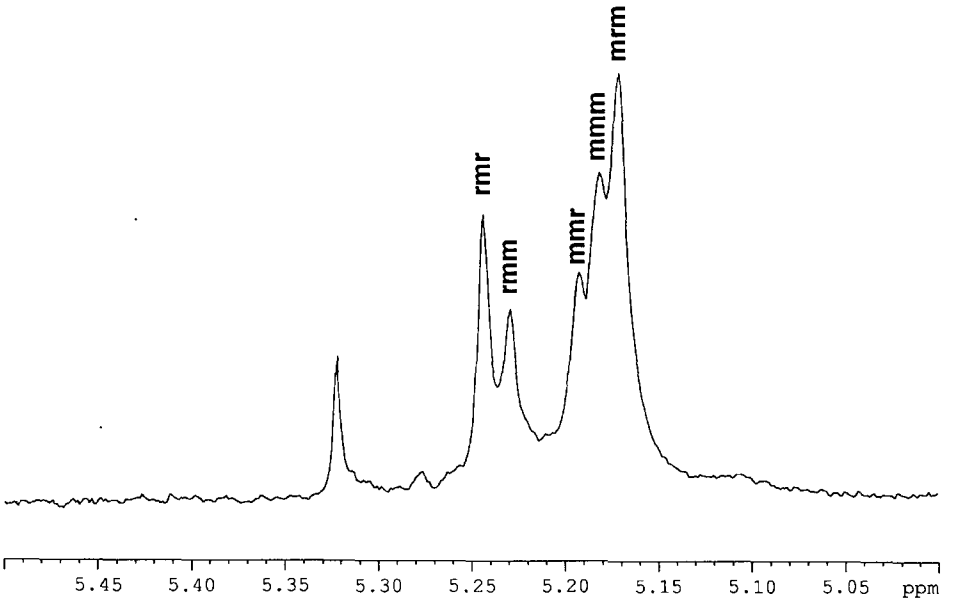

Figure 2.4. Methine region of decoupled ^{1}H NMR for atactic PLA stars (A-I).

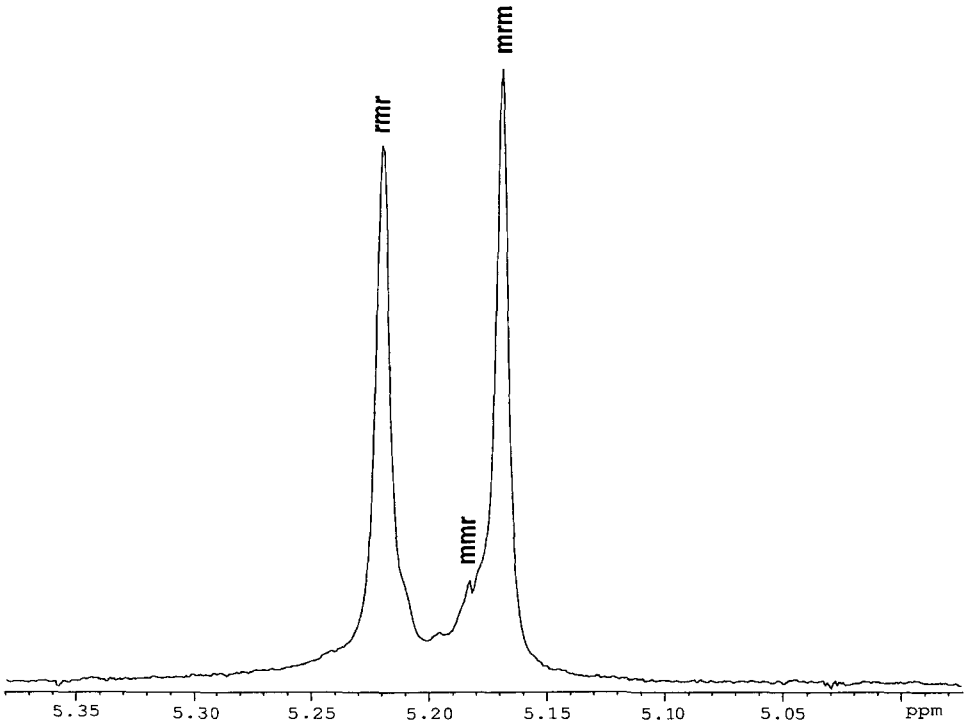

Figure 2.5. Methine region of decoupled ^{1}H NMR for heterotactic PLA stars (H-I).

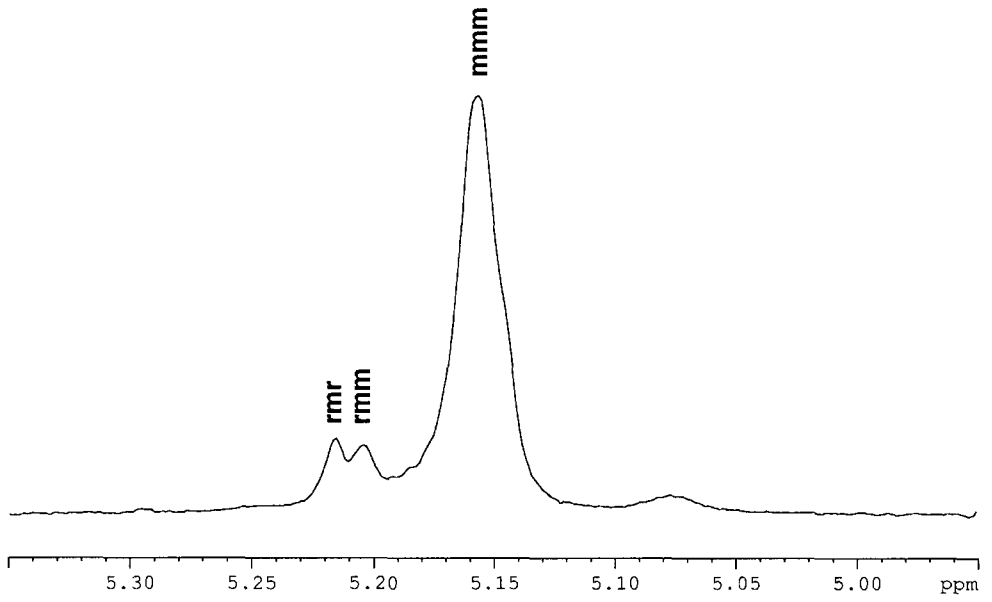

Figure 2.6. Methine region of decoupled ^{1}H NMR for isotactic-*rac* PLA stars (IR-I).

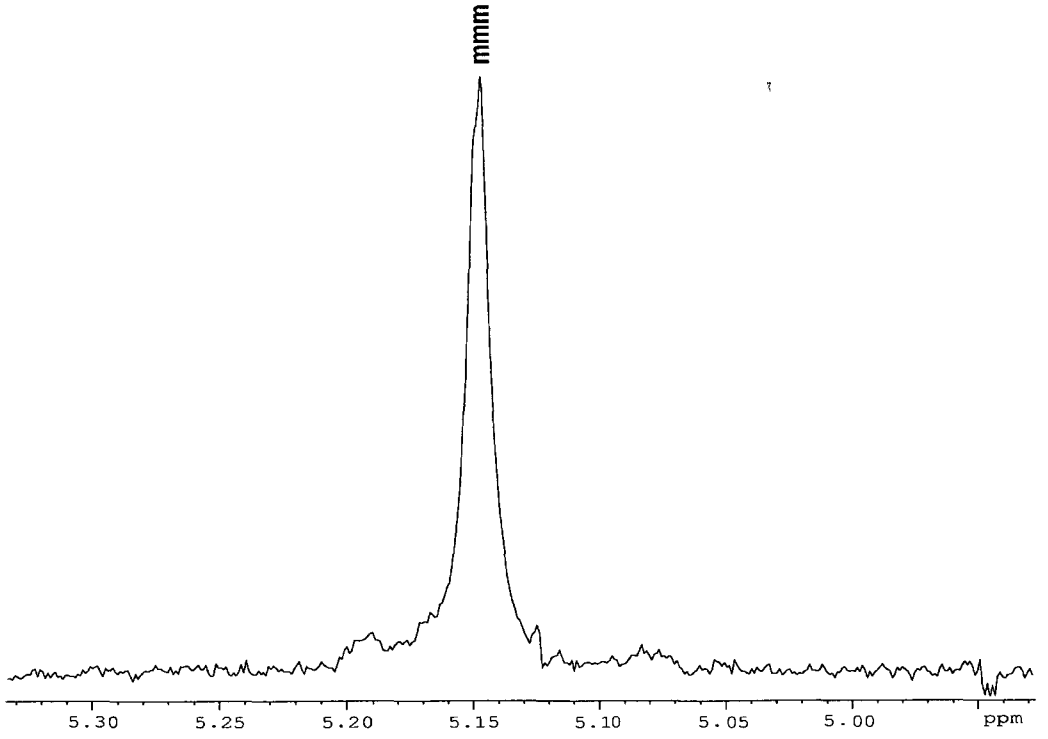

Figure 2.7. Methine region of decoupled ^{1}H NMR for isotactic-*L* PLA stars (IR-I).

From these Figures (2.4-2.7), the stereocontrol can be clearly observed.[19] The five stereosequences of atactic PLA derived from *rac*-lactide are shown in Figure 2.4. The relatively similar intensity of these peaks is a strong indication of the random character of the polymer chains, and it is worth noting that the most intense peaks are attributed to the mrm and the mmm tetrads. This indicates the propensity for this catalytic system to enchain two successive lactide monomers randomly, with roughly equivalent prevalence of the iso-enchainment (RRRR/SSSS) from mmm and the hetero-enchainment (RRSS/SSRR) from the mrm/rmr tetrads.

The heterotactic stars (Figure 2.5), synthesized utilizing the ^{Cl}[salan]AlMe catalyst (**2**), exhibit a strong presence of the rmr and mrm tetrads. Representing the RSSR/SRRS and RRSS/SSRR stereosequences, these two signals are indistinguishable by NMR spectroscopy.[76] Resulting from the alternating enchainment of lactide monomers, a condition imposed by the chain end control mechanism, the presence of these two tetrads in roughly equivalent intensity indicate the strong heterotactic bias of these polymer stars, which has been calculated to be 86%. This represents a decrease from the literature report (P_r = 0.96), but is a very appreciable retention of heterotactic bias at greatly elevated temperature in a vastly different reaction medium and in the formation of a multi-armed product. The more intimate monomer:catalyst interface under molten conditions, coupled with the increased thermal energy of the system can lead to insertions that are thermodynamically, rather than kinetically, driven.

The isotactic-enriched polymer stars also exhibit decoupled ^{1}H NMR spectra characteristic of high tacticity bias. Isotactic DPE-stars derived from *rac*-lactide possess the mmm tetrad (RRRR/SSSS) in high intensity with respect to the other possibilities (all other 4 possible tetrads for *rac*-lactide are observed for isotactic PLA polymers). Calculated to possess an isotacticity bias of 82%, the ^{tBu}[salen]AlMe catalyst retained a high capacity to enchain lactide

monomers in the same conformation. While this P_m value (0.82) also represents a decrease from the literature, this catalyst exhibits a better retention of stereocontrol at the higher temperatures.

When considering the differences between this reaction methodology and the conditions under which these Al-based catalysts have previously been screened, high retention of tacticity control is observed even at elevated temperatures with improved rates (21 h vs 16 h for >90% conversion with ^{Cl}[salan]AlMe) as a result of the elimination of solvent in the reaction process. Additionally, the issues associated with DPE solubility in traditional PLA polymerization solvents were solved, providing a method that may be expanded to application of these systems for other cyclic ester ROP processes including PLA-poly(glycolic acid) copolymers.

2.1.2 Thermal properties of DPE-PLA stars

Thermal characterization of the polymer stars was investigated by two methods, thermogravimetric analysis (TGA) and differential scanning calorimetry (DSC). Both of these techniques imparted valuable information about the thermal integrity and properties of these materials, as well as their suitability for applications, especially those requiring structural integrity at higher temperatures.

From investigations into the published literature, a severe lack of understanding of how molecular weight differences affect the observed thermal properties of star polymers of PLA is evident, and that the concept of utilizing stereocontrol to influence the thermal properties was largely unexplored.[183] To this end, a series of DPE-centred star PLAs of various tacticities were analyzed by TGA. These results are presented in Table 2.3 and Figure 2.8.

Table 2.3. TGA data for stereocontrolled DPE-PLA stars.[a]

Sample	Onset[b] (°C)	50%[c] (°C)	T_{max}[d] (°C)	ΔT_{decomp}[e](°C)
A-I	232.2	255.1	320.5	88.3
A-II	234.7	256.7	321.2	86.6
H-I	275.8	305.3	351.2	75.4
H-II	278.7	309.1	351.2	72.5
IR-I	274.5	306.2	375.5	100.6
IR-II	278.5	306.7	374.7	96.2
IL-I	275.2	302.2	350.0	74.8
IL-II	276.4	304.5	354.3	77.9

[a] Collection parameters: 10°C min^{-1} heating rate under N_2 atmosphere, 60 mL min^{-1} sample purge flow, 40 mL min^{-1} balance purge flow, on inert platinum pans [b] Onset of rapid thermal decomposition, [c] Measure of mass retention, [d] Maximum decomposition temperature, [e] Thermal decomposition window (T_{max}-T_{onset})

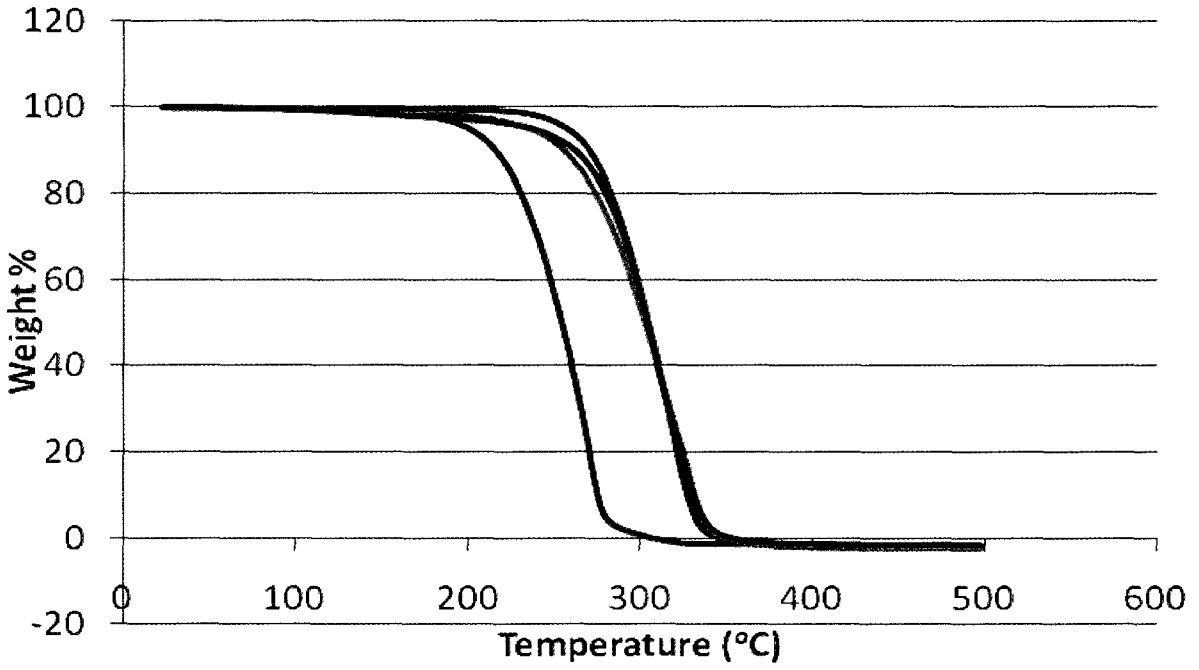

Figure 2.8. A TGA overlay of stereocontrolled DPE-PLA stars (blue-atactic, purple-heterotactic, green-isotactic-*rac*, red-isotactic-*L*).

The synthesized stars were analyzed by TGA, by a series of parameters as a means of thermal integrity evaluation. These included the onset temperature of rapid thermal decomposition, a measure of the initial stability of a polymer sample, and the temperature the material can reach without suffering any substantial thermal decomposition. From the data

presented in Table 2.3, the slight differences in molecular weight (M_n in Table 2.2) do not manifest in any clear trends; slight differences in M_n cannot be correlated to significant differences in the onset temperatures of the samples.

The effect that the introduction of stereocontrol has on the thermal onset temperature of these star polymers is clearly observable. The observed onset for atactic stars was ~ 232-234°C, but with an introduction of regularity to the polymer chains, an increase of ~40°C was observed. No large differences were observed for samples bearing the Ht, IR or IL designation, indicating that the presence of stereoerrors, or other non-desirable tetrads, has little effect on the decomposition temperatures; rather the onset is dictated by the presence of a dominant major tetrad component.

Similar trends are observed when examining the point of 50% mass retention, a measure of the samples resistance to thermal decomposition. Here we see little differences between samples possessing stereoregularity, but a ~50°C thermal enhancement over atactic samples. These data support the assertion that stereocontrol has a marked effect on enhancing the thermal stability of these PLA stars. Surprisingly the heterotactic stars exhibit similar onset temperatures to isotactic analogues, indicating that the rmr/mrm tetrads are not more susceptible to the onset of thermal decomposition than mmm tetrads.

The maximum decomposition temperatures reveal another major trend in the observed data. Here we see a greater than 30°C enhancement of the maximum thermal tolerance of the PLA stars bearing a heterotactic bias or an isotactic-*L* bias when compared to the atactic samples. These data support the conclusions regarding the onset and 50% data, namely that stereocontrolled tetrad sequences provide an improved resistance to thermal degradation. The isotactic-enriched stars derived from *rac*-lactide possess a greatly improved maximum thermal

lifetime when compared to the other stereocontrolled samples. An improvement of ~25°C over the heterotactic and isotacic-*L* samples indicates that some other phenomenon is at work. These stars may possess some stereocomplex behaviour, allowing for an enhancement of the maximum decomposition temperatures. By utilizing *rac*-lactide, a racemic mixture of *D*- and *L*-lactide, it is likely that polymer star arms bearing strong RRRR and SSSS character are being synthesized. The ability of these chains to form stereocomplexes with arms of adjacent macromolecules through intermolecular dipole-dipole interactions ($C{=}O^{\delta-}$---- $^{\delta+}H$-C and $C{=}O^{\delta-}$---- $^{\delta+}C{=}O$), lends improved stability to the polymer matrix. This effect is manifest in the T_{max} values because, if the thermal decomposition follows the intramolecular back-biting mechanism,[224,225] these stereocomplex regions may improve thermal stability even if the arms are excised from the core acting as more traditional linear polymers.

Finally, the decomposition window provides additional information on the material properties of these star polymers and the properties that the introduction of stereocontrol provides. The heterotactic and isotactic-*L* stars exhibit the smallest decomposition windows, a result that is expected because of the improved onset stability provided by stereocontrol, coupled with an absence of stereocomplex behavior. The atactic and isotactic-*rac* samples possess the greatest decomposition windows, but for different reasons. The larger ΔT_{decomp} windows for atactic stars can be attributed to the effects of the random polymer arrangement. The lack of a predominant stereosequence(s) in these samples prevents any synergistic effects from occurring, leading to a lower than projected onset. For the isotactic-*rac* samples, the stereocomplex behaviour that results in an enhanced T_{max} of these samples also provides a lengthening of the decomposition window.

Comparisons of star polymers to linear systems will always reveal a decrease in the thermal properties at face value. The factors affecting the depression of these thermal properties are well-known.[226] The presence of more end-groups, less tight packing structures resulting in decreased crystallinity, and an interruption of thermally induced crystallizations are all factors limiting the thermal resistance of PLA stars. The number of chain ends is an especially important factor because the last monomer unit of the polymer chain has been found to be the most susceptible to degradation by the transesterification mechanism, and chain end-scission is the dominant degradation mechanism.[227]

With these factors considered, stereocontrol has emerged as a legitimate option in recovering some of the thermal stability lost in the switch to the more complex macromolecular structure. The ability to synthesize star PLA polymers from lactide with isotactic and heterotactic biases, reported here for the first time, has improved the properties of these materials making them comparable to atactic linear PLAs.

Amorphous PLA from NatureWorks with an M_n of 7000 Da has a thermal decomposition onset above 350°C and a T_{max} of ~410°C. Isotactic stars synthesized from *rac*-lactide in this project have recovered ~35% of the loss in onset temperature and ~61% in the maximum decomposition temperature when switching from the linear to star architectures.[228]

Investigations into the thermal decomposition products of PLA have been completed,[229] and the residual matter from TGA is a variety of organic pyrolysis products including lactide monomer, other PLA ring-formed oligomers, CO_2, CO, acrylic acid, methane, ethylene, propylene, methylketene, acetaldehyde and butane-2,3-dione. Typical residual matter for TGA analyses in this project revealed pyrolysis products constituting <4% of the sample mass.

These star-shaped PLAs were also investigated by DSC, which allowed for analysis of the polymer properties of these materials, and subsequent understanding of the effects of stereocontrol on multi-armed macromolecules. These results are summarized in Table 2.4.

Table 2.4. DSC data for stereocontrolled PLA stars.[a]

Sample	T_g (°C)	T_m (°C)	T_c (°C)	X_c [b](%)
A-I	39.9	-	-	-
A-II	37.3	-	-	-
H-I	41.5	-	-	-
H-II	41.5	-	-	-
IR-I	43.7	114.5, 134.4	-	22
IR-II	43.3	122.4, 133.7	-	34
IL-I	48.3	131.9, 142.9	96.9	30
IL-II	47.7	127.4, 141.9	84.2	43

[a]Collection parameters: 5°C min^{-1} heating and cooling rates, 50 mL min^{-1} N_2 sample purge in hermetically sealed aluminum pans [b]Calculated from $\Delta H_m°$ of crystalline P*L*LA 93.1 J g^{-1}

The polymers were analyzed according to the thermal transitions that they possess, including the glass transition temperature (T_g), the melting temperature (T_m), the crystallization temperature (T_c) and the percent crystallinity (X_c) of the polymer samples.

Glass transition temperatures measure the point at which a polymer material softens. At and above this temperature the polymer chains have enough thermal energy to slide over one another, representing a shift in material consistency from a glass-like material to a rubber-like one. While no actual change in state is observed (a polymer remains a solid above the glass transition temperature), the solid matrix moves from the rigid arrangement associated with glass materials to a freer association of the chains, akin to a rubber material. Indicating an increase in the latent heat capacity of the material, the T_g is associated with an endothermic process.[230] T_g values for the synthesized stereocontrolled stars are shown in Figure 2.9.

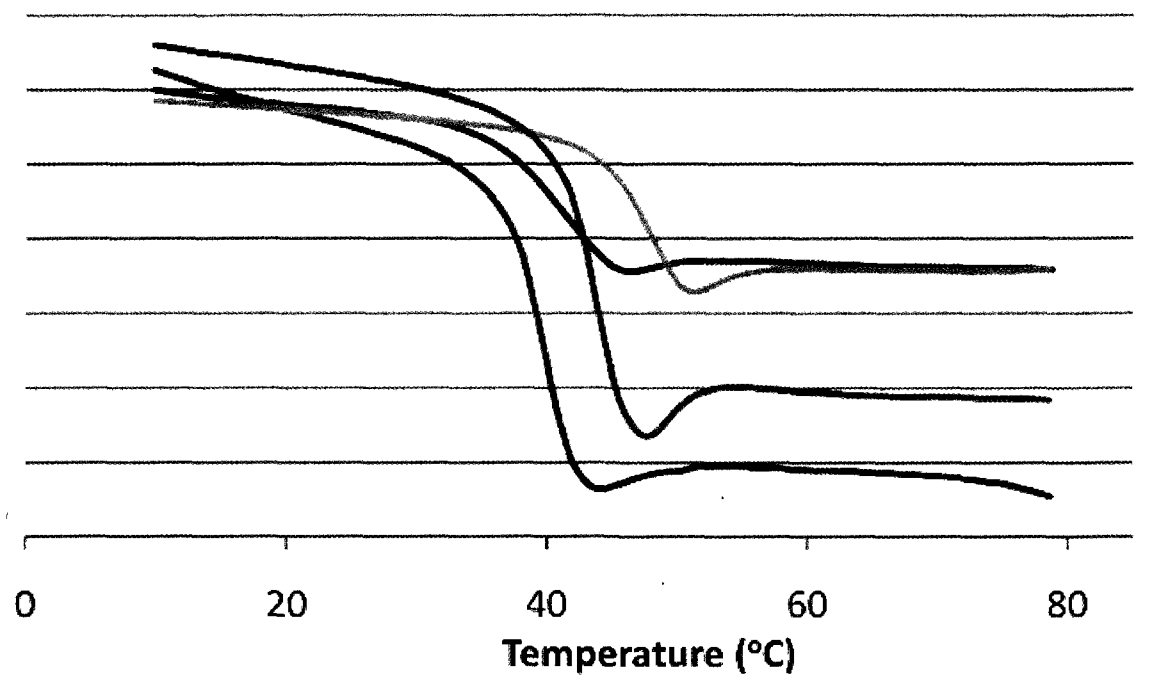

Figure 2.9. A DSC overlay of T_g values of stereoncontrolled stars, blue-atactic, red-heterotactic, purple-isotactic-*rac*, green-isotactic-*L* with y-axis (Heat flow W/g), removed for clarity of comparison.

From the data obtained, stereocontrol is observed to have a considerable effect on the T_g values of star PLA polymers. While the T_g of atactic samples is consistently lower than 40°C (~37-40°C), an increase is observed for the stereocontrolled samples, trending as expected and in line with their linear analogues. Heterotactic PLA stars possessed T_g values of 41.5°C and isotactic-*rac* samples showed an improvement to >43°C. The largest improvement of glass transition temperature was with isotactic-*L* samples, a trend that would be expected from looking at linear systems. The lack of stereoerrors has the effect of improving thermal properties in these samples, to the point where T_g values of ~48°C were achieved for these samples. When compared to the published results for linear PLAs,[199] a decrease in both the T_g values and the T_m values is observed, a trend established in PLA star chemistry.[183] The atactic stars synthesized

possess T_g values similar to those reported in the literature, and exhibit a depressed T_g when compared to linear PLAs.[199,231]

Atactic PLA possesses a T_g value of ~53°C, while purely isotactic P*L*LA possesses T_g values up to 65°C.[61] While our samples exhibit depressed T_g values, the inclusion of stereocontrol improves our T_g values to within 74% of linear systems of similar M_n. Lack of consistency between literature reports makes comparisons difficult, but the isotactic-*L* stars show similar properties to DPE-centred stars of comparable molecular weight.[195]

Melting temperatures of PLA remain an interesting area of study for both linear and star architectures. For a polymeric material to possess a distinct melting signal it must contain some crystalline domains, and so atactic PLA samples do not exhibit a melting transition. Heterotactic PLA has remained the most frustrating of microstructures for material scientists. Calculations of the microstructure indicate that it should possess the crystalline domains necessary to have melting transitions, but this curious microstructure does not exhibit them.[232] Our studies were in line with existing research indicating an absence of melting signals for heterotactic PLA.

The melting signals of isotactic samples were obtained and two signals were observed for these star polymers, consistent with other published reports (Figure 2.10).[233-235] An enhancement of the main melting value for star-PLAs with an isotactic-*L* bias was measured, typically ~10°C over isotactic-*rac* analogues. Additionally, the minor melting signal shows similar improvement but conclusive trends cannot easily be drawn, as the melting signal differential changes variably between the isotactic stars. In a general sense, our studies indicated a greater separation between the minor and major melting signals for isotactic PLA stars derived from *rac*-LA.

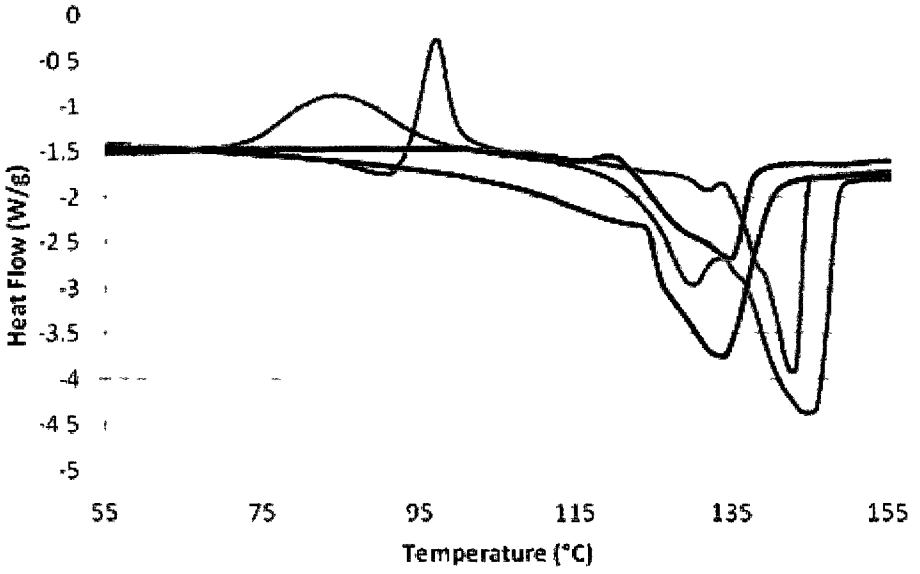

Figure 2.10. A DSC overlay of PLA stars (T_m and T_c illustrated), purple-isotactic-*rac* stars, green-isotactic-*L* stars.

An additional phenomenon observed with the isotactic-*L* stars is the presence of a crystallization temperature, (T_c). This crystallization temperature is the value at which the polymer sample possesses enough thermal energy to undergo a rearrangement to a more favourable orientation. This favourable orientation involves the crystallization of the polymer, a process that is associated with an exothermic release of heat energy. The higher crystallinity of the isotactic-*L* samples allows this rearrangement to occur. The values of our selected T_cs, 96.94°C and 84.19°C, indicate a disparity between the values, a difference that can be affected by precipitation of the polymer from the molten state.[236] Rapid cooling from this disordered molten state will result in a thermodynamically derived crystalline domain that is not as closely packed as kinetically derived domains derived from slower precipitation. The rate of this precipitatory cooling has been found to affect the position of the T_c.[236]

Additional key thermal information was calculated from DSC. This included the percent crystallinity (X_c) of the synthesized star polymers. Since this calculation requires a discernable

melting temperature, it is only applicable to the isotactic PLA stars. The X_c values for the samples were calculated from the following equation (Figure 2.11).

$$X_C = \left(\frac{\Delta H_m - \Delta H_c}{H_m^\circ}\right) \times 100$$

Figure 2.11. Formula for percent crystallinity (X_c) where ΔH_m and ΔH_c are the heats of melting and crystallinity, ΔH_m° is the standard heat of melting for P*L*LA (93.1 J g^{-1}).

While the values of X_c for linear PLA polymers increase when comparing isotactic-*rac* vs. isotactic-*L* systems, the more irregular packing arrangement of polymer stars minimizes these differences. There were similar observed percent crystallinities for isotactic PLA stars and additional experimentation revealed that the averages of these samples tended towards 30% for isotactic-*rac* samples and upwards of 40% for isotactic-*L* samples.

The disparities in these reported X_c values is indicative of the highly variable crystallization nature of PLAs. Numerous factors have been found to affect the crystallization temperatures and the percent crystallinities. Annealing above the glass transition temperature, rate of thermal quenching, M_n and the presence of nucleating agents have all been found to have effects on the resulting crystallization properties of PLAs.[237] The quenching of samples from an elevated temperature (120°C), the rate of quenching, the temperature of the MeOH precipitating solution and the variable possible nucleating agents (catalyst and unreacted monomer) all contribute to our observed crystallization properties.

Finally, the materials properties of these samples were analyzed by powder X-ray diffraction. Loose powder samples were analyzed on inert glass substrates, the results of which are summarized in Table 2.5. This technique was employed as a method of further confirming conclusions with respect to the high tacticity bias of stereocontrolled stars. The diffraction

angles, crystallite size and d-spacing of the samples were analyzed (Table 2.5). These diffractograms can be observed in Figures 2.13-2.16.

Table 2.5. Powder-XRD data for stereocontrolled PLA stars.[a]

Sample	Angle of Diff. (°)	Crystallite Size[b] (nm)	d-spacing (Å)
A-I	-	-	-
A-II	-	-	-
H-I	-	-	-
H-II	-	-	-
IR-I	16.9	178	5.2
IR-II	16.9	160	5.2
IL-I	16.9	169	5.2
IL-II	16.8	188	5.3
rac-lactide	11.5	-	7.7

[a] Collected as loose powder on glass substrate, θ-2θ mode, 2-60° [b] Calculated from Scherrer equation for determination of crystallite size

The amorphous character of atactic and heterotactic samples is revealed through the lack of clear diffraction peaks. These samples exhibit the broadened, featureless spectra characteristic of amorphous materials.[238] The atactic and heterotactic pXRD data differed in the onset of the amorphous features. The location of the 'hump' is indicative of differences in the composition of glassy-materials.[239] The pXRD of the amorphous and heterotactic samples contrast with the isotactically-enriched samples which possess a clear diffraction signal at ~16.9 degrees. The confirmation of this peak as belonging to PLA was achieved through analysis of the diffraction qualities of both core and monomer.

The crystallite size of the samples was calculated by the Scherrer equation (Figure 2.12), where τ, the crystallite size in nm, is equivalent to K, the featureless shape form factor (0.9) multiplied by the wavelength of radiation from the X-ray source divided by β, the line broadening (radians) at half the maximum intensity multiplied by the cosine of the Bragg diffraction angle (θ).

$$\tau = \left(\frac{K\lambda}{\beta \cos\theta}\right)$$

Figure 2.12. Scherrer equation for crystallite size determination.[240]

From this equation, the crystallite size in nanometers was calculated and found to be in the range of 160-190 nm for all isotactic samples, providing further evidence of the similarity in microstructure between the isotactic-*rac* and isotactic-*L* samples (Table 2.5). Additionally, the d-spacing, the interlayer spacing of the material, is consistent throughout the isotactic samples. Representative pXRD patterns for the isotactic-*L*, isotactic-*rac*, atactic and heterotactic stars can be seen in Figures 2.13-2.16 respectively.

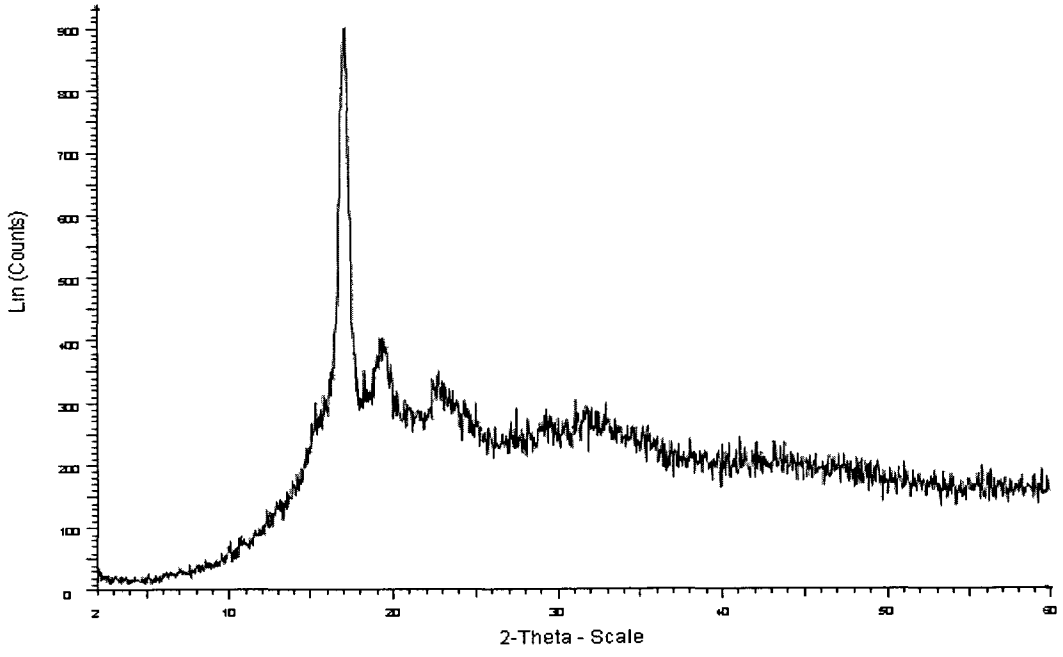

Figure 2.13. pXRD pattern of isotactic-*L* DPE-PLA stars.

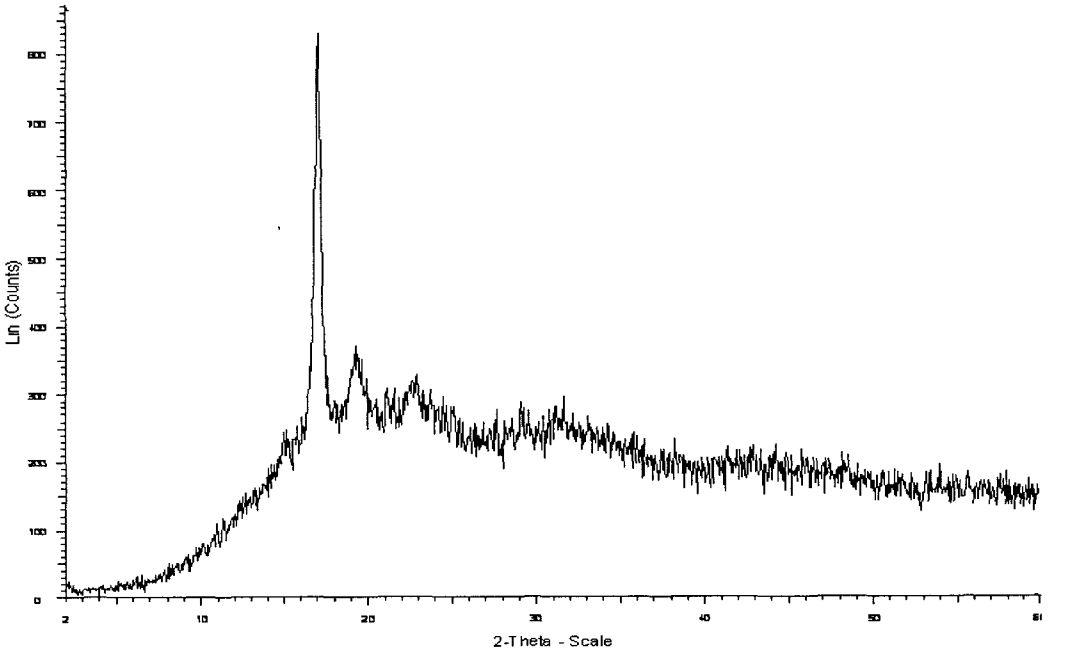

Figure 2.14. pXRD pattern of isotactic-*rac* DPE-PLA stars.

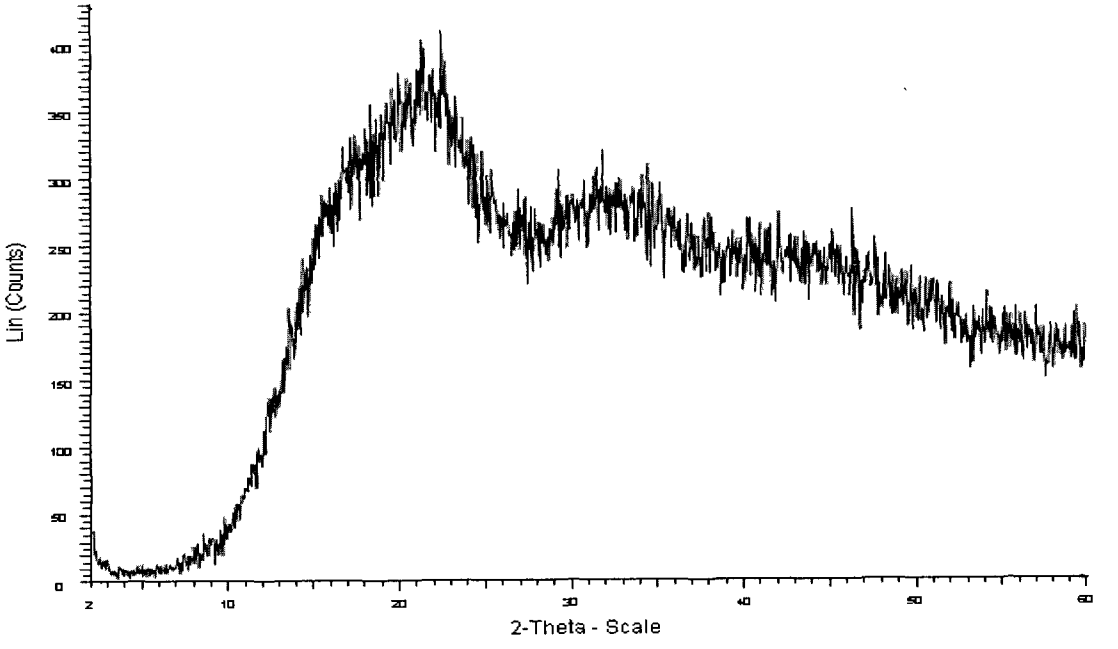

Figure 2.15. pXRD pattern of atactic DPE-PLA stars.

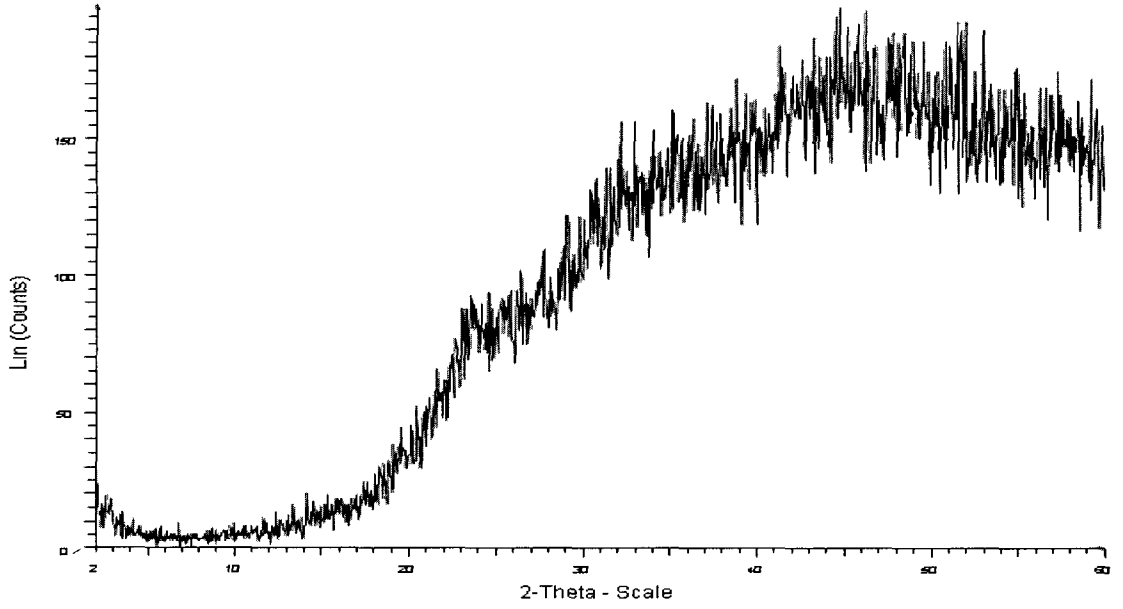

Figure 2.16. pXRD pattern of heterotactic DPE-PLA stars.

2.1.3 Degradation of DPE-PLA stars

Apart from a thorough materials characterization, the stereocontrolled PLA stars were also examined for solution properties, specifically hydrolytic degradation. PLA stars have previously been investigated for resistance to hydrolytic degradation, but a systematic investigation of the effect of stereocontrol on the degradation profiles of stereocontrolled stars has not been reported.[183]

The degradation of these materials follows the uptake of solvent (in our case methanol), followed by hydrolysis of the ester linkages. There are many factors that affect the rate of hydrolysis, including the pH of the solution, crystalline phase, molecular architecture, molecular weight and stereomeric composition.[241]

The pH is an important consideration because hydrolysis may occur under both acidic and basic conditions. Our investigations into the degradation of PLA stars employed basic

conditions. Although there is open debate concerning the site of hydrolysis, chain-end scission vs. random scission, the mechanism is thought to follow an activated intramolecular transesterification mechanism (Figure 2.17).

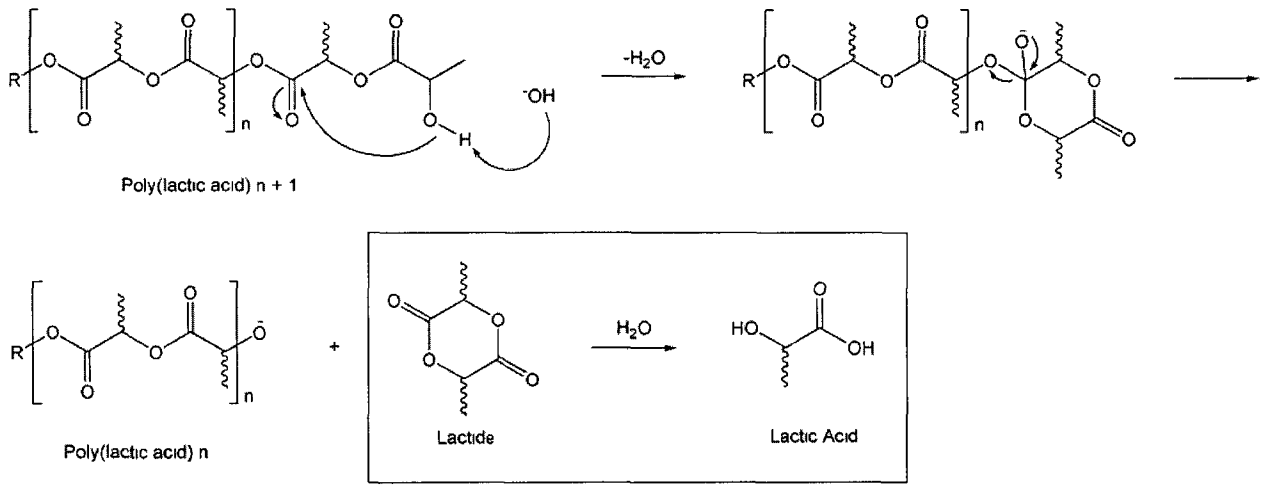

Figure 2.17. Base-catalyzed intramolecular transesterification 'back-biting' mechanism.

This proposed mechanism is similar to that of transesterification for polymerization catalysts. The presence of the base, (OH^-), increases the nucleophilicity of the terminal oxygen, promoting the back-biting mechanism of nucleophilic attack on the second carbonyl group and leading to the formation of a stable six-membered ring. This ring is lactide, produced in conjunction with an oligomeric PLA segment. The lactide is not usually detected as its solution lifetime is quite short (the monomer quickly degrades to lactic acid), however end-group modification has confirmed the role of the hydroxyl end-group in alkaline degradation studies.[241] Studies have also revealed that factors such as hydrophobicity and dielectric constant play a key role in the degradation rates of PLAs.[241]

An increase of pH within the P*L*LA matrices has been observed when accompanied by increases in the degree of degradation.[241] This has been attributed to an increase in the number of COOH groups within the matrix and also an accumulation of water/methanol soluble low

molecular weight degradation products. Conclusions drawn from these data indicate that, in a degradation study performed at physiological pH (7.365), the rate of degradation should decrease until it effectively stops at a pH of 3-4. Countering this is a positive change in the hydrophilicity of the matrix, resulting in an increased dielectric constant. This increase in dielectric constant will result in an increase in the degradation rate. Low dielectric constant organic solvents have been shown to stabilize the PLA 'ground state' while discouraging the transesterification transition state.[241] Improved hydrophobicity protects the highly susceptible endgroups from exposure to the degradation solution, similar to biological micelles. The simple observation that PLA samples degrade completely in solution indicates that the increase in hydrophilicity has a greater impact on degradation kinetics than the decrease in pH.

Crystallinity of PLA plays a key role in the degradation rates of PLA samples, as amorphous and semi-crystalline samples have been found to degrade through different pathways.[241] Amorphous PLA degradation, similar to the atactic and heterotactic stars, is thought to proceed heterogeneously, with faster internal rates of degradation than surface kinetics. This is believed to occur because of a larger contribution from auto-catalysis, the ability of carboxylic acid groups to degrade the polymer chain. In these samples, the initial degradation through hydrolysis of the ester bonds proceeds homogeneously throughout the matrix. The switch to a heterogeneous effect is the result of two factors. These are the increase in COOH terminal groups which are known to autocatalyze, and the ability of soluble oligomers to escape from the matrix before they are fully degraded. Motility of these oligomers from the surface is contrasted with the entrapment of oligomers in the core of the sample, a phenomenon which leads to a lowering of the pH at the core, which in turn leads to an accelerated degradation rate, dominated by the acid-catalyzed degradation mechanism.

Degradation of semicrystalline PLA samples, such as the isotactically-enriched stars is thought to proceed by a two-step process.[255] In the initial stage, water diffuses into the amorphous regions of PLA, resulting in random scission of ester bonds. This destruction of the amorphous domains has been shown to increase the overall crystallinity of the PLA samples.[242] A retardation of the rate of degradation has been observed in the amorphous regions through the formation of a crystalline phase of an oligomeric stereocomplex intermediate.[243] This stereocomplex intermediate, arising only in P*DL*LA samples has been found to be highly resistant to hydrolysis. After most of the amorphous character has been degraded, the hydrolysis intensifies, from occurring solely at the surface of the crystalline domains to degrading the centre of the domain.

The molecular architecture has also been found to affect degradation rates. Hyperbranched and dendritic PLAs present a much higher concentration of terminal hydroxyl groups than linear analogues of comparable molecular weight. If the hydrolysis predominantly occurs through the chain-end scission mechanism, this will allow for an enhancement of the degradation rate. Star polymers, while not possessing the type of hydroxyl functionality observed with hyperbranched systems, provide an increase of endgroups over linear systems, and are therefore expected to have, and exhibit, increased degradation kinetics vs. linear PLAs.

The molecular weight of linear PLA is also capable of profoundly affecting the degradation rates. Increases in molecular weight are observed to cause a slowing of the degradation rates, an outcome that can be explained by a decrease in the number of highly susceptible terminal groups, when compared to lower molecular weight samples with the same mass.

Finally, the stereospecificity of the polymer chains can also have a profound effect on the degradation rates. The introduction of an isotactic bias into the polymer chain can enhance the resistance to degradation through an increase in the crystallinity of the polymer sample. An isotactic P*DL*LA sample can have a much faster degradation rate than a P*L*LA sample simply because of the enhanced crystallinity. The results of our stereocontrolled PLA samples exposed to the degradation solution are summarized in Table 2.6.

Table 2.6. Degradation lifetimes of PLA samples of various tacticities.

Sample Bias	Lifetime (min)	Standard Deviation (min)
Atactic	20.5	0.5
Heterotactic	23.0	0.5
Isotactic-*rac*	58.5	7.5
Isotactic-*L*	175.5	8.5

In a typical experiment, samples of polymer were pressed into thin pellets (d = 1.3 cm, m = 200 mg) under 2000 psi. The pellets were exposed to a solution of 1,5,7-triazabicyclo[4.4.0]dec-5-ene (TBD) in methanol (4.34×10^{-2} M, pH = 12.85). The samples were agitated at 23°C and monitored until all PLA had dissolved. The resultant solution contents were then analyzed by ^{1}H NMR spectroscopy to reveal oligomeric PLA chains.

From these data it is clear that the inclusion of stereocontrol has a profound effect upon the lifetime of these stars. Atactic star samples possessed an average lifetime of 20.5 minutes, while heterotactic stars had a slightly improved lifetime of 23.0 minutes. The greatest enhancement of solution stability resulted from the introduction of an isotactic bias. Isotactic samples derived from *rac*-lactide exhibited lifetimes averaging 58.5 minutes, while isotactic-*L* samples persisted in solution for an average of 175.5 minutes. From these data several conclusions can be drawn.

Firstly, the amorphous character of the atactic and heterotactic samples played a key role in their shorter lifetimes. The presence of these amorphous domains resulted in quicker uptake of the TBD solution into the polymer matrix, which allowed increased COOH auto-catalyzed scission to occur at the core of the polymer samples.[241] The morphology of heterotactic PLA does not differ greatly from atactic samples, and while the heterotactic PLAs possessed a strong bias for the mrm and rmr tetrads, these stereosequences did not afford the sample any great enhancement of lifetime. These results indicate an increased susceptibility of racemic linkages to the scission mechanism.

The noticeable enhancement of lifetime for isotactically-enriched samples can be attributed to their semicrystalline nature. The presence of crystalline domains retarded the uptake of the degradation solution and provided enhanced solution stability to these samples. The strong bias for the mmm tetrad plays a key role in this enhanced crystallinity and the consequent enhancement of lifetime. These trends are observed in Figure 2.18.

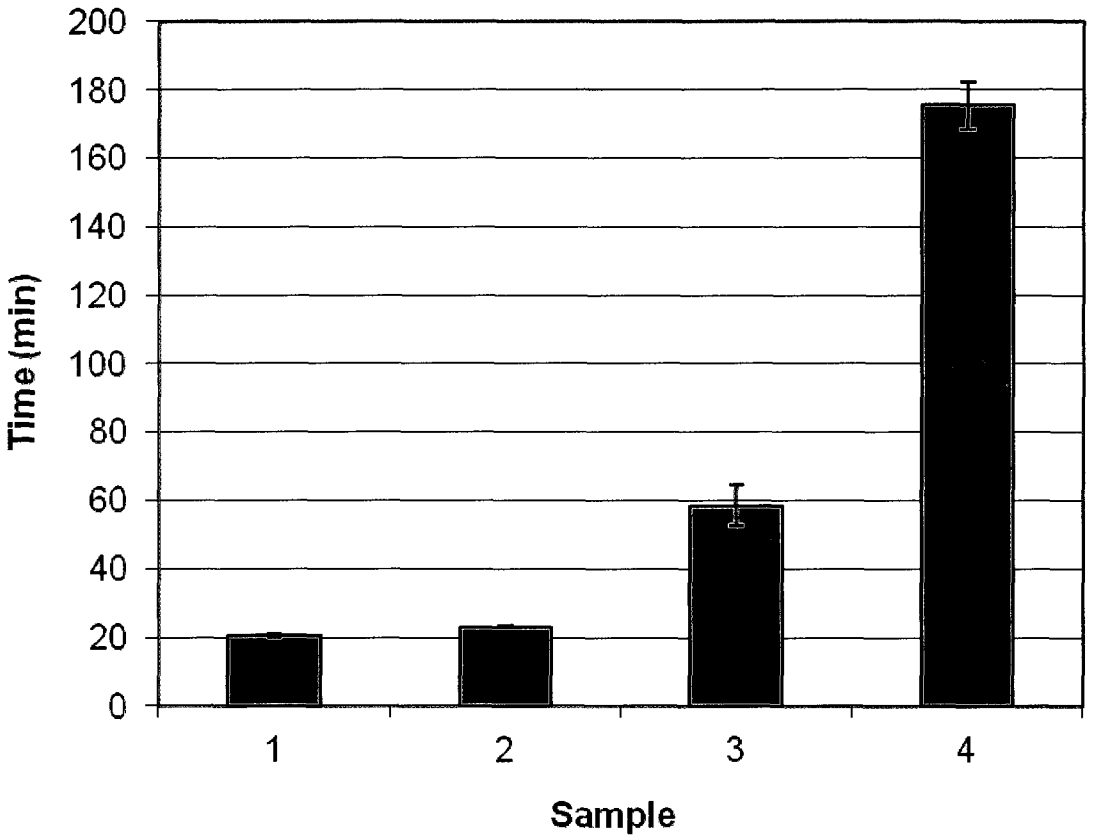

Figure 2.18. Bar graph illustrating the lifetimes of stereocontrolled samples with error bars indicating the standard deviations (Table 2.6). Samples 1 (atactic), 2 (heterotactic), 3 (isotactic-*rac*), 4 (isotactic-*L*). n = 4

The other prominent factor in this study was the effect of molecular weight. While known to affect the rates of degradation of PLA samples, it has not been fully quantified for stereocontrolled star PLAs. From these data, little effect of molecular weight on atactic and heterotactic samples is observed. This is attributed to the amorphous character of these samples dominating the effects of M_n. The morphology of these samples allows for such a rapid uptake of the degradation solution that slight differences in M_n were not discernable by these methods. However an effect of molecular weight on degradation rate for the isotactic samples was observed.

Preliminary results for the degradation of PLA samples yielded ranges of lifetimes. These were found to be 51 to 66 minutes for isotactic-*rac* samples and 167-184 minutes for isotactic-*L* samples. These results, while not relatable to physiologically relevant conditions still provide valuable information on the effect of stereocontrol on the sample lifetimes. Observing slight differences in the molecular weights, experiments were undertaken to decipher the relationship between solution lifetimes of samples bearing the same isotacticity bias but different molecular weights. These results for isotactic-*rac* and isotactic-*L* samples are illustrated in Figures 2.19 and 2.20.

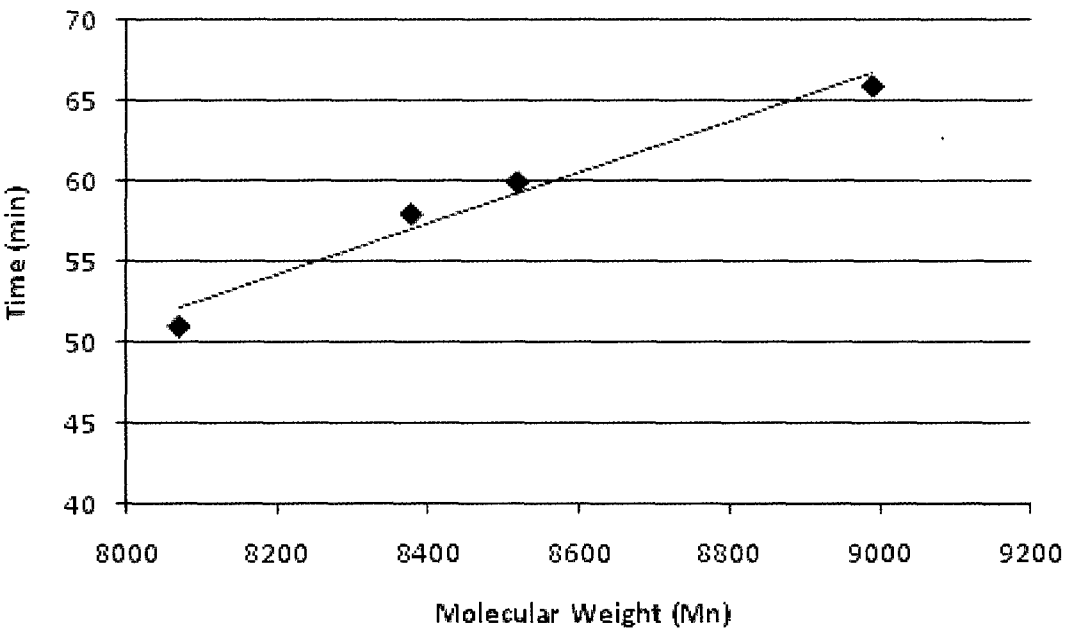

Figure 2.19. Relationship of M_n and solution stability for isotactic-*rac* DPE-PLA stars.

The linearity of Figure 2.19 was calculated to be high (R^2 = 0.97), indicating a strong correlation between the time required to fully degrade vs. molecular weight (M_n) of isotactic-*rac* samples. This accounts for the large variance observed in the lifetimes of isotactic-*rac* pellets (Table 2.6).

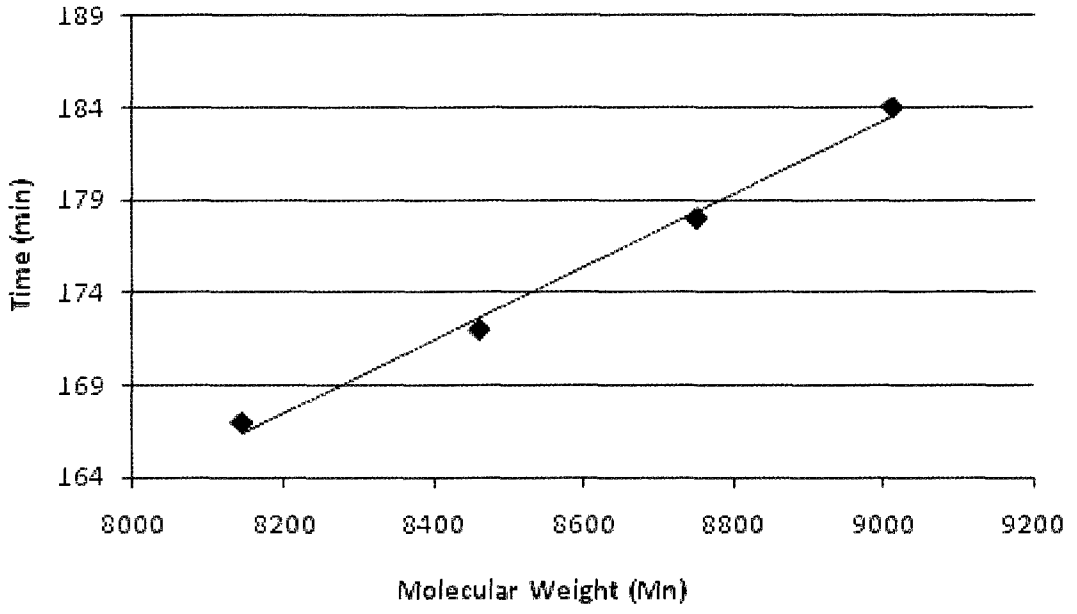

Figure 2.20. Relationship of M_n and solution stability for isotactic-*L* DPE-PLA stars.

The linearity of Figure 2.20 was also very high ($R^2 = 0.99$), indicating strong correlation. From these data we can see that there is a strong linear relationship between the lifetimes of isotactic-*L* samples and the molecular weight of the polymer star. The legitimacy of the degradation values were examined through quadruplicate analysis of pellets. For the isotactically biased samples that were investigated at various molecular weights, quadruplicate analysis was also employed.

2.2 Isotactic-enriched DPE-PLA stars of longer arm lengths

There are concerns that the striking differences noted in the PLA star thermal data could be attributed strictly to differences in molecular weight. A typical M_n of ~8700 is sometimes considered too low to properly assess the materials properties. To alleviate these concerns, isotactic-*rac* and isotactic-*L* samples of significantly larger molecular weights were synthesized to determine the accuracy of the method. Possessing a theoretical arm length of 50 monomer units, these experiments proved an interesting study in the initiation efficiency of our system and arm length uniformity it provided. These results are presented in Table 2.7.

Table 2.7. Polymer properties of isotactic-rac$_{50}$ and isotactic-L$_{50}$ DPE-PLA stars.

Sample	$M_{n,GPC}$	$M_{n,th}$	PDI	PDI_{arm}	P_m(%)
Isotactic-*rac*	41403	43038	1.16	2.10	86
Isotactic-*L*	40726	42754	1.08	1.60	100

Initial attempts at preparing these higher molecular weight stereocontrolled stars revealed the limitations of this solvent-free synthetic methodology. While highly efficient for the synthesis of stars with oligomeric arm lengths, this system proved incapable of synthesizing the longer armed stars. Preliminary results for neat polymerizations at 120°C revealed improper initiation of the DPE system, resulting in broad PDI values accompanied by inconsistent molecular weights.

This was remedied by returning to a solvent-based polymerization, utilizing toluene at 70°C. This proved successful in synthesizing DPE-centred isotactic stars with controlled polymer properties, albeit at longer reaction times.

A close correlation between GPC-determined M_n and the theoretical M_n was observed, especially considering the tendency of size exclusion chromatography techniques to underestimate the molecular weights of star polymers.[244] While this effect becomes more

pronounced at the higher molecular weights, there is still sufficiently good correlation between the values. The PDI values of these stars were also quite narrow, indicating uniformity of the molecular weight distribution. As a measure of dispersity, the PDI of the arms was calculated to be 2.10 and 1.60 for isotactic-*rac* and isotactic-*L* stars respectively. These values are an improvement over those observed for the polymer stars bearing arms of 10 monomeric units in length. Unfortunately, conclusive statements concerning the accuracy of these differences cannot be made because of the dominant effect that star molecular weight has on the calculation. Confirmation of the uniformity of the polymer star arms in these instances could not be obtained without the aid of GPC equipped with triple detection, capacity that we do not currently possess. However, it can be conclusively surmised that all hydroxyl functionalities of DPE have been initiated, from the disappearance of DPE-core CH_2 peaks in the ^1H NMR spectrum of these star polymers (δ: 4.15 vs. 3.38 ($OCH_2C(CH_2)_3$ and δ: 3.34 vs. 3.31 (OCH_2)). The conversion of these polymerizations remained high (>90%) and the isotacticity bias of the ^{tBu}[salen]AlMe catalyst (0.86) was improved over the solvent free results, more accurately representing the known P_m value of 0.88.[155]

These enlarged stars were exposed to the same characterization techniques as the lower molecular weight stars, TGA, DSC and pXRD. Significant changes in the thermal properties of the DPE-PLA stars with an increase in the molecular weight were observed. These results are summarized in Table 2.8.

Table 2.8. Materials properties of isotactic-rac_{50} and isotactic-L_{50} DPE-PLA stars.

Sample	T_g (°C)	T_m (°C)	T_c (°C)	T_{onset} (°C)	T_{max} (°C)	Degrad. (min)
Iso-rac_{50}	61.3	185.8	-	316.8	375.7	475
Iso-L_{50}	63.4	165.1	107.1	290.8	362.4	1266

The analysis of these samples corroborated trends that have been reported with respect to star PLA chemistry.[183] An increase in the molecular weight of the samples revealed an enhancement of the T_g values by DSC. The increase from ~43.5°C to >61°C illustrated the effect that an increase in M_n has on the thermal properties. A roughly 5-fold increase in molecular weight resulted in an 18°C (42%) increase in T_g for isotactic-*rac* stars. Similar enhancement was shown for isotactic-*L* stars, where a 5-fold increase in molecular weight increased the T_g values from ~48°C to 63°C (31%).

A similar trend is observed for the melting temperatures of these higher molecular weight stars. There is an increase of ~25°C (18%) in the melting temperature of P*L*LA DPE-stars with an increase of M_n from 8700 to 42000. While this trend can be attributed to the widely established correlation between M_n and melting temperatures, the results for iso-rac_{50} samples cannot. Here an improvement in the melt stability of >50°C is observed, which cannot be explained by simple increases in M_n alone. If this were the case the melting temperature should still remain below that of P*L*LA stars, however there is an enhancement of this value to a melt temperature that exceeds that observed for purely isotactic stars derived from *L*-lactide. We believe the reason for this is the ability for these iso-rac_{50} stars to exhibit stereocomplex behaviour, as previously explained in this chapter (Figure 2.21).

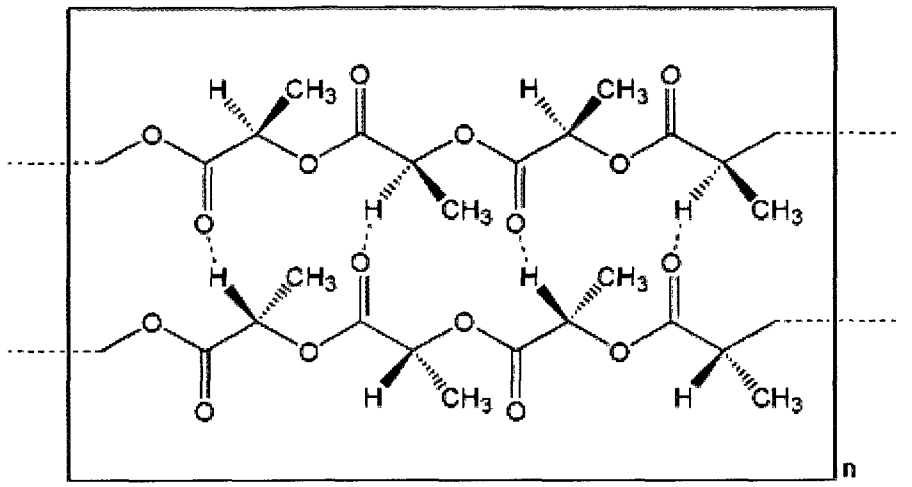

Figure 2.21. Stereocomplex behaviour (dipole-dipole ineratctions), of two linear PLA arms (P*D*LA and P*L*LA).

Similar to the phenomenon observed in the TGA of isotactic-*rac* samples, the presence of longer chains of PLA that could possess alternating arrangements allow for the presence of stereocomplex PLA. This stereocomplex, predominantly driven by the intermolecular hydrogen bonding between the oxygen atoms of C=O groups and the C-H methine protons on the polymer backbone, is known to greatly enhance the thermal properties of a PLA material.[34] While the greatest enhancement is shown to occur at 50:50 mixtures of P*D*LA and P*L*LA, a significant improvement in properties can be observed even at small P*D*LA compositions. The enhanced properties that this intermolecular complex affords can reasonably result in the increased melt resistance that we have observed.

This stereocomplex behaviour is also observed in the TGA analysis of these stars. An enhancement of the thermal stability of these larger stars is to be expected, and improved stability with an increase in M_n for the isotactic-L_{50} stars is shown. In agreement with our other results, a greater than expected enhancement of the thermal stability for the isotactic-rac_{50} stars is observed by TGA analyses (Figure 2.22). The DSC analyses of these elongated stars is shown in Figures 2.23 and 2.24.

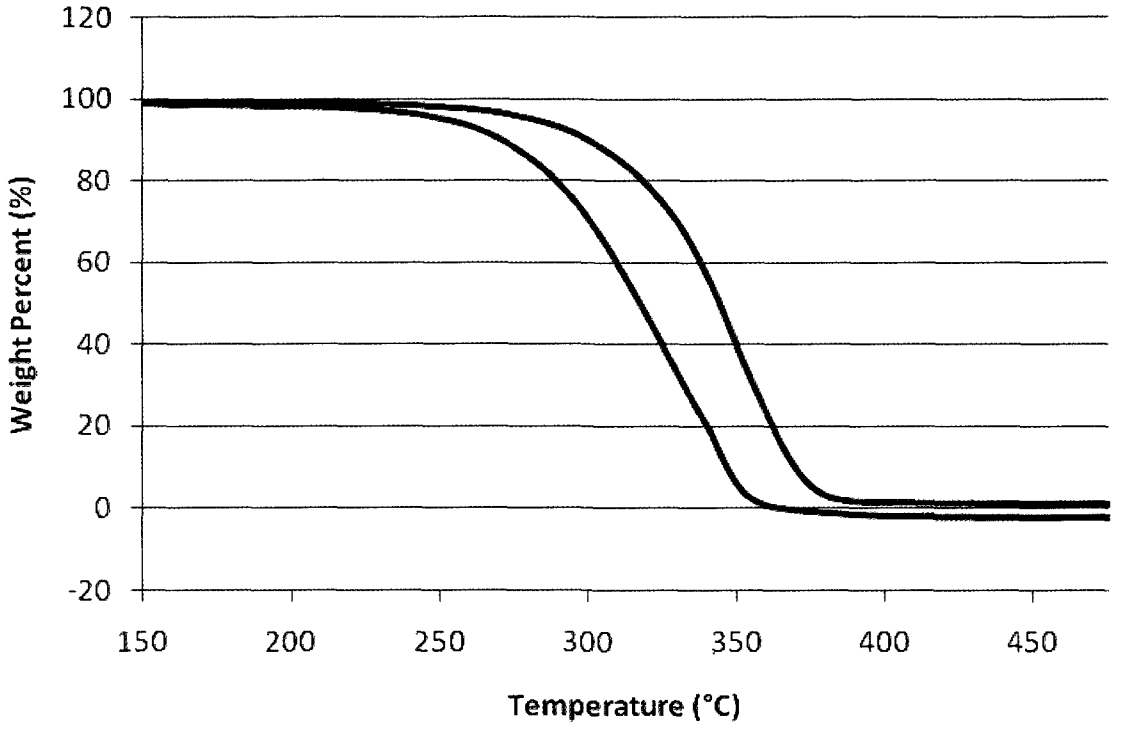

Figure 2.22. A TGA overlay of isotactic-L_{50} (red) and isotactic-rac_{50} (blue).

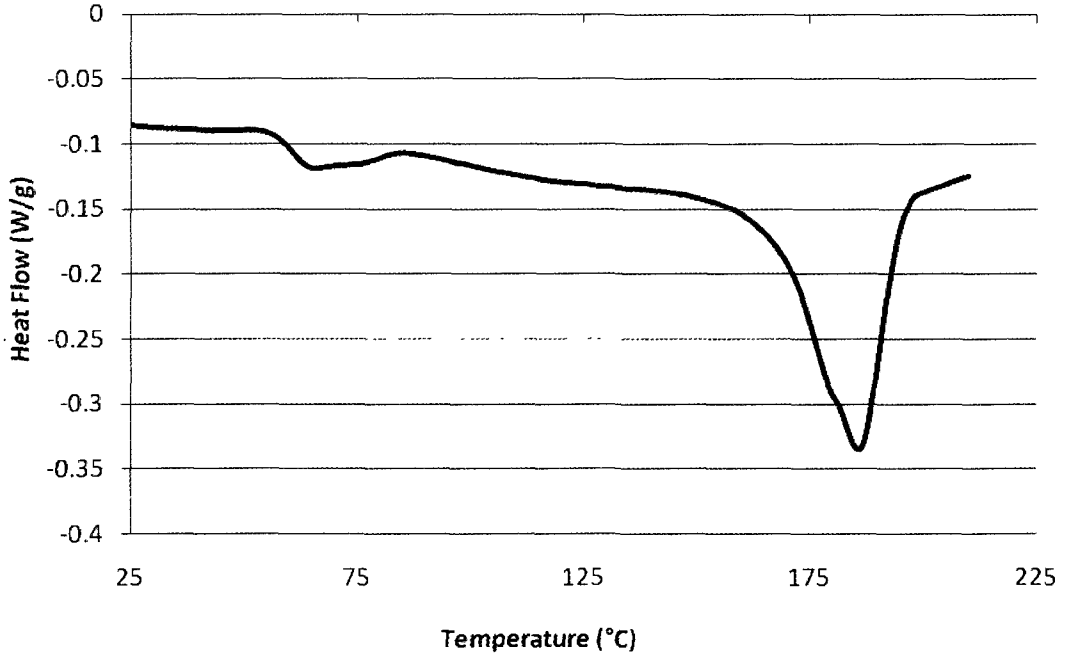

Figure 2.23. DSC of isotactic-rac_{50} DPE-PLA stars.

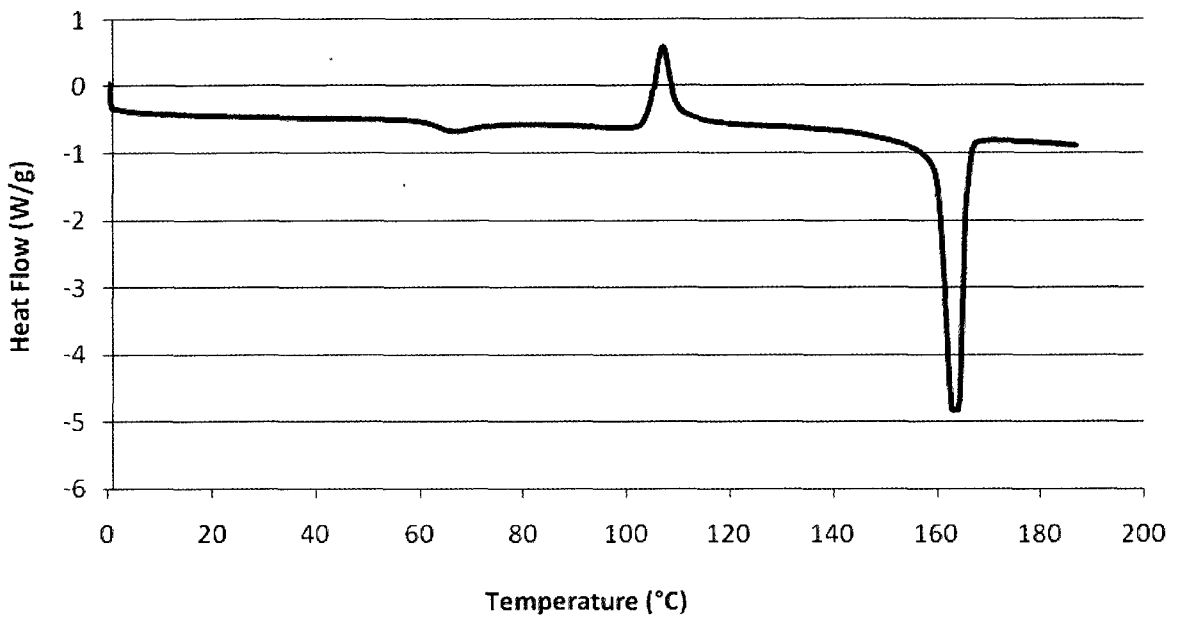

Figure 2.24. DSC of isotactic-L_{50} DPE-PLA stars.

Figures 2.23 and 2.24 illustrate the enhanced thermal transitions of our isotactic$_{50}$ stars, indicating that the thermal properties of these materials can be tuned both by differing the tacticity of the polymer chains and by changing the molecular weight of the polymer stars.

Percent crystallinity calculations on these materials revealed an increase in crystallinity for isotactic-*rac*$_{50}$ stars compared to their oligomeric analogues, with values averaging to 38%, a roughly 8% increase over the average for iso-*rac* stars, and 4% greater than the highest observed for the iso-*rac* system. X_c values of 45% were observed for the isotactic-L_{50} stars, an improvement of roughly 5% from the iso-*L* oligomeric stars. These results indicate that molecular weight increases have a positive effect on the percent crystallinity of DPE-PLA stars, which is to be expected. Increases in M_n should allow for larger crystalline domains to form (derived from longer isotactically biased chains), that will increase the overall crystallinity of these materials.

The solution lifetimes of these stars also exhibited great enhancement with an increase in the molecular weight. Isotactic-rac_{10} stars that possessed a lifetime of just over 58 minutes were enhanced to an average of 475 minutes for the isotactic-rac_{50} samples. Additionally, lifetime of the isotactic-*L* stars was enhanced from 175 ± 4 minutes for the iso-L_{10} samples to 1266 ± 4 minutes for the iso-L_{50} samples. In each case this represents a greater than 7-fold increase in solution persistence for a 5-fold increase in M_n.

2.3. Mixed monomer DPE-PLA stars with various *L*:*rac*-lactide ratios

Initial investigations into stereocontrolled polymer stars revealed the versatility of this system. With an ability to tune the materials' properties by tacticity control and molecular weight, the limits of this versatility through the production of a series of isotactically-enriched DPE-PLA stars bearing different tacticity biases was of particular interest. Rather than utilize a series of catalysts, the results from which could not be considered consistent, a method where $Sn(Oct)_2$ coupled with a series of monomer blends (*L*-lactide and *rac*-lactide) was employed to prepare polymers with various isotacticites. By employing a single catalyst, reproducibility of the results was assured, as well as consistent reaction times, kinetics and conversions. The results for a series of these experiments are presented in Table 2.9.

Table 2.9. Polymerization data for DPE-PLA stars with various isotacticity biases.

Composition (*L*:*rac*)	$M_{n,GPC}$	$M_{n,th}$	PDI	PDI_{arm}	Conversion (%)
100:0	8771	8781	1.18	2.51	99
90:10	8552	8930	1.16	2.39	92
80:20	8405	8645	1.15	2.34	92
70:30	8300	8645	1.12	2.15	93
60:40	8473	9065	1.11	2.07	90
50:50	8223	8787	1.11	2.09	90
0:100	8873	9464	1.14	2.24	94

From these data, close relationships between the analytically determined M_n and the theoretical values, along with very narrow PDI values are observed. This demonstrates the living nature of the polymerization with this combination of monomers. From these experiments, very high conversions of >90% were achieved, which were determined gravimetrically. The dispersity of the stars was calculated by the Szymanski method to reveal PDI_{arm} values <2.4. Additionally, these samples were investigated by ^1H NMR spectroscopy, DSC and TGA analyses to assess their qualities (Table 2.10).

Table 2.10. Thermal properties of mixed monomer DPE-PLA stars.

Sample Composition (*L*:*rac*)	**Tacticity (%)**	**T_g (°C)**	**T_m (°C)**	**T_{onset} (°C)**	**T_{max} (°C)**
90:10	93	47.4	125.6 + 138.5	276.1	353.1
80:20	83	44.7	121.6 + 132.8	273.6	350.3
70:30	74	43.7	117.3 + 128.3	264.8	332.8
60:40	62	43.5	-	258.2	330.4
50:50	51	43.2	-	251.1	328.6

^1H NMR spectra revealed that the tacticity bias increased fairly consistently, illustrated through an increase in the P_m value with an increase in the *L*-lactide composition, a result that was expected. Additionally, there was an increase in isotacticity bias greater than the *L*-lactide percent content in all samples. As *rac*-lactide is a racemic mixture of *D*- and *L*-lactide, our contents should read, for example, 80:20 *L*:*rac* as 90:10 *L*:*D*. Due to the ability of the *D*-monomer to affect the linkage at both its ends, it should be projected as an isotacticity bias of 80% for this sample. The increase observed above this would presumably account for the statistical possibility of two *D*-lactide monomers being inserted adjacent to each other.

TGA analyses of these mixed monomer star polymers revealed that the onset temperature (T_{onset}) and the maximum decomposition temperature (T_{max}) were both dependant upon the isotacticity bias (Figure 2.25).

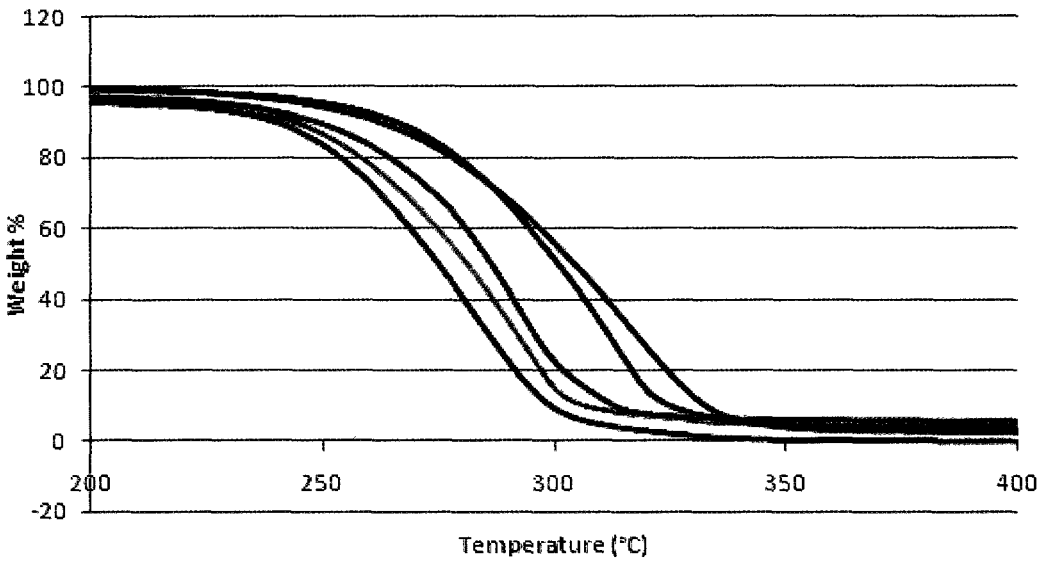

Figure 2.25. A TGA overlay of mixed monomer DPE-PLA stars, blue-50:50, green-60:40, red-70:30, purple-80:20 and light blue-90:10.

The thermal properties of these samples collected by DSC revealed little trending in the T_g values for samples between 51% and 74% isotacticity bias (Figure 2.26). While slight differences are observed for the T_g values for the 50:50, 60:40, 70:30 samples, (43.2-43.7°C), conclusive statements regarding specific trends cannot be made with such slight differences. However, there is an improvement of the T_g by movement to higher P_m values, with an average T_g of 44.7 and 47.4°C for the 80:20 and 90:10 composite samples. This reinforces the assertion that tacticity bias, and the crystalline character of these stars, has a profound effect on the polymer properties.

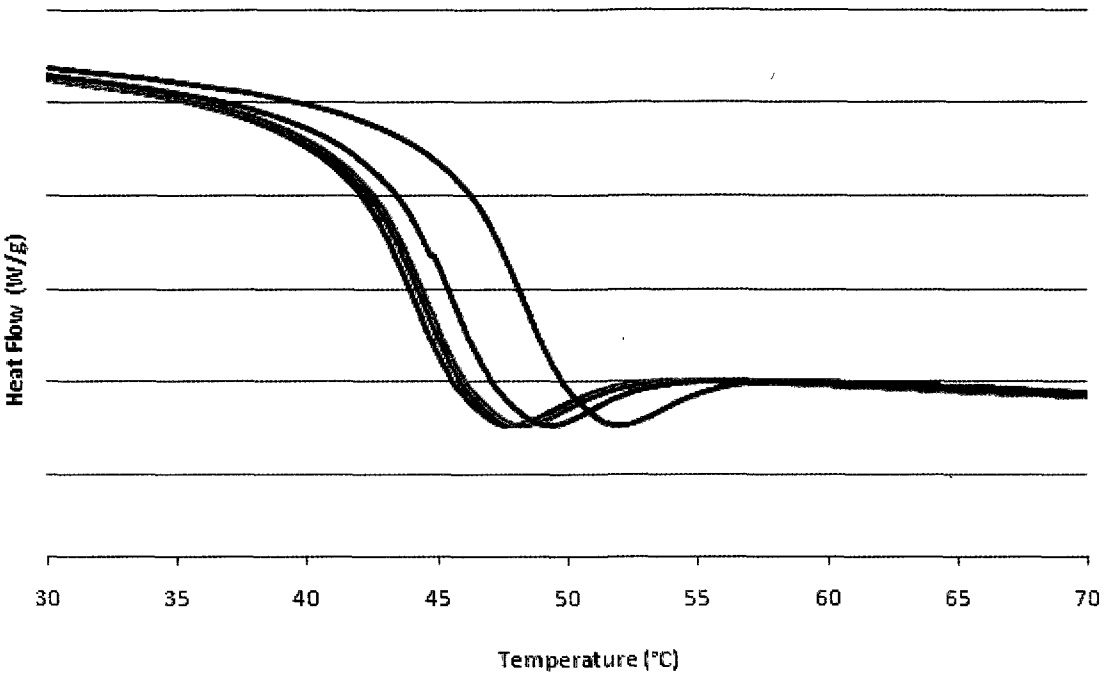

Figure 2.26. A DSC overlay (only T_g region shown) of mixed monomer DPE-PLA stars, blue-50:50, red-60:40, green- 70:30, purple-80:20, light blue-90:10.

The melting signals of these mixed monomer stars became an interesting area of study. Distinct melting signals were observed for only the 90:10, 80:20 and 70:30 composites, which extends the isotacticity range we observed with isotactic-*rac* stars with 82% isotacticity bias.[19] The X_c values of the mixed monomer stars were calculated and the observed trend indicates that the crystallinity of the samples bearing a distinct melting transition decreased with increasing content of *rac*-lactide. The propensity for *L*-lactide to form crystalline domains allows for the prediction of this trend. The observed X_c values were found to increase from the 70:30 composites, which had an initial crystallinity of 15%, to the 80:20 composites, which possessed an average X_c value of 23%. The 90:10 composites more closely resembled the iso-*rac* composites, possessing an average X_c value of 31% which indicated that the percent crystallinity can be tuned by this method through a range of 25%. Additionally, 15% crystallinity seems to be

the threshold for these materials, below which no discernable melting transitions can be observed.

To better understand the lack of true melting signals for some of these composites, pXRD analysis was performed on them. These data can be observed in Table 2.11 and Figure 2.27. In analyzing these samples by pXRD, information was collected that was key in identifying questions concerning our observed results in other techniques. The lack of melting signals for our 60:40 and 50:50 composites was revealed through the characteristics of these materials in pXRD, and the dependence of crystallite size upon percent crystallinity was also revealed.

Table 2.11. pXRD data for mixed monomer DPE-PLA stars.

Composition (*L*:*rac*)	**Angle of Diff. (°)**	**Crystallite Size[a] (nm)**	**d-spacing (Å)**
90:10	16.9	110	5.2
80:20	16.9	138	5.2
70:30	16.9	213	5.2
60:40	-	-	-
50:50	-	-	-

[a] Crystallite size calculated from the Scherrer equation

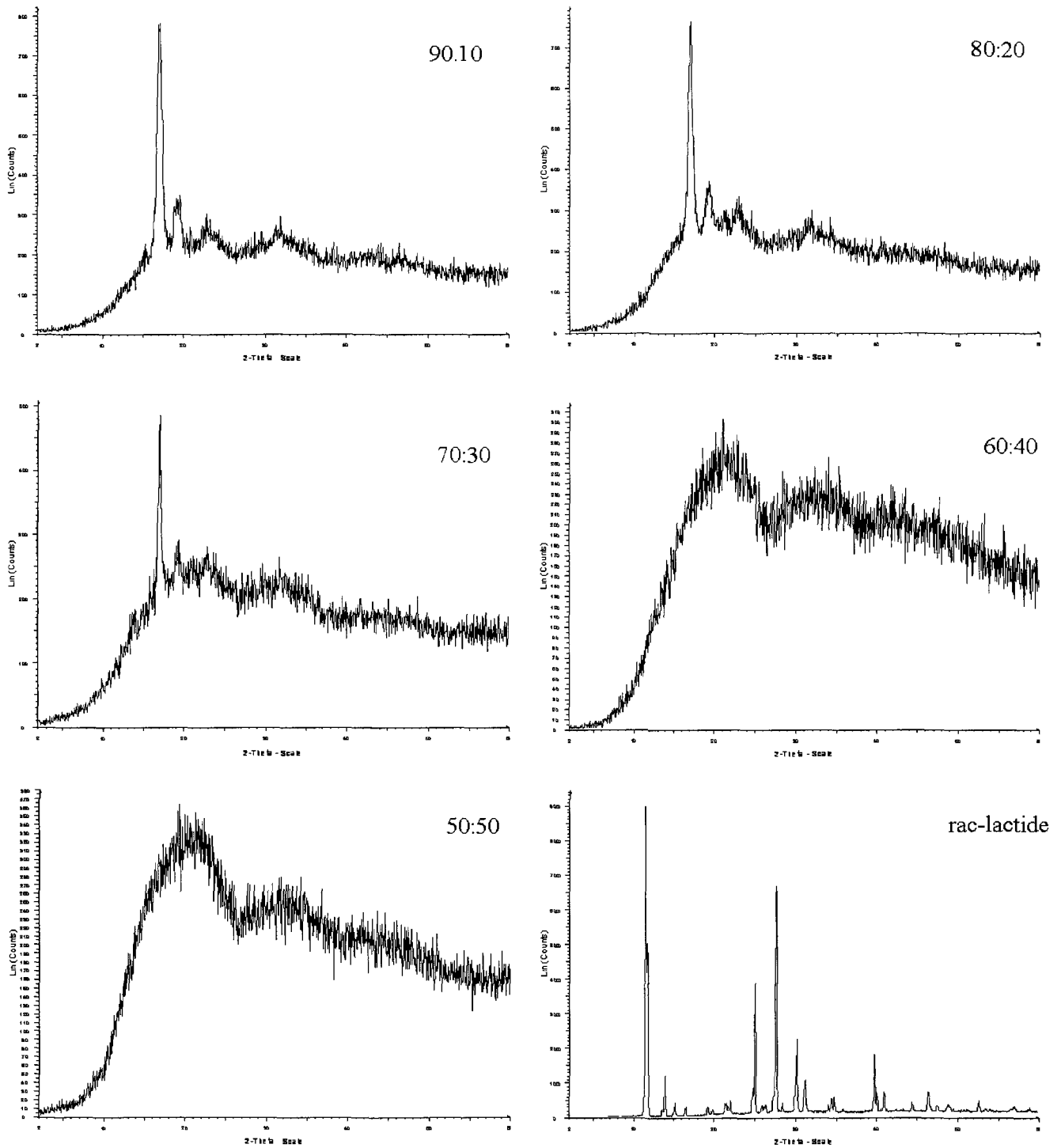

Figure 2.27. pXRD patterns for DPE-PLA stars derived from mixed monomers and *rac*-lactide monomer.

From the data in Table 2.11 it is obvious that while the diffraction angles and interlamellar d-spacing of these composite materials does not change with differing isotacticity biases, this parameter clearly affects the crystallite size. Changes in the isotacticity from a high of 93% to 74% have raised our average crystallite size from 110 to 230 nm. Considering the tendency of highly crystalline materials to form single crystals, as well as the enhanced ability of amorphous materials to agglomerate, this trend in crystallite size is not unexpected.

From the pXRD patterns themselves, the onset of amorphous characteristics is observed from the 90:10 composites to the 50:50 samples. Decreases in the diffraction intensity (linear counts) occur when the content of *L*-lactide is decreased, until at 60% *L*-lactide content a loss of the semicrystalline nature of isotactically-enriched PLA is observed. Samples below this threshold show featureless pXRD patterns characteristic of amorphous materials. It was unexpected that such an increase in the isotacticity bias would be required to achieve a semi-crystalline material. While parameters have been established, with regards to where these PLA stars undergo the transition from an amorphous material to a semi-crystalline polymer, the exact monomeric ratios have not been established.

The degradation profiles of these composite samples were analyzed in attempts to decipher if the system was tunable for solution stability. As previously described, pressed PLA samples were exposed to a standard solution of TBD in MeOH. The results of this analysis are presented in Figure 2.28 and Table 2.12.

Table 2.12. Degradation lifetimes of samples bearing various *L*:*rac*-lactide compositions.

Composition	Tacticity Bias (%)	Degradation (min)	Standard Dev. (min)
90:10	93	164	1
80:20	83	140	1
70:30	74	89	2
60:40	62	44	1
50:50	51	40	1

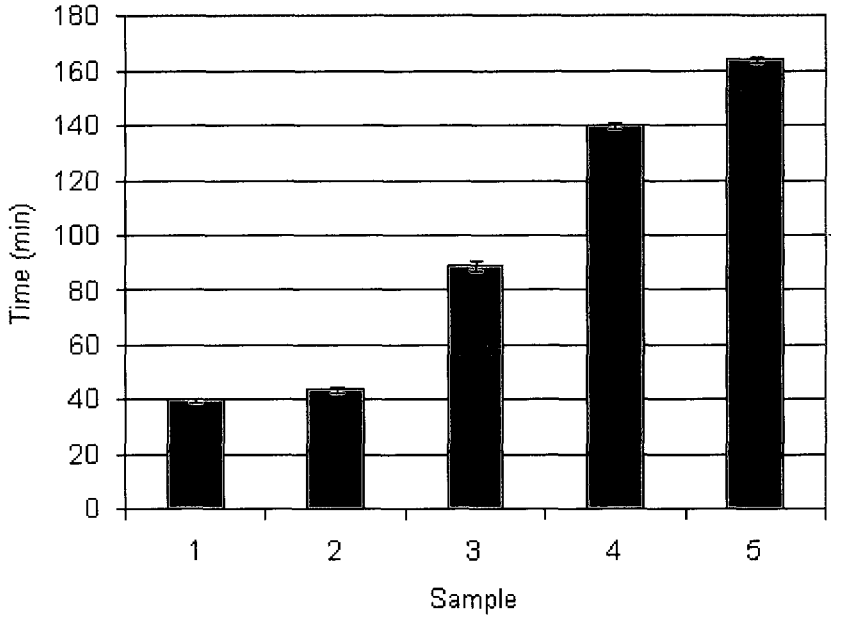

Figure 2.28. Bar graph demonstrating the degradation lifetimes of mixed monomer pellets. Samples 1 (50:50), 2 (60:40), 3 (70:30) 4 (80:20) 5 (90:10), n = 4.

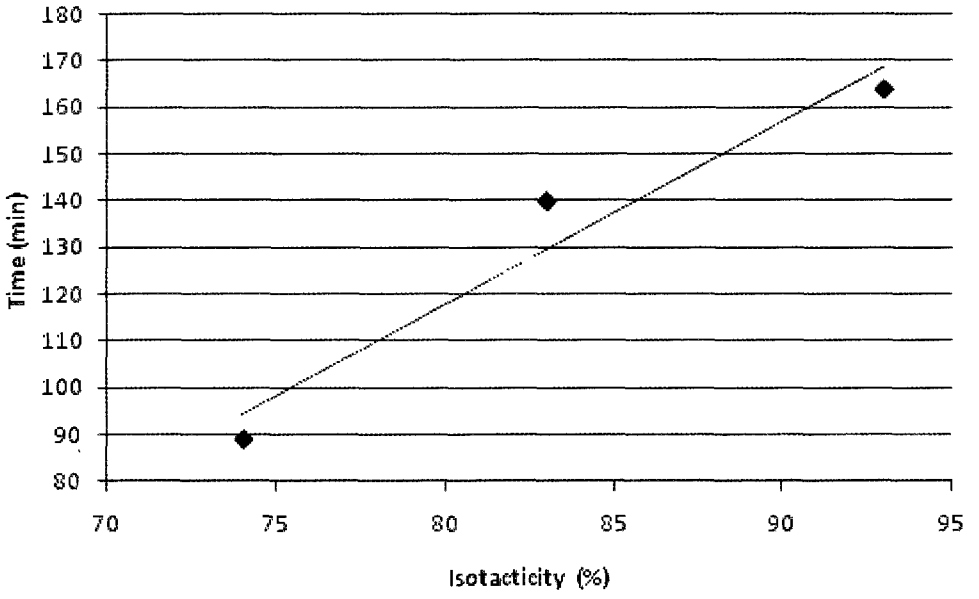

Figure 2.29. Linear relationship between degradation lifetimes and % isotacticity for mixed monomer samples from isotacticity bias of 74% to 93%.

The features revealed in the pXRD patterns are manifest in distinct differences in the observed lifetimes of pellets of mixed monomers. The two amorphous samples (50:50) and (60:40) were observed to have solution lifetimes significantly shorter than the other semi-crystalline samples. The cause of this has been determined to be the swifter uptake of the degradation solution by amorphous materials, a phenomenon that was discussed previously. The composite materials that have been confirmed as semi-crystalline exhibit a greater enhancement of the solution lifetimes. Beyond the 70:30 composite samples, enhancement of the isotacticity is observed to increase the lifetime of the pellets in solution. This relationship was analyzed by regression analysis and the dependence was found to be linear in nature with an R^2 value of 0.9456.

Chapter Three

Synthesis, characterization and lactide polymerization screening of anilido-aldimine aluminum complexes

3.1 Complex synthesis and characterization

A new adaptation in N-only donor ligands has been anilido-aldimine ligands. These ligands typically contain two types of donor atoms, with the anilido nomenclature arising from the presence of a univalent radical derived from aniline, and aldimines, the aldehyde analogue of an imine. These ligands remain largely underdeveloped with few reports of metal complexes being prepared. A variety of ligands possessing different denticities have been prepared including bidentate,[245,246] tridentate,[247-250] tetradentate or bis(bidentate).[251-256] These systems are illustrated in Figure 3.1.

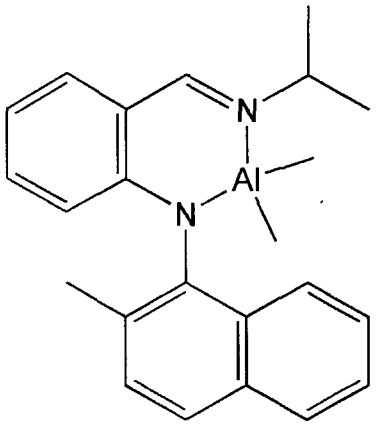

Mu (2005)[246]

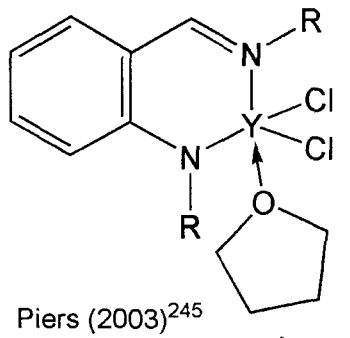

Piers (2003)[245]

R = 2,6-$^{i}Pr_2C_6H_3$

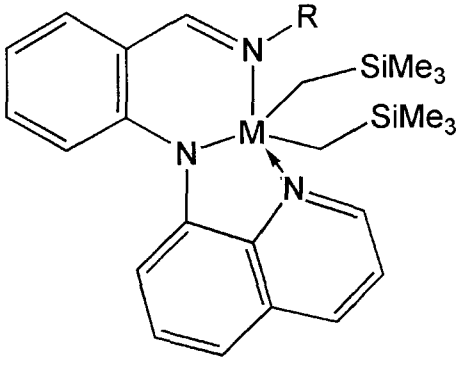

Mu (2008)[248]

M = Lu, Sc, Y
R = 2,6-$^{i}Pr_2C_6H_3$

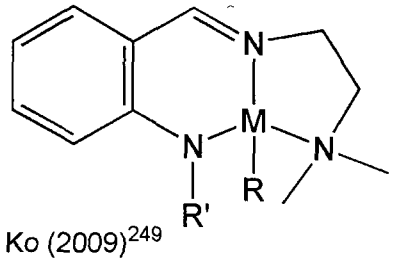

Ko (2009)[249]

M = Mg, Zn
R_{Mg} = ^{n}Bu
R_{Zn} = Et
R' = 2,6-$^{i}Pr_2C_6H_3$

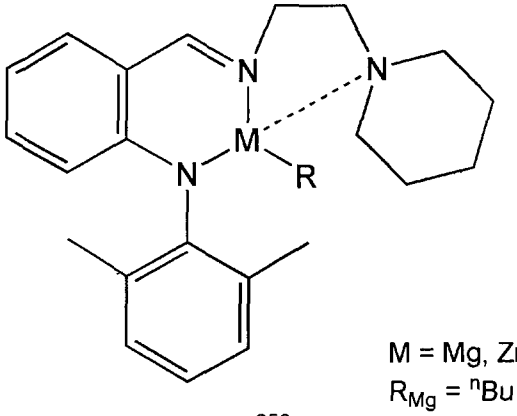

Ko (2010)[250]

M = Mg, Zn
R_{Mg} = ^{n}Bu
R_{Zn} = Et

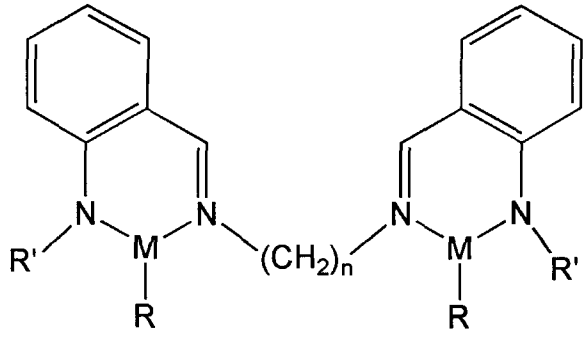

Mu (2008)[252]
Gibson (2007)[251]

M = Al, Zn
n = 2,3,6
R_{Al} = Me_2 or $^{i}Pr_2$
R_{Zn} = Et
R' = 2,6-$^{i}Pr_2C_6H_3$

Figure 3.1. Literature survey of anilido-aldimine ligands and complexes.

The bidentate systems have been used as stabilizers for organoyttrium cations,[245] and in the preparation of dialkylaluminum complexes, which exhibit fluorescent properties both in solution and in the solid state.[246] Variation of the *ortho* substituent on the rotatable aryl ring allowed for tuning of the emission colour the complex exhibits in solution.

The tridentate N,N,N anilido-aldimine ligands have been complexed with a variety of metals including the rare earth metals lutetium,[248] scandium[248] and yttrium,[247,248] as well as magnesium and zinc.[249] The rare earth complexes were shown to be effective ROP catalysts for ϵ-caprolactone, with high conversions and a linear dependence of conversion with respect to time. This was tempered with mediocre PDI values, which were the result of fluxionality of the quinoline derived pendant arm.[248] The magnesium and zinc complexes bearing dimethyl amino or piperidine pendants were shown to polymerize ϵ-caprolactone and *L*-lactide quite effectively with conversions >90% and low PDIs of 1.1-1.2.[249]

The bis(bidentate) N,N,N,N ligands have been successfully complexed with aluminum and zinc to prepare bimetallic catalysts.[251-256] These complexes have been shown to catalyze the ROP of ϵ-caprolactone, however the openness of the co-ordination sphere has led to broadened PDIs.[251] Finally some of these bis(bidentate) ligands have been tethered to create a macrocyclic ligand, in hopes of synthesizing bimetallic zinc complexes that mimic the β-diiminato complexes of Coates.[257] Possessing an alkyl sulfoxide bridge these bimetallic zinc complexes have been employed in the copolymerization of carbon dioxide and epoxides.[255,256]

The second component of this project involved the development and screening of novel aluminum catalysts supported by these anilido-aldimine ligands. The anilido-aldimine ligand sets were investigated because of their capacity for creating very different steric environments adjacent to the metal centre through different substitution patterns of the N,N,N,N co-ordinating

sphere. Aluminum was chosen as the metal because of its known proficiency in lactide ROP, as well as being a hard Lewis acidic metal with good orbital overlap and polarizability match when combined with the chosen ligand set, bearing the nitrogen donors. This improved overlap promotes better thermal stability for these catalysts, which was necessary for the conducting of polymerization experiments at high temperatures (120°C). Additionally, literature reports suggest a dependence upon steric crowding of the metal centre for the production of highly isotactic PLA.[155]

This trend has been elucidated through investigations of the activation energies of lactide polymerization. Subsequent enchainment of a lactide monomer in an isotactic insertion pattern is not solely dependant upon the energy of the second transition state, which involves the opening of the lactide ring after insertion into the M-O metal-organic bond. The four statistical probabilities: RRRR, SSSS, RRSS and SSRR have free energies of 20.2, 25.4, 18.9 and 28.1 kcal mol^{-1} respectively.[245] The similarity of these values indicates that some other geometric effect is necessary to produce isotactic PLA. Increasing the steric crowding at the vacant coordination site will help to control the stereochemistry of the inserted lactide monomer.

The standard salen framework has been highly successful in the isotactic polymerization of *rac*-lactide. The initial report by Spassky[134] of an unsubstituted [salen]AlOMe catalyst achieving a P_m of 0.68 has evolved into a ^tBu substituted salen ligand set capable of achieving P_m values of 0.88 when complexed with aluminum.[155] In this vein it was envisaged that movement of bulky R-substituents from the ortho-phenoxy position of the salen framework to the amino nitrogen of an anilido-aldimine framework. The shift in proximity of the R group to the metal centre is illustrated in Figure 3.2.

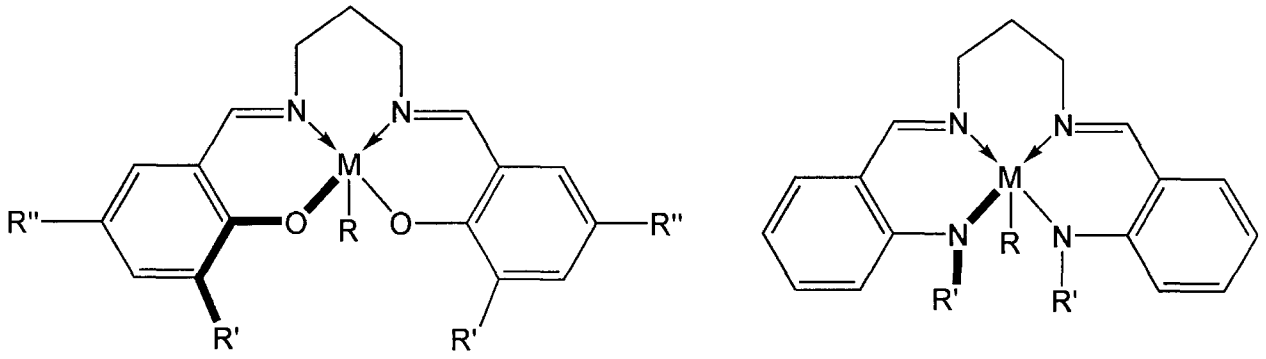

Figure 3.2. Proximity of substituent R to the metal centre in salen and anilido-aldimine type ligand frameworks.

From Figure 3.2 it is observed that the proximity of the sterically cumbersome group to the metal centre, M, has been drastically decreased from the anilido-aldimine ligand framework on the right to the substituted salen ligand framework on the left. The crowding of the metal co-ordination sphere should then lead to an improvement in the isotacticity bias (P_m) of the PLA produced by such a catalyst. To accomplish this, a series of substituted (2,6-diisopropylphenyl and cyclohexyl), anilido-aldimine ligands were prepared and attempts to complex them with aluminum were made.

The synthesis of the target anilido-aldimine ligands was performed through the preparation of two flourinated proligands, N,N'-bis(2-fluorobenzylidene)ethane-1,2-diamine (**4**) and N,N'-bis(2-fluorobenzylidene)propane-1,3-diamine (**5**). The synthesis of these ligand precursors is shown in Scheme 3.1.

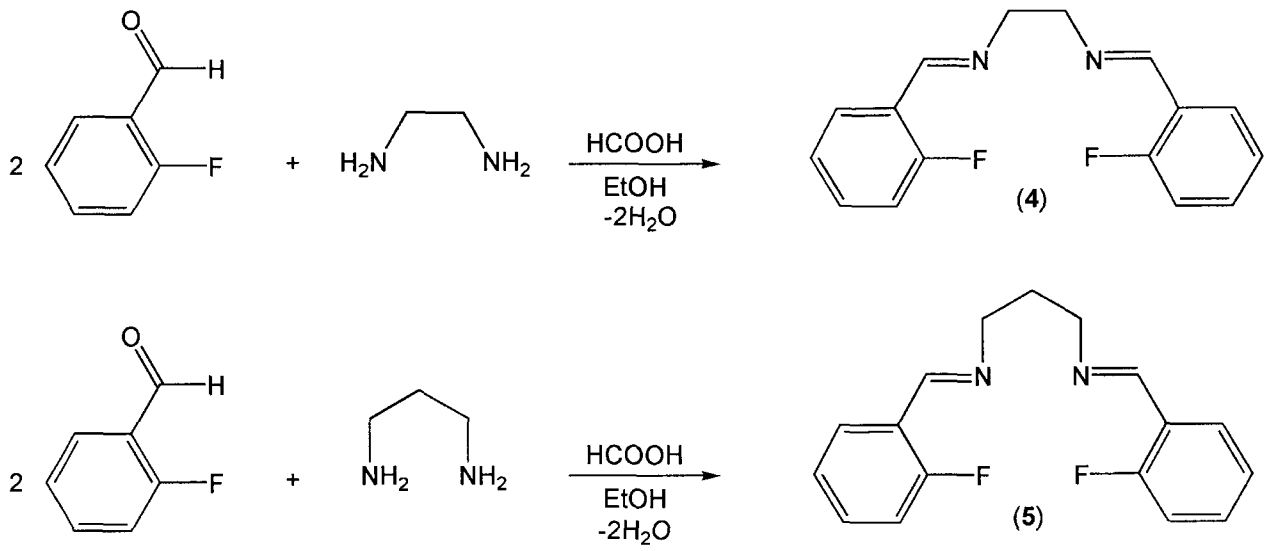

Scheme 3.1. Formation of fluorinated precursors from substituted benzaldehyde and appropriate diamine.

Fluorinated precursors (**4** and **5**) were prepared via the acid-catalyzed condensation of two equivalents of 2-fluorobenzaldehyde and one equivalent of the appropriate diamine. Condensation of water is the driving force in this reaction to promote the imine formation. A catalytic amount of formic acid (HCOOH) was added to increase the electrophilicity of the C=O carbon to facilitate nucleophilic attack by the amine nitrogen. Purification of the precipitate was accomplished via vacuum filtration and washing with ethanol (EtOH). Determination of the product formation was achieved via ^{1}H and ^{13}C NMR, which are described in Chapter 5.

Preparation of the anilido-aldimine ligand was accomplished by adaptation from literature synthesis.[228] Initial studies involving the synthesis of the diisopropylphenylamino derivatives, (N, N' –bis(2-(2,6-diisopropylphenylamino)benzylidene)ethane-1,2-diamine (**6**) and N, N' –bis(2-(2,6-diisopropylphenylamino)benzylidene)propane-1,3-diamine (**7**)), utilized an in situ generated lithium salt, however very low yields necessitated a switch to the synthesis and isolation of the appropriate lithium amide. Isolation of the amido lithium salt allowed for greater

control of the stoichiometric ratios, which promoted higher yields for the reaction processes. The general reaction scheme for ligand synthesis is outlined below (Scheme 3.2).

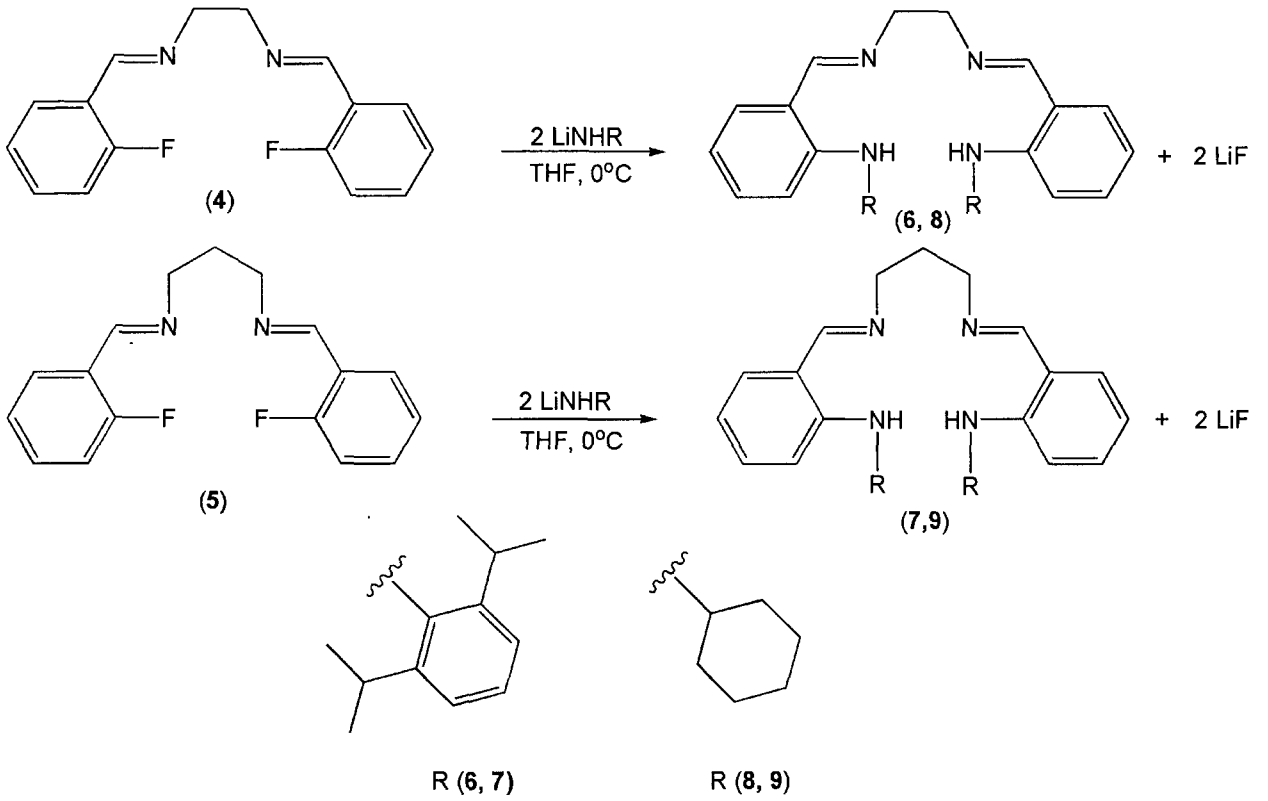

Scheme 3.2. Synthesis of substituted anilido-aldimine ligands from (**4**), (**5**) and lithiated amines.

Isolation of the lithiated amines, ($LiNC_6H_3(CH(CH_3)_2)_2$ and $LiNHC_6H_{11}$) was achieved via reaction of the substituted amines, (2,6-diisopropylaniline and cyclohexylamine), and ^nBuLi in THF. The lithium salts precipitated from solution and were filtered in vacuo to afford the grey solid product in high yields (90%).

Formation of the target ligands was achieved through a typical metathesis reaction. The driving force for this reaction is the formation of LiF, an inorganic salt that possesses a high lattice energy, which promotes its formation *in situ*.[258] A dropwise addition of a slurry of the appropriate lithium salt in THF to a stirred and chilled (-35°C) solution of the fluorinated precursors (**4** and **5**), also in THF, produced the target ligands. As the addition went to

completion, the solution darkened from yellow to deep red in color. The reaction contents were allowed to warm to room temperature and left to stir overnight (12 h). An aqueous workup eliminated LiF salts. Addition of degassed deionized water to the reaction mixture resulted in the formation of yellow precipitates, which redissolved to afford a yellow solution. The reaction solvent, THF, was removed by rotary evaporation, and the organic product was extracted by water:hexanes separation (3 x 100 mL). Removal of the solvent afforded the impure target compound in low to moderate yields.

Isolation of the ligands remained a difficult process throughout. Low reaction yields (<20% for cyclohexyl substituted derivatives) and the similar solubility of both the ligand and fluorinated precursor prevented simple filtration and washing from isolating the ligands in a high purity. Diisopropylphenylamino derivatives (**6** and **7**) were purified by recrystallization in acetonitrile (ACN) to afford the desired ligands in moderate yields (40 and 45% for the ethylene and propylene linked ligands respectively), and the ligands were characterized by ^{1}H and ^{13}C NMR. The cyclohexylamino derivatives (**8** and **9**) could not be isolated by means of recrystallization. Purification was adapted from the literature and utilized alumina columns pretreated with a 1% v/v solution of triethylamine (NEt_3) in hexane.[226] Both (**8**) and (**9**) were collected as yellow oils (15 and 20% for the ethylene and propylene linked ligands respectively) as confirmed by ^{1}H and ^{13}C NMR. Formation of the products was confirmed by the presence of the N*H* peak in ^{1}H NMR and the shift in the C*H*=N signal from 8.63 ppm in the precursor to 8.37 ppm in the ligand.[228]

The aluminum complexes of these ligands, **10-13** were to be prepared via protonolysis reaction with trimethylaluminum (TMA) in toluene at 110°C (24 h). Since the target catalysts were monometallic in nature, attempts were made to isolate the monometallic species (Figure

3.3), through the reaction of stoichiometric ratios of ligand to metal despite the precedence for these complexes to adopt bimetallic arrangements.

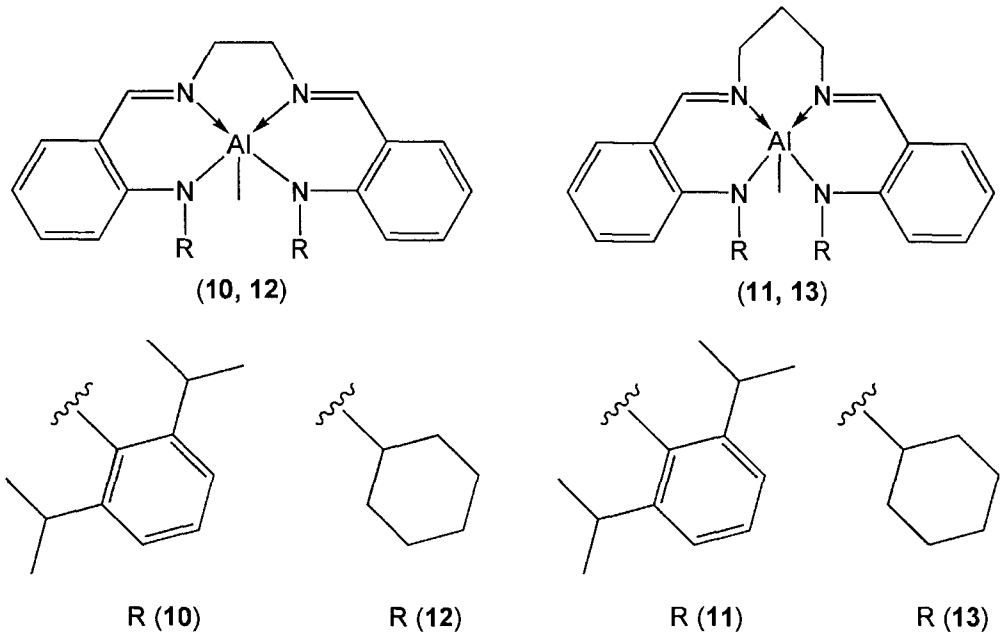

Figure 3.3. Target monometallic anilido-aldimine aluminum complexes (**10-13**).

These reactions yielded mixed results. Rather than isolating the preferred monometallic species (from stoichiometric reaction of TMA and ligand), these reactions yielded mixtures of the *bis*-metal complex (Figure 3.5) or an interesting monometallic species exhibiting a free pendant arm. The presence of bimetallic structures was determined by a 1:6 *H*C=N Al-C*H*$_3$ integration by ^{1}H NMR, and mono-complexed catalyst that still possessed the ^{1}H signal for an uncoordinated amido proton (N*H* at 10.47 ppm). This structure was revealed by single crystal X-ray crystallography.

Crystals of **14,** a represrentative mono-metallic compound possessing the free pendant arm, were grown from a saturated acetonitrile solution and analyzed by X-ray crystallography. An interesting geometry of **14** was characterized and is shown in Figure 3.4. Relevant bond

lengths and angles are listed in Tables 3.1 and 3.2 respectively, and crystallographic parameters are located in Table 3.3.

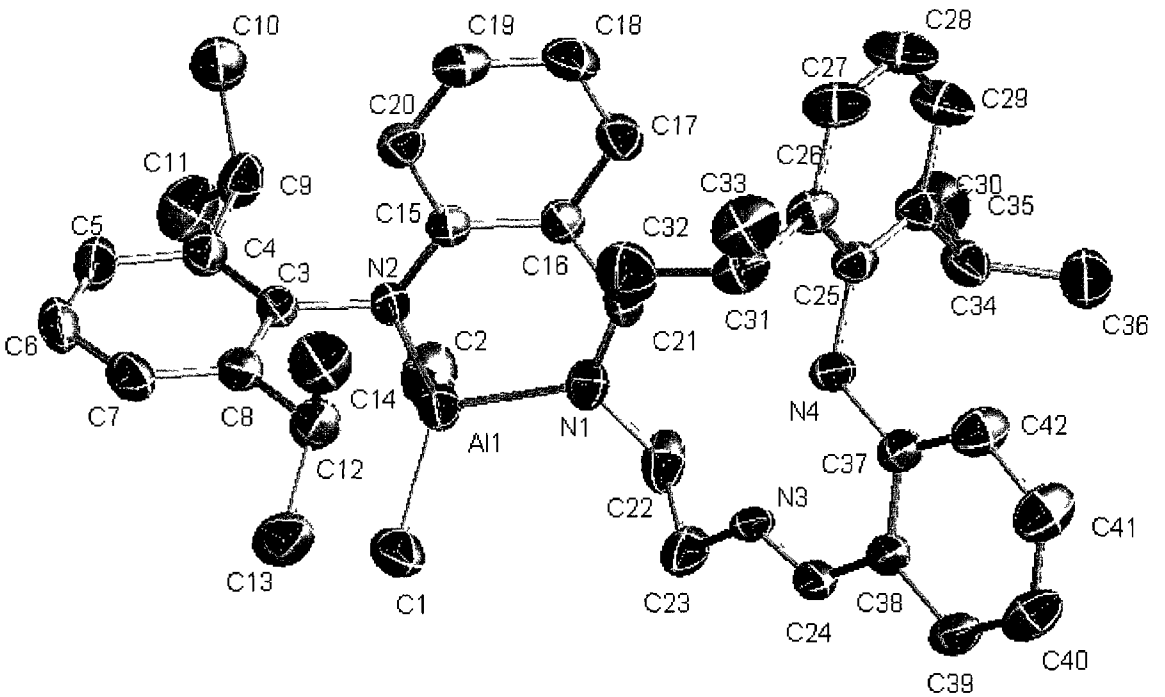

Figure 3.4. Molecular structure of complex (**14**) with free pendant arm. Hydrogens omitted for clarity.

Table 3.1. Selected bond lengths for (**14**) ([**6**]$AlMe_2$).

Bond	Length (Å)	Bond	Length (Å)
Al(1)-N(1)	1.9292(18)	N(2)-C(15)	1.369(3)
Al(1)-N(2)	1.8881(18)	N(3)-C(23)	1.52(4)
Al(1)-C(1)	1.958(3)	N(3)-C(24)	1.15(3)
Al(1)-C(2)	1.967(3)	N(4)-C(25)	1.430(3)
N(1)-C(21)	1.295(3)	N(4)-C(37)	1.378(3)
N(1)-C(22)	1.468(3)	C(16)-C(21)	1.429(3)
N(2)-C(3)	1.449(2)	C(22)-C(23)	1.506(4)

Table 3.2. Selected bond angles for (**14**) ([**6**]$AlMe_2$).

Bond	Angle (°)	Bond	Angle (°)	Bond	Angle (°)
N(1)-Al(1)-C(1)	110.23(8)	C(3)-N(2)-Al(1)	115.25(12)	C(22)-N(1)-Al(1)	117.25(14)
N(1)-Al(1)-C(2)	104.12(10)	Al(1)-C(1)-H(1A)	109.5	C(24)-N(3)-C(23)	123.0(3)
N(2)-Al(1)-C(1)	115.16(10)	C(15)-N(2)-Al(1)	127.07(13)	C(24)-(N3')-C(23)	113.0(2)
N(2)-Al(1)-C(2)	117.58(10)	C(15)-N(2)-C(3)	117.65(16)	C(25)-N(4)-H(4)	118.5
N(2)-Al(1)-N(1)	94.38(8)	C(21)-N(1)-Al(1)	123.84(15)	C(37)-N(4)-C(25)	122.54(17)
C(1)-Al(1)-C(2)	112.82(13)	C(21)-N(1)-C(22)	118.50(18)	C(37)-N(4)-H(4)	118.7

Table 3.3. Crystallographic data and details for (**14**) ([**6**]$AlMe_2$).

Empirical Formula	$C_{42}H_{55}AlN_4$	Formula weight	642.88
Crystal system	Monoclinic	Space group	$P2_1/c$
a, b, c (Å)	13.496(2), 13.913(3), 20.820(5)		
α, β, γ (°)	90, 99.431(2), 90		
V, $Å^3$	3856.7(13)	Total reflections	25597
Z	4	Unique reflections	8584
D_{calc}, mg m^{-3}	1.107	Parameters	437
Wavelength, Å	0.71073	R_1[a]	0.1010
T, K	173(1)	wR_2[b]	0.1701
θ range (°)	1.53 to 27.50°	Goodness-of-fit	1.052

[a] $R_1 = \Sigma (F_o-F_c)/\Sigma F_o$ [b] $wR_2 = (\Sigma w(F_o^2-F_c^2)^2/\Sigma(wF_o^4)^{1/2}$

The molecular structure supports these catalysts favouring a *bis*-metal configuration and the anilido-aldimine ligand sets acting as bidendate ligands. Despite lacking the necessary stoichiometry to synthesize the true bimetallic complex, the preferred geometry of these systems can be seen from Figure 3.4. This provides an enhanced view of these ligand systems as it allows for comparison of the bond lengths and angles of the complexed and free ligands.

First we see that the Al(1)-N(2) bond is shorter than the Al(1)-N(1) bond. This indicates that the strongest coordination is the amido nitrogen to the aluminum metal centre. The reason for this shorter bond length can be attributed to the enhanced electronegativity of the amido nitrogen from the close proximity to two aromatic rings. Ligand integrity is seen to be maintained through the very short N(1)-C(21) bond which at 1.295(3) Å is representative of a double bond. This value is consistent with reported literature values, however there are examples of similar structures that lose this double bond character.[229] This is compared to the N(3)-C(24)

bond length of 1.40(3) Å. In this case it appears that complexation to the metal centre has caused a contraction, or strengthening of the imino bond.

Additionally, comparing the lengths of the N(2)-C(15) bond and the N(4)-C(37) bonds reveals valuable information. From these bond lengths, 1.369(3) Å vs 1.378(3) Å, it can be seen that complexation to the metal centre has a far less significant effect in this instance. The length of our amido N(2)-C(3) (1.449(2) Å) for the complexed half-ligand vs. that of N(4)-C(25) (1.430(3) Å), representing the free half-ligand. This indicates that complexation to the metal causes a slight elongation of this N-C bond. The N(1)-C(22) (1.468(3) Å) vs. N(3)-C(23) (1.41(4) Å) bonds which unite the imino nitrogen and the aliphatic linker show that complexation to the metal centre leads to lengthening of this bond.

From the bond angles we can see that the inclusion of the metal aluminum atom causes a pinching of the ligand framework and a contraction of the bond angles. The disorted tetrahedral geometry at the metal centre is shown from the bond angles, with the shortest observed being the N(2)-Al(1)-N(1) (94.38(8)°), which is compressed based upon the geometry of the anilido-aldimine ligand set. Additionally, comparing the N(1)-C(21)-C(16) angle of 126.80(19)° to that of the uncomplexed pendant arm which is 125(2)° for the N(3)-C(24)-C(38), indicating that the inclusion of the metal centre has little effect on the geometry of this angle. Comparatively the N(2)-C(15)-C(16) angle is measured at 121.31(18)° while the N(4)-C(37)-C(38) is revealed to be 119.83(19)°. Here the metal centre has actually caused an expansion of the bond angle, although a rather small one.

The other product that formed via 1:1 reactions of the appropriate anilido-aldimine ligand (**6-9**) and TMA were bis-metal complexes (**15-18**) (Figure 3.5). This geometry has previously been reported,[252] and plagues attempts to prepare monometallic anilido-aldimine complexes. Changes in the reaction strategy, by employing stoichiometric ratios of 1:2 (ligand:TMA) allowed for the exclusive formation of the bimetallic species (**15-18**).

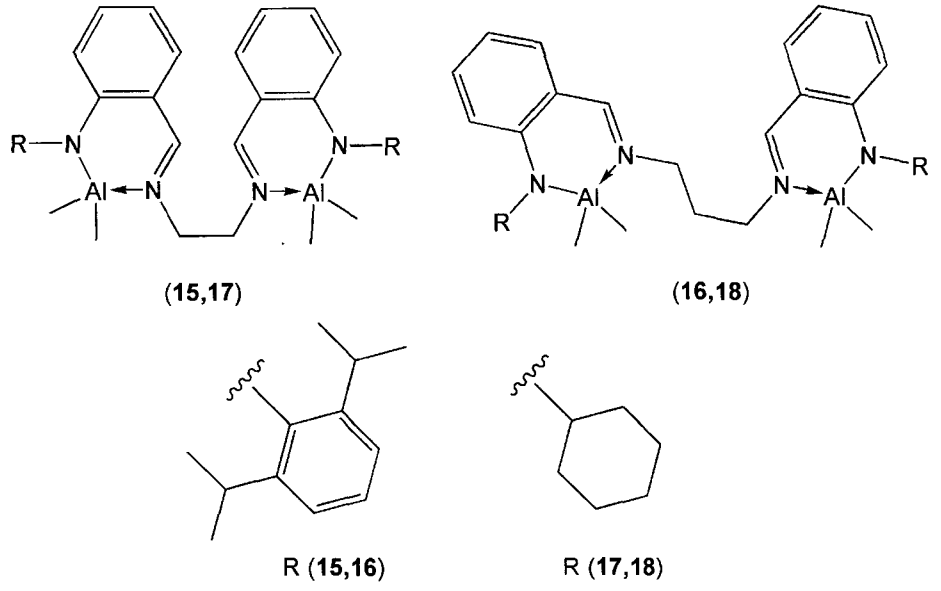

Figure 3.5. *Bis*-metal geometry for substituted anilido-aldimine aluminum complexes. (**15-18**)

By switching to the reaction strategy to utilize excess equivalents of TMA the yields were greatly increased, and the purity of the products (**15-18**) was enhanced. For complex **16**, (Figure 3.6) crystals were also grown from a saturated solution of ACN and analyzed by X-ray crystallography. The bimetallic complex is favoured.

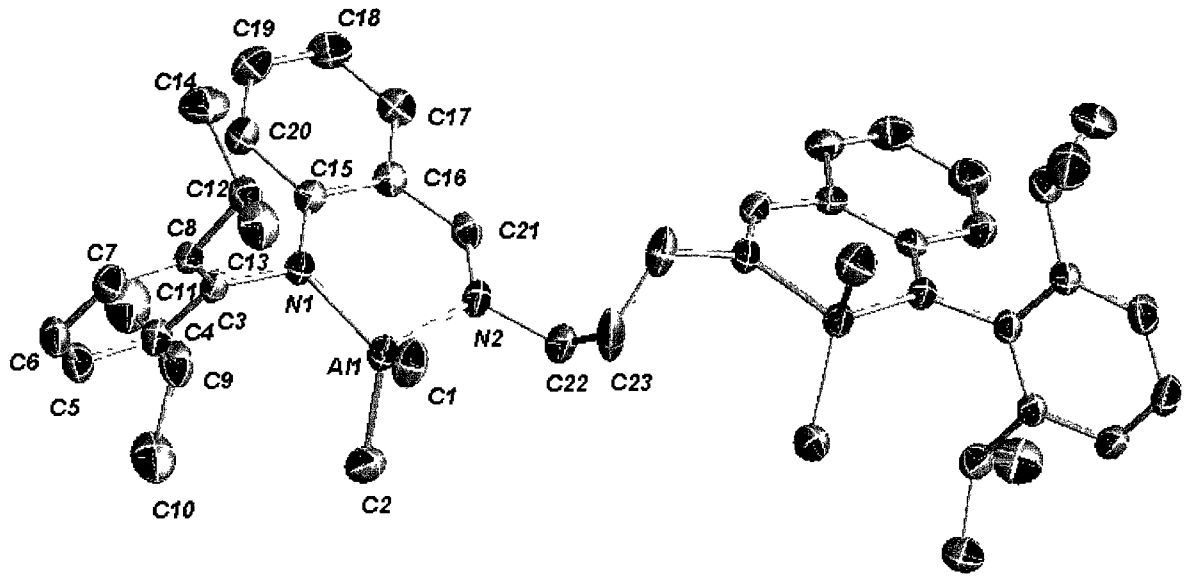

Figure 3.6. Molecular structure of complex **16**. Hydrogens omitted for clarity.

Table 3.4. Bond lengths for (**16**) [7]$(AlMe_2)_2$.

Bond	Length (Å)	Bond	Length (Å)
N(1)-Al(1)	1.8918(14)	N(1)-C(3)	1.445(2)
N(2)-Al(1)	1.9482(15)	N(2)-C(22)	1.481(2)
Al(l)-C(1)	1.963(2)	C(22)-C(23)	1.512(3)
Al(1)-C(2)	1.965(2)	C(16)-C(21)	1.436(2)
N(2)-C(21)	1.293(2)	C(8)-C(12)	1.518(2)
N(1)-C(15)	1.365(2)	C(4)-C(9)	1.521(3)

Table 3.5. Bond angles for (**16**) [7]$(AlMe_2)_2$.

Bond	Angle (°)	Bond	Angle (°)	Bond	Angle (°)
N(1)-Al(1)-N(2)	95.15(2)	C(3)-N(1)-Al(1)	113.89(11)	N(1)-C(15)-C(16)	121.66(15)
N(1)-Al(1)-C(1)	114.35(8)	C(21)-N(2)-C(22)	118.03(16)	C(15)-C(16)-C(21)	124.21(16)
N(1)-Al(1)-C(2)	115.45(8)	C(21)-N(2)-Al(1)	123.78(12)	N(2)-C(21)-C(16)	127.24(16)
N(2)-Al(1)-C(1)	112.55(9)	C(22)-N(2)-Al(1)	117.76(13)	C(3)-C(8)-C(12)	122.47(15)
N(2)-Al(1)-C(2)	104.90(8)	C(17)-C(16)-C(21)	115.99(16)	C(3)-C(4)-C(9)	122.73(16)
C(1)-Al(1)-C(2)	112.70(11)	C(13)-C(12)-C(14)	109.33(18)	N(2)-C(22)-C(23)	112.10(15)
C(15)-N(1)-C(3)	118.30(13)	C(22)-C(23)-C(22)	114.9(8)	C(18)-C(17)-C(16)	122.22(18)
C(15)-N(1)-Al(1)	127.65(11)	C(10)-C(9)-C(11)	109.9(12)	N(1)-C(15)-C(20)	122.15(15)

Table 3.6. Crystallographic data for (**16**) [**7**]$(AlMe_2)_2$.

Empirical Formula	$C_{45}H_{62}Al_2N_4$	Formula weight	712.95
Crystal system	Orthorhombic	Space group	Pbcn
a, b, c (Å)	15.7648(16), 17.2749(17), 15.2425(15)		
α, β, γ (°)	90, 90, 90		
V, $Å^3$	4151.1(7)	Total reflections	27336
Z	4	Unique reflections	4742
D_{calc}, mg m^{-3}	1.141	Parameters	355
Wavelength, Å	0.71073	R_1[a]	0.0676
T, K	173(1)	R_w[b]	0.1339
θ range (°)	1.75 to 27.50	Goodness-of-fit	1.123

[a]$R_1 = \Sigma (F_o-F_c)/\Sigma F_o$ [b]$wR_2 = (\Sigma w(F_o^2-F_c^2)^2/\Sigma(wF_o^4)^{1/2}$

This structure, (Figure 3.6) reveals the preferred bimetallic geometry that these complexes adopt. The bidentate coordination of the anilido-aldimine framework to the aluminum centre linked with a flexible aliphatic chain to produce a bimetallic species.

When investigating the bond lengths, the co-ordinating N(1)-Al(1) and N(2)-Al(1) show lengths of 1.8918(14) and 1.9482(15) Å respectively. Again this indicates that the amido nitrogen is more strongly co-ordinated to the metal centre. Additionally the characteristic imino double bond N(2)-C(21), with length of 1.293(2) Å is shown to be maintained. This is consistent with the data acquired for [**6**]$AlMe_2$ and with literature.[229] The N(1)-C(15) bond (1.365(2) Å) is consistent with Figure 3.4, (1.369(3) Å), while the N(2)-C(22) linking bond (1.481(2) Å) is slightly longer than the 1.468(3) Å calculated for the [**6**]$AlMe_2$ (**14**) structure.

With respect to bond angles similar results to the first structure are observed. The distorted tetrahedral geometry at the metal centre is displayed by the bond angles which deviate slightly from the theoretical value of 109.5°. Again, the smallest observed angle is the N(1)-Al(1)-N(2) (95.15(2)°) which represents the angle of the co-ordinating nitrogens through the metal centre. The differences in the linker group can be observed when examining the C(22)-

C(23)-C(22) bond angle. At 114.9(8)° this represents a slight compression of the theoretical 120° bond angle.

The cyclohexylamido complexes (**17** and **18**) have also revealed a propensity to take the bimetallic conformation. Preliminary reactions with TMA at 1:1 ratios revealed complex metal environments, (attributed to the bis-metal complex and cyclohexyl analogues of complex **14**), by ^{1}H NMR. To alleviate this, 2:1 reactions were carried out in hopes of isolating strictly the *bis*-metal complex. Analysis by ^{1}H NMR revealed that reactions at these stoichiometric ratios afforded strictly the *bis*-metal complex. Full NMR characterization of these complexes can be found in Chapter 5.

Diagnostic peaks for these complexes were again the formation of the Al-C*H*$_3$ (-0.17 ppm) peak and the correct integration of this to our ligand imine signal. The shifting of this imine was also characteristic of catalyst formation with the shift being in line with those observed for the diisopropylphenyl substituted bis-aluminum catalysts. Finally reaction progress/completion was monitored by the disappearance of the N*H* amino proton peak at 9.4 ppm. By use of these tools the synthesis of the cyclohexyl substituted anilido-aldimine *bis*-aluminum complexes was confirmed. Unfortunately crystals could not be obtained by conventional means to be included in this document. Further experimentation to elucidate the crystal structure is continuing.

3.2 Lactide screening and kinetics

After the isolation of the *bis*-metal complexes (**15-18**) they were investigated for proficiency as ROP catalysts in the production of PLA. Reactions were carried out in toluene at 70°C and under neat conditions at 120°C. The polymerization results are summarized in Table 3.7.

Table 3.7. Polymerization data for catalysts bimetallic anilido-aldimine aluminum catalysts (**15-18**) with *rac*-lactide[a,b]

Catalyst	Time (hr)	Conversion (%)	$M_{n,GPC}$	$M_{n,th}$	PDI
15	2	8	1222	1146	1.06
15	4	24	3289	3437	1.10
15	8	43	6866	6157	1.15
15	16	67	9010	9594	1.17
15	24	69	9412	9880	1.26
16	2	9	1812	1288	1.11
16	4	20	4175	2864	1.16
16	8	45	5875	6444	1.22
16	16	60	9123	8592	1.25
16	24	66	9450	9451	1.28
17	2	21	2867	3007	1.21
17	4	46	6282	6587	1.27
17	8	62	8468	8878	1.22
17	16	82	11244	11742	1.23
17	24	84	10890	12028	1.25
18	2	12	1452	1718	1.19
18	4	20	2762	2864	1.21
18	8	38	4952	5442	1.33
18	16	65	9034	9308	1.37
18	24	68	8822	9738	1.45

[a]benzyl alcohol (BnOH) initiator, [b] Monomer:initiator:catalyst ratios of 200:2:1

From this initial screening data, the novel anilido-aldimine aluminum catalysts exhibit moderate to good control over the ROP of *rac*-lactide to prepare linear PLA in the presence of benzyl alcohol initiator. Conversion was found to increase over time to approximately 16 hours in all trials. When the polymerizations were sampled at 24 h it was revealed that conversion had not increased as anticipated and that polymer properties had worsened (decrease in M_n was observed). Polymerization experiments carried beyond this point (48 h) revealed that the

polymerization was effectively completed after the 16-18 h mark. Loss of capability at this point could be attributed to a number of factors, including the decomposition of the catalyst by thermal stress or the possibility of protic impurities terminating the polymer chains. The lack of any induction period was to be expected as these bimetallic aluminum catalysts are not especially crowded at the coordination site, allowing for access of the lactide monomer to coordinate to the metal centre. Conversion by **15**, **16** and **18** typically was maximized at 63-68 percent, with typical transesterification data collected beyond the 16 h mark. The cyclohexyl substituted ethylene catalyst (**17**) achieved the highest conversions approaching 84% as determined by gravimetry.

Molecular weight control and the living nature of the catalysts were determined through plots of M_n vs. conversion. These can be seen in Figures 3.7-3.10. From these data it can be shown that the catalysts exhibit living characteristics with a linear increase in M_n with respect to conversion. Typical R^2 values for these catalysts were found to be in the range of 0.97-0.99.

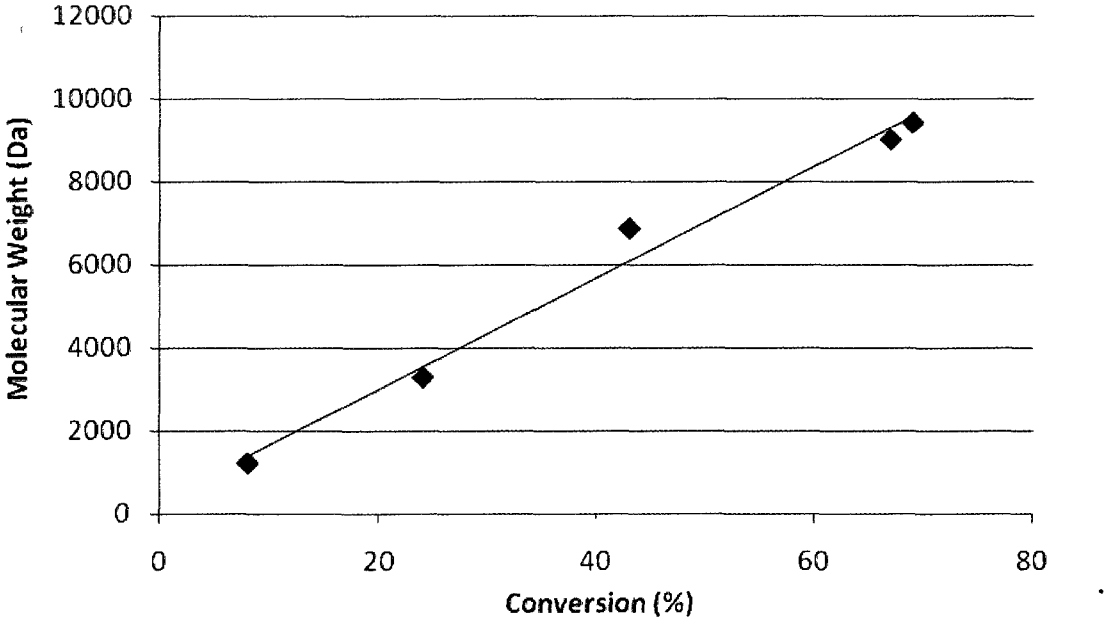

Figure 3.7. M_n vs. conversion for **15** [**6**]$(AlMe_2)_2$.

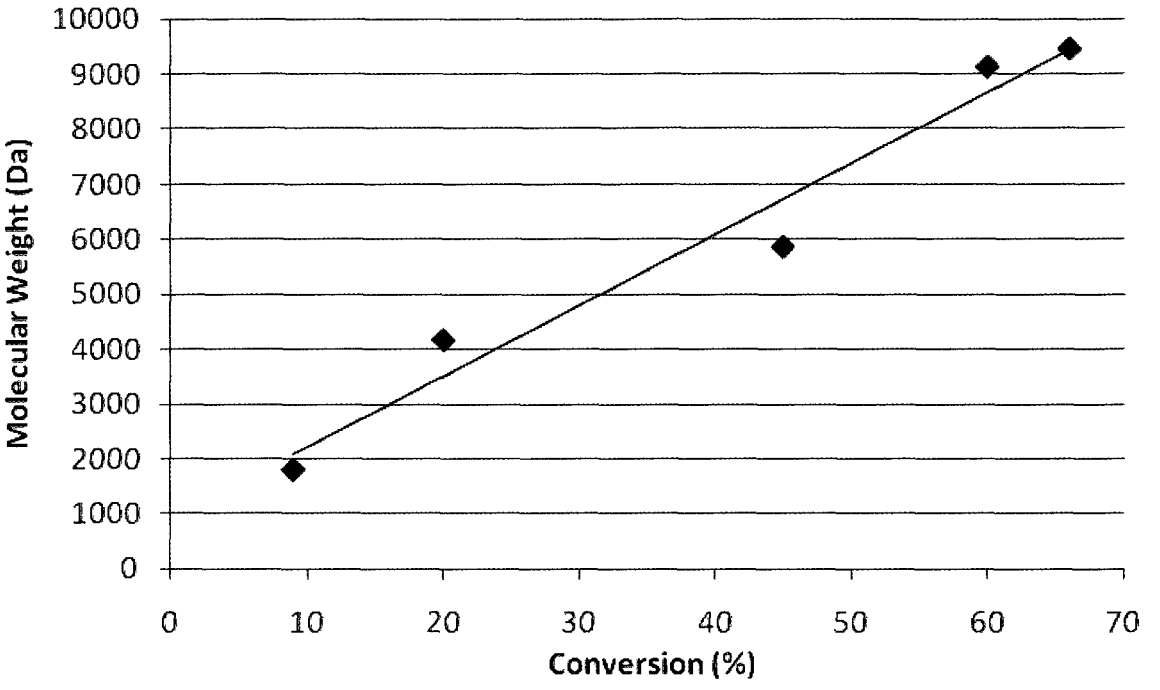

Figure 3.8. M_n vs. conversion for **16** [7]$(AlMe_2)_2$.

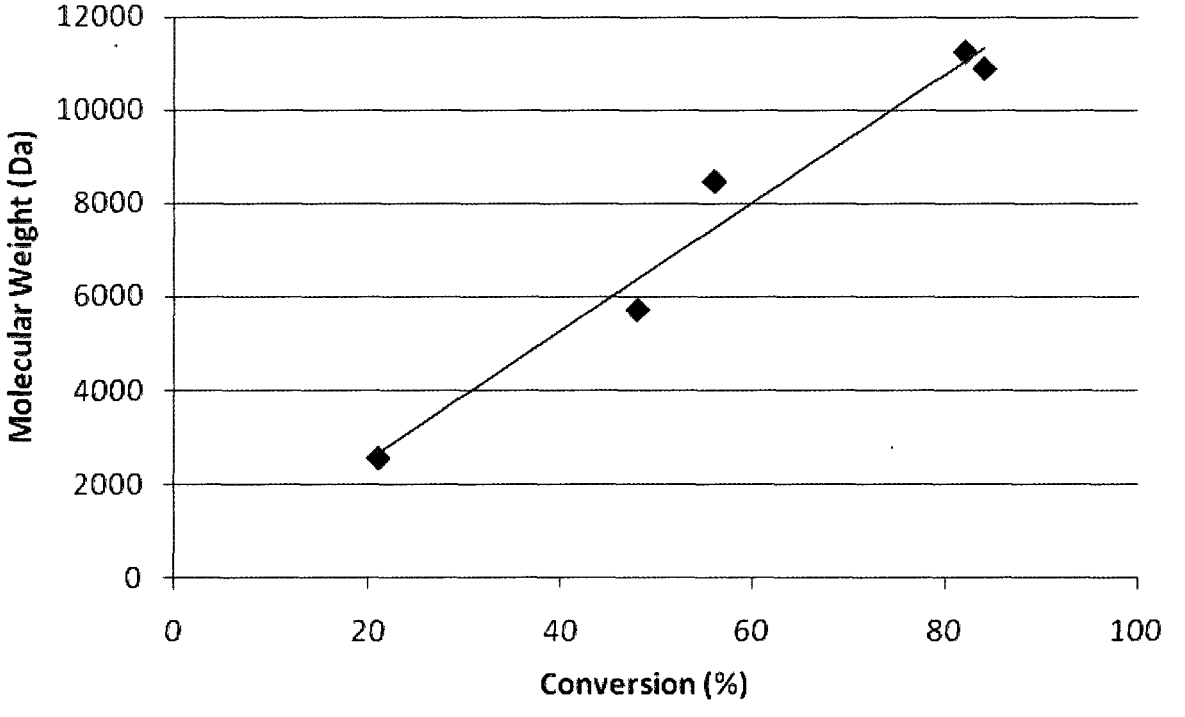

Figure 3.9. M_n vs. conversion for **17** [**8**]$(AlMe_2)_2$.

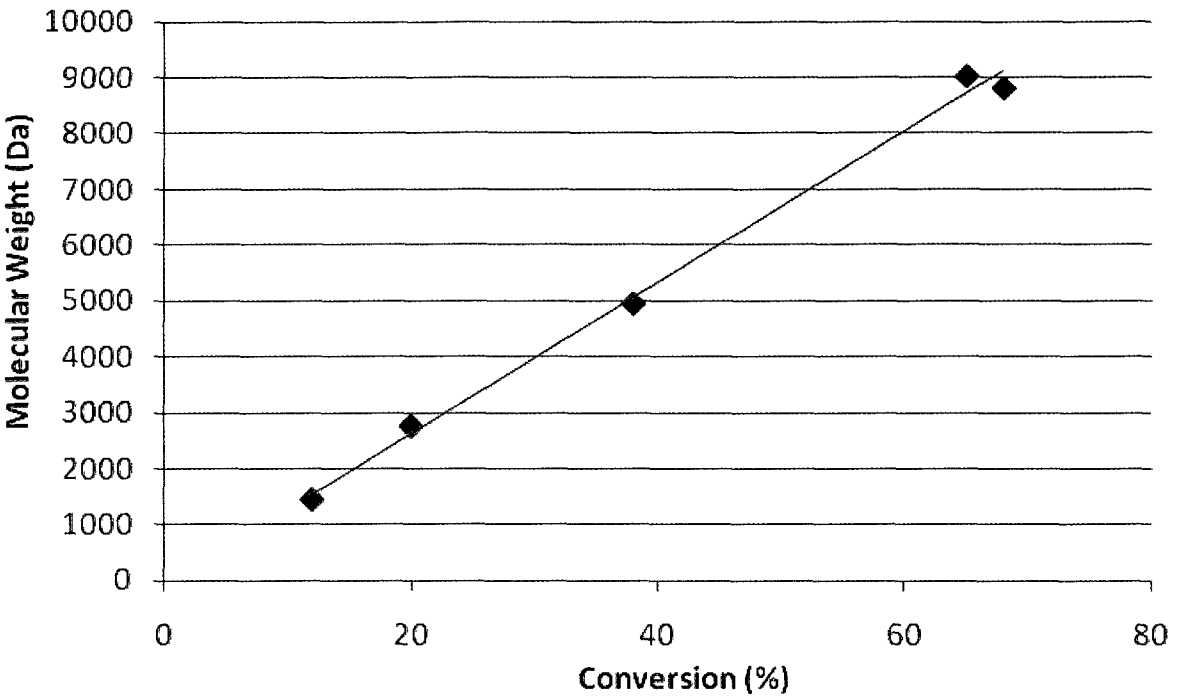

Figure 3.10. M_n vs. conversion for **18** [**9**]$(AlMe_2)_2$.

The plots of M_n vs conversion illustrate the living characteristics of our catalysts. Linear relationships with R^2 of 0.97-0.99 demonstrate this, along with our experimental observations of little induction period, monomodal GPC distributions and relatively good PDI values.

The rates of polymerization for these reactions (k_{obs}), was also calculated from the $\ln(M_o/M_t)$ vs time plot of each kinetic run. The plots revealed a linear character that deviated slightly with the last transesterification point. This point was omitted from the linear approximations. The results are summarized in Table 3.8, and illustrated with a representative plot, Figure 3.11.

Table 3.8. Rate data for bimetallic aluminum anilido-aldimine catalysts (**15-18**).

Catalyst	Linearity (R^2)	Rate (s^{-1})
15	0.997	2.00×10^{-5}
16	0.961	1.64×10^{-5}
17	0.985	2.80×10^{-5}
18	0.997	1.86×10^{-5}

The rates of these catalysts deviated between 1.64 and 2.80×10^{-5} s^{-1} which is considerably lower than those reported for the conventional lactide polymerization catalysts. The rate of polymerization for $Sn(Oct)_2$ has been reported as 1.4×10^{4}-4.56×10^{4} s^{-1} [259,260] which represents a dramatic increase in the rate over our most efficient catalyst. Aluminum salen initiators have been shown to possess k_{obs} first order rate constants in the range of 10^{1} s^{-1} still demonstrating an increase of 6 orders of magnitude in polymerization efficiency.[136]

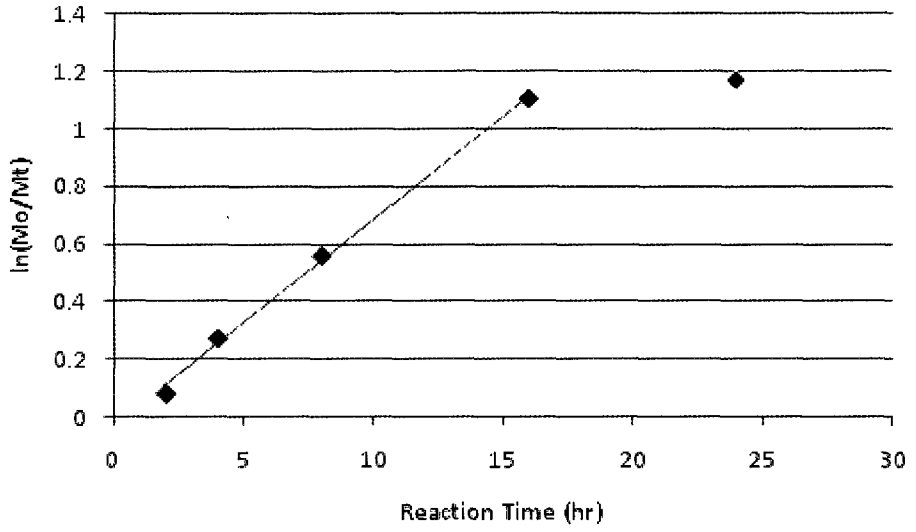

Figure 3.11. Kinetic plot of $\ln(M_o/M_t)$ vs. time (h) for **15** ([**6**]$(AlMe_2)_2$).

From the sample plot above the approximation of the rate (k_{obs}) from the linear part of the graph is observed. At higher conversion these bimetallic aluminum catalysts appear to undergo catalyst death. Drastic decreases in the conversion beyond the 16 h mark for all systems (**15-18**), indicate the loss of capacity for these systems. While this leveling off of the $\ln(M_o/M_t)$ vs. time plot can be a characteristic feature representing the point at which the monomer concentration has been depleted, polymerization rate is slowed and a monomer/polymer equilibrium is achieved,[260] this would not seem the case in these systems as conversion is maximized at ~70%.

The anilido-aldimine aluminum catalysts were also screened under neat polymerization conditions. The results from these studies are summarized in Table 3.9.

Table 3.9. Polymerization data for **15-18** @ 120°C.[a]

Catalyst	Conversion (%)	$M_{n,GPC}$	$M_{n,th}$	PDI
15	82	18626	9447	1.59
16	85	30539	9792	1.64
17	86	16132	9908	1.47
18	78	26507	8986	1.49

[a] Monomer:initiator:catalyst ratios of 200:2:1

Data collected for these bimetallic aluminum anilido-aldimine catalysts at 120°C revealed that at higher temperatures control over molecular weight is lost. The produced polymers, while exhibiting higher conversions and faster reaction times (3-4 hrs) were found to have much broader PDIs and uncorrelated M_n values. This was to be expected based upon the increased thermal energy that the system possessed and the more intimate reaction conditions in the absence of solvent.

In all cases these bimetallic aluminum catalysts (**15-18**) were found to possess no capacity for tacticity control in the polymerization of *rac*-lactide. Investigation of the decoupled ^{1}H NMR spectrum of the resultant PLA revealed the presence of the five possible tetrads arising from *rac*-lactide, characteristic of an atactic chain.

Experimentation with these complexes does not yield the desired monometallic product in all cases. The steric influence of the diisopropylphenyl and cyclohexyl substituents is thought to prevent a monometallic aluminum complex from forming. Investigations of smaller R groups such as isopropyl or *n*-alkyls, might allow for the formation of the desired geometry. Positively, this is the first report of these bimetallic complexes successfully polymerizating lactide, and while they do not control the polymerization (M_n variance and broad PDI as a result of the highly open co-ordination sphere), further investigations of these ligands with different substitution patterns could greatly enhance the quality of this family of catalysts.

Chapter Four

Conclusions and Future Work

4.1 Conclusions

A thorough examination of the effects of stereocontrol on the properties of PLA polymer stars has been completed. We have determined that the inclusion of stereoregularity into the polymer chain arms of DPE-centred stars of PLA derived from *rac*-lactide has had wide-ranging effects on the observed properties. Additonally we have developed a methodology for preparing these materials in neat molten monomer. By synthesizing these stars in the melt, and utilizing the solubilizing properties of our monomer, we have improved the efficiency of our reaction processes, both in terms of conversion and reaction rate. Removal of the reaction solvent has decreased the overall waste of the process, moving in the direction of greener reaction processes that produce less waste.

Thermal characterization of the prepared stars has revealed that transitions such as the T_g, T_m and T_c are all heavily dependant upon the tacticity of the stars. Atactic, heterotactic, isotactic-*rac* and isotactic-*L* stars have shown that an increase in the isotacticity bias leads to an increase in the T_g, T_m and also may reveal the presence of a T_c. Percent crystallinity (X_c) has also been

effected by the isotacticity bias. The thermal stability of these materials has been effectively enhanced by the introduction of stereocontrol. The presence of regularity in the tetrads has improved the onset stability of these PLA stars by 42°C. The isotactic-*rac* samples also exhibited the highest T_{max}, an artifact attributed to the possibility of stereocomplex behavior occurring during the precipitation/crystallization process.

The solution stability of these materials was also investigated. When stereocontrol was introduced to these samples, lifetimes of pressed PLA star pellets were enhanced by upwards of a factor of 7 when exposed to a harsh basic solution. Investigations at higher M_n reveal that these trends hold true with differences in molecular weight.

The tunable nature of these materials was investigated by varying the monomer composition of these stars to prepare isotactically biased stars with different P_m values. We determined that there was a direct correlation between the P_m, and the observed thermal, solution and X-ray properties of these materials. Additionally, the range at which these materials transition from an amorphous featureless arrangement to a more regular semi-crystalline polymeric material was pinpointed (60-70% isotactic).

Novel anilido-aldimine aluminum catalysts have also been prepared. Full characterization of these complexes by NMR spectroscopy and X-ray characterization of selected complexes reveals that they prefer a bimetallic structure, as opposed to the preferred and targeted monometallic species. Screening of these catalysts for lactide polymerization found them to be active, however control over the molecular weight, molecular weight distribution and the tacticty was found to be less than desirable in all cases, both at 70°C and at 120°C. Kinetic analysis revealed these catalysts to be slow initiators of ROP, with rates several orders of magnitude slower than conventional [salen]AlMe metal catalysts.

4.2 Future Work

There are several avenues of research that should be investigated to both enhance the totality of this work as well as extend it for various applications. The kinetics of star PLA formation has not been investigated, and a comparison of the rates for the $Sn(Oct)_2$, ^{Cl}[salan]AlMe and ^{tBu}[salen]AlMe catalysts employed in the production of linear polymers vs the star macroinitiators could be examined.

While it has been confirmed that all arms of DPE-centred PLA stars (M_n ~42000) are initiating, the true shape of these macromolecules is not known. Investigation of these materials by triple equipped GPC would allow for a determination of the radius of gyration and the hydrodynamic volume, parameters that would allow for qualified analysis about the overall shape of these stars, whether they be spherical or ellipsoid in solution. Expansion of this study to include different cores will allow for determination of its role in the observed polymer star properties.

While the propensity for these isotactically-biased PLA stars to exhibit a switch in materials properties from an amorphous to semi-crystalline polymer between 62 and 74% isotacticity has been confirmed, the exact value at which this transition occurs is not known. Further examination of this by careful polymerization of select monomer ratios could elucidate the actual P_m value where this transition occurs.

While we have extensively studied the DPE-PLA star polymer system, there exist other non-linear polymer architectures to which the stereoregularity strategy has yet to be applied. The production of stereoregular PLA polymer brushes, dendrimers or hyper-branched has yet to be explored. The ability to combine lactide with other cyclic monomers, (β-butyrolactone, ϵ-

caprolactone or glycolide for example), to create copolymers make this an expansive field. Combining ROP techniques with other polymerization strategies via multi-functional initiators, make the possibilities for new materials almost limitless.

While NMR spectroscopy suggested a bimetallic structure of the cyclohexyl substituted anilido-aldimine catalysts, X-ray characterization would allow for confirmation of these results and allow for a comparison of the cyclohexyl substituted complexes to the more widely studied diisopropylphenyl substituted anilido-aldimine ligand systems.

While our ligands have neglected the *ortho* and *para* aromatic substitutions documented for the salen frameworks, expansion of the ligand set to include these, as well as changing the linking group, will have wide ranging steric and electronic effects for the coordination sphere. These changes should alter the observed polymerization results, allowing for expanded tuning of this framework.

Chapter Five

Experimental

5.1 General Procedures

All chemicals and solvents were obtained from Sigma Aldrich unless otherwise stated. Purasorb *D,L*-lactide (PURAC Biomaterials) and *L*-lacitde were sublimed under vacuum twice prior to use. DPE (tech.) was recrystallized from ethyl acetate. 2,6-diisopropylaniline (90%), benzyl alcohol (99%), cyclohexylamine, and tin(II) *bis*(2-ethylhexanoate) were distilled under nitrogen prior to use.

Reagent grade pentane, tetrahydrofuran and toluene were collected from an Innovative Technologies glovebox equipped with an inline solvent purification system, consisting of alumina columns and a copper catalyst. The solvents were then degassed by three consecutive freeze-pump-thaw cycles. All other solvents were used as received.

All air-sensitive syntheses were performed in an MBraun Labmaster sp glovebox equipped with -35°C freezer, [O_2] and [H_2O] analyzers and built-in Siemens Simantic touch panel. All other inert atmosphere manipulations were performed under dinitrogen atmosphere on a dual manifold Schlenk line utilizing standard Schlenk techniques.

^{1}H and ^{13}C NMR spectra were collected on a 300 MHz Bruker Avance Spectrometer. GPC analyses were performed on a Polymer Laboratories PL-GPC 50 Plus system equipped with three 300 × 7.5 mm Resipore columns and a refractive index detector. Samples were dissolved and eluted in HPLC grade THF at a flow rate of 1 mL min^{-1} at 50°C. TGA analyses were carried out on a TA Instruments TGA Q500 under N_2 atmosphere with balance and purge flow rates of 40 and 60 mL min^{-1} respectively and a heating rate of 10°C min^{-1}. A furnace purging time of 15 minutes was employed prior to the start of data collection. DSC analyses were completed on a TA Instruments DSC Q100 in hermetically sealed aluminum pans. A flow rate of 50 mL min^{-1} and heating parameters of 5°C min^{-1} for heating and cooling were employed. Powder X-ray diffractograms were collected on a Bruker AXS Advance D8 diffractometer equipped with a graphite monochromator, variable divergence slit, variable antiscatter slit and a scintillation detector. Cu(Kα) radiation (λ = 1.542 Å), θ-2θ detection mode and 2-60° collection parameters were utilized. Samples were collected as loose powders on glass substrates.

Crystals of **14** and **16** were grown by precipitation from an ACN solution at -35°C. Single crystals were coated in Paratone-N oil, mounted using a polyimide MicroMount and frozen in the cold nitrogen stream of the goniometer. A hemisphere of data was collected on a Bruker AXS P4/SMART 1000 diffractometer using ω and θ scans with a scan width of 0.3° and 30 s exposure times. The detector distance was 5 cm. The data were reduced (SAINT) and corrected for absorption (SADABS). The structure was solved by direct methods and refined by full-matrix least squares on F^2(SHELXTL).

5.2 Syntheses

Synthesis of N,N'-bis(2-fluorobenzylidene)ethane-1,2-diamine (4)

12.0 g (96.7 mmol) of 2-fluorobenzaldehyde (124.11 g mol^{-1}) was dissolved in 30 mL ethanol in an Erlenmeyer flask. To this stirred solution was added 2.91 g (48.4 mmol) of 1,2-diaminoethane (60.1 g mol^{-1}) dropwise. To this solution was added several drops of formic acid (46.03 g mol^{-1}). Heat was evolved and the mixture was allowed to stir at room temperature for 12 h. The solution was then chilled (-25°C) and a white solid precipitated. This precipitate was collected by vacuum filtration and washed with cold EtOH. $C_{16}H_{14}F_2N_2$ (272.11 g mol^{-1}) Yield: 18.4 g (70%). ^1H NMR (300 MHz, $CDCl_3$, 25°C) δ: 8.62 (s, 2H, *H*C=N), 7.96 (td, 2H, Ar-*H*, 7.5 Hz, 2.0 Hz), 7.39 (m, 2H, Ar-*H*), 7.17 (t, 2H, Ar-*H*, 7.5 Hz), 7.06 (m, 2H, Ar-*H*), 4.02 (s, 4H, C*H*$_2$). ^{13}C NMR (75 MHz, $CDCl_3$, 25°C) δ: (164.1, 160.7, 132.3, 129.5, 127.9, 124.5, 115.8, 70.5).

Synthesis of N,N'-bis(2-fluorobenzylidene)propane-1,3-diamine (5)

12.0 g (96.7 mmol) of 2-fluorobenzaldehyde (124.11 g mol^{-1}) was dissolved in 30 mL ethanol in an Erlenmeyer flask. To this stirred solution was added 3.60 g (48.6 mmol) of 1,3-diaminopropane (74.15 g mol^{-1}) dropwise. To this solution was added several drops of formic acid (46.03 g mol^{-1}). Heat was evolved and the mixture was allowed to stir at room temperature for 12 hours. The solution was then chilled (-25°C) and a white solid precipitated. This precipitate was collected by vacuum filtration and washed with cold EtOH. $C_{17}H_{16}F_2N_2$ (286.13 g mol^{-1}) Yield: 17.4 g (63%). ^1H NMR (300 MHz, $CDCl_3$, 25°C) δ: 8.63 (s, 2H, *H*C=N), 8.00 (t, 2H, Ar-*H*, 7.5 Hz), 7.40 (m, 2H, Ar-*H*), 7.18 (t, 2H, Ar-*H*, 9.9 Hz), 7.08 (m, 2H, Ar-*H*) 3.77 (t, 4H, C*H*$_2$CH$_2$C*H*$_2$, 6.7 Hz), 2.15 (p, 2H, CH$_2$C*H*$_2$,CH$_2$, 6.8 Hz, 13.7 Hz). ^{13}C NMR (75 MHz, $CDCl_3$, 25°C) δ: (164.1, 160.8, 132.3, 128.0, 126.4, 124.6, 115.9, 59.9, 32.2).

Synthesis of N,N' –bis(2-(2,6-diisopropylphenylamino)benzylidene)ethane-1,2-diamine (6)

3.50 g (19.7 mmol) of 2,6-diisopropylaniline (177.29 g mol^{-1}) was dissolved in 12 mL of tetrahydrofuran (THF). To this stirred solution was added 12.4 mL (19.7 mmol) of *n*-butyllithium (1.6 M solution in hexanes) dropwise. Evolution of heat and gas was observed. Reaction contents were allowed to stir at room temperature for 12 h, at which point a gray solid was observed. This precipitate was collected by vacuum filtration and utilized without further purification. Yield: 3.25 g (90%). 3.25 g (17.7 mmol) of lithium 2,6-diisopropylanilide (183.22 g mol^{-1}) was added to 40 mL of THF to create a reaction slurry. This mixture was placed in an addition funnel and stored prior to use. Concurrently, 2.19 g (8.1 mmol) of **4** was dissolved in 5 mL of THF in a 125 mL Erlenmeyer flask and cooled to -35°C. The $LiC_{12}H_{18}N$ slurry was then added dropwise to a stirred and chilled solution of **4**. Solution changed from colorless to a deep red. Reaction was capped and allowed to stir at room temperature for 12 hours, at which point it was transferred to a sealed glass ampoule and removed from the glovebox. To this mixture was added 20 mL of deionized water sparged with N_2 gas. Solution changed from a deep red to orange color. The mixture was poured into a separatory funnel and extracted 3 times with hexanes (100 mL). The organic phase was collected and the aqueous phase discarded. The product was dried in vacuo to yield a yellow oil, which was recrystallized from acetonitrile (ACN) to afford a white product. $C_{40}H_{50}N_4$ (586.40 g mol^{-1}) Yield: 1.90 g (40%). ^{1}H NMR (300 MHz, $CDCl_3$, 25°C) δ: 10.47 (s, 2H, N*H*), 8.39 (s, 2H, *H*C=N), 7.33-7.20 (m, 4H Ar-*H*), 7.10 (m, 2H, Ar-*H*), 7.03 (m, 2H, Ar-*H*), 6.55 (m, 4H, Ar-*H*), 6.16 (m, 2H, Ar-*H*), 3.90 (s, 4H, CH_2CH_2), 3.07 (s, 4H, CH_3CHCH_3), 1.27 (dd, 24H, CH_3, 5.8 Hz, 3.6 Hz). ^{13}C NMR (75 MHz, $CDCl_3$, 25°C) δ: (161.0, 142.3, 138.8, 132.1, 131.3, 127.7, 125.8, 124.4, 123.1, 119.1, 115.7, 62.3, 28.5, 23.5, 23.3).

Synthesis of N,N' –bis(2-(2,6-diisopropylphenylamino)benzylidene)propane-1,3-diamine (7)

3.50 g (19.7 mmol) of 2,6-diisopropylaniline (177.29 g mol^{-1}) was dissolved in 12 mL of tetrahydrofuran (THF). To this stirred solution was added 12.4 mL (19.7 mmol) of *n*-butyllithium (1.6 M solution in hexanes) dropwise. Evolution of heat and gas was observed. Reaction contents were allowed to stir at room temperature for 12 h, at which point a gray solid was observed. This precipitate was collected by vacuum filtration and utilized without further purification. Yield: 3.25 g (90%). 3.25 g (17.7 mmol) of lithium 2,6-diisopropylanilide (183.22 g mol^{-1}) was added to 40 mL of THF to create a reaction slurry. This mixture was placed in an addition funnel and stored prior to use. Concurrently, 2.32 g (8.1 mmol) of **5** was dissolved in 5 mL of THF in a 125 mL Erlenmeyer flask and cooled to -35°C. The $LiC_{12}H_{18}N$ slurry was then added dropwise to a stirred and chilled solution of **5**. The solution changed from colorless to a deep red. The reaction was capped and allowed to stir at room temperature for 12 h, at which point it was transferred to a sealed glass ampoule and removed from the glovebox. To this mixture was added 20 mL of deionized water sparged with N_2 gas. The solution changed from a deep red to orange color. The mixture was poured into a separatory funnel and extracted 3 times with hexanes (100 mL). The organic phase was collected and the aqueous phase discarded. Product was dried in vacuo to yield a yellow oil, which was recrystallized from acetonitrile (ACN) to afford a white product. $C_{41}H_{52}N_4$ (600.88 g mol^{-1}) Yield: 2.19 g (45%). ^{1}H NMR (300 MHz, $CDCl_3$, 25°C) δ: 10.42 (s, 2H, N*H*), 8.42 (s, 2H, *H*C=N), 7.33 (m, 2H Ar-*H*), 7.17 (m, 2H, Ar-*H*), 7.00 (m, 2H, Ar-*H*), 6.58 (m, 4H, Ar-*H*), 6.24 (m, 2H, Ar-*H*), 3.90 (m, 4H, $CH_2CH_2CH_2$), 3.07 (m, 4H, CH_3CHCH_3), 2.22, (p, 2H, $CH_2CH_2CH_2$, 6.8 Hz, 13.7 Hz), 1.27 (dd, 24H, CH_3, 5.9 Hz, 3.7 Hz). ^{13}C NMR (75 MHz, $CDCl_3$, 25°C) δ: (162.3, 144.7, 138.6, 132.3, 131.3, 128.3, 125.4, 124.6, 123.6, 119.4, 116.1, 62.5, 32.6, 28.9, 23.8, 23.5).

Synthesis of N,N' –bis(2-(cyclohexylamino)benzylidene)ethane-1,2-diamine (8)

5.50 g (55.5 mmol) of cyclohexylamine (99.17 g mol^{-1}) was dissolved in 12 mL of tetrahydrofuran (THF). To this stirred solution was added 34.7 mL (55.5 mmol) of *n*-butyllithium (1.6 M solution in hexanes) dropwise. Evolution of heat and gas was observed. Reaction contents were allowed to stir at room temperature for 12 h, at which point a gray solid was observed. This precipitate was collected by vacuum filtration and utilized without further purification. Yield 5.25 g (90%). 2.50 g (23.9 mmol) of lithium cyclohexylamide (105.1 g mol^{-1}) was added to 40 mL of THF to create a reaction slurry. This mixture was placed in an addition funnel and stored prior to use. Concurrently, 3.21 g (11.8 mmol) of **4** was dissolved in 10 mL of THF in a 125 mL Erlenmeyer flask and cooled to -35°C. The $LiC_6H_{12}N$ slurry was then added dropwise to a stirred and chilled solution of **4**. The solution changed from colorless to a deep red. Reaction was capped and allowed to stir at room temperature for 12 h, at which point it was transferred to a sealed glass ampoule and removed from the glovebox. To this mixture was added 20 mL of deionized water sparged with N_2 gas. The solution changed from a deep red to orange color. The mixture was poured into a separatory funnel and extracted 3 times with hexanes (100 mL). The organic phase was collected and the aqueous phase discarded. The product was dried in vacuo to reveal an impure red oil. This oil (2.50 g) was loaded on a packed alumina column (25 g) pretreated with 50 mL of 1% (v,v) solution of triethylamine (NEt_3) and hexane. The product was eluted with hexanes (300 mL) to afford a yellow oil. $C_{28}H_{38}N_4$ (430.31 g mol^{-1}) Yield: 1.02 g (20%). ^{1}H NMR (300 MHz, $CDCl_3$, 25°C) δ: 9.44 (br s, 2H, N*H*), 8.37 (s, 2H *H*C=N), 8.00 (m, 2H, Ar-*H*), 7.39 (m, 2H, Ar-*H*) 6.70 (m, 2H, Ar-*H*) 6.57 (m, 2H, Ar-*H*) 3.48 (s, 4H, CH_2CH_2) 2.56 (m, 2H, NHC*H*C_5H_{10}), 2.00-1.05 (m, 20H, 2(C_5H_{10})). ^{13}C NMR (75 MHz, $CDCl_3$, 25°C) δ: (162.0, 149.6, 133.8, 133.4, 117.3, 114.6, 113.8, 61.9, 61.2, 33.4, 26.7, 25.1).

Synthesis of N,N' –bis(2-(cyclohexylamino)benzylidene)propane-1,3-diamine (9)

5.50 g (55.5 mmol) of cyclohexylamine (99.17 g mol^{-1}) was dissolved in 12 mL of tetrahydrofuran (THF). To this stirred solution was added 34.7 mL (55.5 mmol) of *n*-butyllithium (1.6 M solution in hexanes) dropwise. Evolution of heat and gas was observed. Reaction contents were allowed to stir at room temperature for 12 hours, at which point a gray solid was observed. This precipitate was collected by vacuum filtration and utilized without further purification. Yield: 5.25 g (90%). 2.50 g (23.9 mmol) of lithium cyclohexylamide (105.1 g mol^{-1}) was added to 40 mL of THF to create a reaction slurry. This mixture was placed in an addition funnel and stored prior to use. Concurrently, 3.38 g (11.8 mmol) of **5** was dissolved in 10 mL of THF in a 125 mL Erlenmeyer flask and cooled to -35°C. The $LiC_6H_{12}N$ slurry was then added dropwise to a stirred and chilled solution of **5**. Solution changed from colorless to a deep red. The reaction was capped and allowed to stir at room temperature for 12 h, at which point it was transferred to a sealed glass ampoule and removed from the glovebox. To this mixture was added 20 mL of deionized water sparged with N_2 gas. The solution changed from a deep red to orange color. The mixture was poured into a separatory funnel and extracted 3 times with hexanes (100 mL). The organic phase was collected and the aqueous phase discarded. The product was dried in vacuo to reveal an impure red oil. This oil (1.50 g) was loaded on a packed alumina column (25 g) pretreated with 50 mL of 1% (v,v) solution of triethylamine (NEt_3) and hexanes. The product was eluted with hexanes (300 mL) to afford a yellow oil. $C_{29}H_{40}N_4$ (444.33 g mol^{-1}) Yield: 0.786 g (15%). ^1H NMR (300 MHz, $CDCl_3$, 25°C) δ: 9.41 (s, 2H, N*H*) 8.34 (s, 2H, *H*C=N) 7.98 (m, 2H, Ar-*H*) 7.18 (m, 2H, Ar-*H*) 6.67 (m, 2H, Ar-*H*) 6.56 (m, 2H, Ar-*H*) 3.11 (m, 4H, $CH_2CH_2CH_2$) 2.55 (m, 2H, $NHCHC_5H_{10}$), 2.07-1.14 (m, 22H, $CH_2CH_2CH_2$ and $(C_5H_{10})_2$).

^{13}C NMR (75 MHz, $CDCl_3$, 25°C) δ: (161.7, 149.8, 134.5, 133.2, 117.7, 114.2, 113.6, 62.3, 61.6, 33.1, 33.0, 26.5, 25.4).

Syntheses of anilido-aldimine aluminum complexes (15-18)

Synthesis of [6](AlMe$_2$)$_2$ (15)

1.00 g (1.71 mmol) of **6** was dissolved in 3 mL of toluene, in a glass ampoule equipped with mechanical stir bar. To this stirred solution was added 1.71 mL of trimethylaluminum (TMA, 2.0 M solution in heptane), dropwise with stirring. Heat and evolution of gas was observed. The glass ampoule was sealed, removed from glovebox and allowed to stir at 110°C for 24 h. Solvent was removed under reduced pressure to reveal an impure orange solid. Washing with pentane gave the aluminum complex in high yield. $C_{44}H_{60}NAl_2N_4$ (698.44 g mol^{-1}) Yield: 0.893 g (75%). ^1H NMR (300 MHz, C_6D_6, 25°C) δ: 7.67 (s, 2H, *H*C=N), 7.37-7.06 (m, 8H, Ar-*H*), 6.82 (d, 2H, Ar-*H*, 9.0 Hz), 6.34 (t, 2H, Ar-*H*, 7.0 Hz) 3.90 (s, 4H, C*H*$_2$C*H*$_2$), 3.48 (m, 4H, CH$_3$C*H*CH$_3$), 1.48 (d, 12H, C*H*$_3$, 7.0 Hz), 1.18 (d, 12H, C*H*$_3$, 7.0 Hz), -0.33 (s, 12H, Al-C*H*$_3$). ^{13}C NMR (75 MHz, C_6D_6, 25°C) δ: (161.0, 142.3, 138.8, 132.1, 131.3, 127.7, 125.8, 124.4, 123.1, 119.1, 115.7, 62.3, 28.5, 23.6, 23.3, -9.1).

Synthesis of [7](AlMe$_2$)$_2$ (16)

1.00 g (1.66 mmol) of **7** was dissolved in 3 mL of toluene, in a glass ampoule equipped with mechanical stir bar. To this stirred solution was added 1.66 mL of trimethylaluminum (TMA, 2.0 M solution in heptane), dropwise with stirring. Heat and evolution of gas was observed.The glass ampoule was sealed, removed from glovebox and allowed to stir at 110°C for 24 h. Solvent was removed under reduced pressure to reveal an impure orange solid. Washing with pentane gave the aluminum complex in high yield. $C_{45}H_{62}Al_2N_4$ (712.46 g mol^{-1}) Yield: 0.972 g (82%). ^{1}H NMR (300 MHz, C_6D_6, 25°C) δ: 7.57 (s, 2H, *H*C=N), 7.35-7.10 (m, 8H, Ar-*H*), 6.94 (d, 2H, Ar-*H*, 9 Hz), 6.43 (t, 2H, Ar-*H*, 7.0 Hz), 3.90 (m, 4H, C*H*$_2$CH$_2$C*H*$_2$), 3.50 (m, 2H, CH$_2$C*H*$_2$CH$_2$), 3.17 (m, 4H, CH$_3$C*H*CH$_3$), 1.48 (d, 12H, C*H*$_3$, 7.0 Hz), 1.18(d, 12H, C*H*$_3$, 7.0 Hz), -0.34 (s, 12H, Al-C*H*$_3$). ^{13}C NMR (75 MHz, C_6D_6, 25°C) δ: (162.3, 144.7, 138.6, 132.3, 131.3, 128.3, 125.4, 124.6, 123.6, 119.4, 116.1, 62.5, 32.6, 28.9, 23.8, 23.5, -9.1).

Synthesis of [8](AlMe$_2$)$_2$ (17)

1.00 g (2.32 mmol) of **8** was dissolved in 3 mL of toluene, in a glass ampoule equipped with mechanical stir bar. To this stirred solution was added 2.32 mL of trimethylaluminum (TMA, 2.0 M solution in heptane), dropwise with stirring. Heat and evolution of gas was observed. The glass ampoule was sealed, removed from glovebox and allowed to stir at 110°C for 24 h. Solvent was removed under reduced pressure to reveal an impure orange solid.. Washing with pentane revealed the aluminum complex in high yield. $C_{32}H_{48}Al_2N_4$ (542.71 g mol^{-1}) Yield: 0.820 g (65%). ^{1}H NMR (300 MHz, C_6D_6, 25°C) δ: 7.57 (s, 2H, *H*C=N), 7.22-7.14 (m, 4H, Ar-*H*), 6.84 (d, 2H, Ar-*H*, 8 Hz), 6.42 (t, 2H, Ar-*H*, 7 Hz), 3.48 (s, 4H, C*H*$_2$C*H*$_2$) 2.56 (m, 2H, NHC*H*C$_5$H$_{10}$)

2.00-1.05 (m, 20H, $(C_5H_{10})_2$), -0.17 (s, 12H, Al-CH_3). ^{13}C NMR (75 MHz, C_6D_6, 25°C) δ: (162.0, 149.6, 133.8, 133.4, 117.3, 114.6, 113.8, 61.9, 61.2, 33.4, 26.7, 25.1, -5.1).

Synthesis of [9](AlMe$_2$)$_2$ (18)

1.00 g (2.25 mmol) of **9** was dissolved in 3 mL of toluene, in a glass ampoule equipped with mechanical stir bar. To this stirred solution was added 2.25 mL of trimethylaluminum (TMA, 2.0 M solution in heptane), dropwise with stirring. Heat and evolution of gas was observed. The glass ampoule was sealed, removed from glovebox and allowed to stir at 110°C for 24 h. Solvent was removed under reduced pressure to reveal an impure orange solid. Washing with pentane revealed the aluminum complex in high yield. $C_{33}H_{50}Al_2N_4$ (556.74 g mol^{-1}) Yield: 0.852 g (68%). ^1H NMR (300 MHz, C_6D_6, 25°C) δ: 7.57 (s, 2H, HC=N), 7.22-7.14 (m, 4H, Ar-*H*), 6.84 (d, 2H, Ar-*H*, 8 Hz), 6.42 (t, 2H, Ar-*H*, 7 Hz), 3.48 (m, 4H, $CH_2CH_2CH_2$), 3.22 (m, 2H, $CH_2CH_2CH_2$), 2.56 (m, 2H, $NHCHC_5H_{10}$) 2.00-1.05 (m, 20H, $2(C_5H_{10})$), -0.17 (s, 12H, Al-CH_3). ^{13}C NMR (75 MHz, C_6D_6, 25°C) δ: (161.7, 149.8, 134.5, 133.2, 117.7, 114.2, 113.6, 62.3, 61.6, 33.1, 33.0, 26.5, 25.4, -10.4).

Synthesis of N,N'-bis(3,5-di-*tert*-butyl-2-hydroxybenzaldehyde)-1,3-propanediamine[155]

This compound was prepared according to a modified literature method.[155] To a stirring solution of 3,5-di-tert-butyl-2-hydroxybenzaldehyde (5.00 g, 21.3 mmol, 234.34 g mol^{-1}) in ethanol (60 mL) was added 1,3-propanediamine (0.790 g, 10.65 mmol) at room temperature. The reaction mixture was allowed to warm to reflux temperature (90°C) and heated for 12 h. Yellow precipitate was observed to form, and this precipitate was then collected by vacuum filtration and washed with cold EtOH to obtain a yellow solid. $C_{33}H_{50}N_2O_2$ (506.76 g mol^{-1}) Yield 2.69 g

(50%) ^{1}H NMR (300 MHz, $CDCl_3$, 25°C) δ: 8.42 (s, 2H, *H*C=N), 7.44 (d, 2H, Ar-*H,* 2.3 Hz), 7.10 (d, 2H, Ar-*H,* 2.3), 3.73 (t, 4H, N($CH_2CH_2CH_2$)N, 6.4 Hz), 2.17 (q, 2H, N($CH_2CH_2CH_2$)N, 6.5 Hz), 1.49 (s, 18H, ArC(CH_3)$_3$), 1.31 (s, 18H, ArC(CH_3)$_3$). ^{13}C NMR (75 MHz, $CDCl_3$, 25°C) δ: (166.49, 158.13, 140.051, 136.70, 126.97, 125.83, 117.84, 56.71, 35.023, 34.06, 31.69, 31.54, 29.46).

Synthesis of N,N'-dibenzyl-N,N'-bis[(3,5-dichloro-2-hydroxyphenyl)methylene]-1,2-diaminoethane[147]

This compound was prepared according to a modified literature method.[147] To a mixture of 2,4-dichlorophenol (10.0 g, 61.3 mmol, 163.00 g mol^{-1}) and N,N'-dibenzylethylenediamine (7.33 g, 30.5 mmol, 240.35 g mol^{-1}) in ethanol (150 mL) was added paraformaldehyde (1.84 g, 61.3 mmol) at reflux temperature (90°C). Disappearance of para-formaldehyde was noticed to occur gradually, giving a clear solution after 2 h. The solution was allowed to stir overnight (12 h), and precipitate was observed to form upon cooling to room temperature. The precipitate was then collected by vacuum filtration and washed with EtOH to obtain a white solid. $C_{30}H_{28}Cl_4N_2O_2$ (590.37 g mol^{-1}) Yield: 3.62 g (20 %).^{1}H NMR (300 MHz, $CDCl_3$, 25°C) δ: 11.52 (br s, 2H, *OH*), 7.38-7.25 (m, 8H, Ar-*H*), 7.17-7.11 (m, 4H, Ar-*H*), 6.80 (d, 2H, Ar-*H*, 2.5 Hz), 3.64 (s, 4H, N$CH_2C_6H_4OH$), 3.54 (s, 4H, N$CH_2C_6H_5$), 2.65 (s, 4H, N(CH_2CH_2)N). ^{13}C NMR (75 MHz, $CDCl_3$, 25°C) δ: (152.17, 135.58, 129.42, 128.97, 128.99, 128.24, 126.82, 123.82, 123.60, 122.59, 58.94, 57.94, 50.12).

Synthesis of ^{tBu}[salen]AlMe (1)

This compound was prepared according to a modified literature method.[155] N,N'-bis(3,5-di-*tert*-butyl-2-hydroxybenzaldehyde)-1,3-propanediamine (2.50 g, 4.93 mmol) was dissolved in 10 mL toluene in a glass ampoule equipped with magnetic stir bar. To this stirred solution was added TMA (2.47 mL, 2.0 M in heptane) dropwise. Heat and gas were evolved. Glass ampoule was sealed and reaction contents were allowed to stir at 110°C for 12 h. A yellow solid was observed to precipitate from solution. The precipitate was collected by vacuum filtration and washed with cold toluene to reveal the desired product as a yellow solid. $C_{34}H_{51}AlN_2O_2$ (546.76 g mol^{-1}) Yield: 1.40 g, (52%). ^{1}H NMR (300 MHz, C_6D_6, 25°C) δ: 7.75 (d, 2H, Ar-*H*, 2.4 Hz), 7.34 (s, 2H, *H*C=N), 6.89 (d, 2H, Ar-*H*, 2.4), 3.07 (m, 2H, N(CH'*H*CH$_2$CH'*H*)N), 2.75 (m, 2H, N(C*H*'HCH$_2$C*H*'H)N), 1.79 (s, 18H, ArC(C*H*$_3$)$_3$), 1.37 (m, 2H, N(CH$_2$C*H*$_2$CH$_2$)N and s, 18H, ArC(C*H*$_3$)$_3$), -0.37 (s, 3H, AlC*H*$_3$). ^{13}C NMR (75 MHz, C_6D_6, 25°C) δ: (170.15, 164.12, 141.29, 137.48, 130.25, 127.45, 118.89, 54.94, 35.94, 34.16, 31.68, 30.18, 27.38).

Synthesis of ^{Cl}[salan]AlMe

This compound was prepared according to a modified literature method.[147] N,N'-dibenzyl-N,N'-bis[(3,5-dichloro-2-hydroxyphenyl)methylene]-1,2-diaminoethane (3.00g, 5.08 mmol) was dissolved in 15 mL toluene in a glass ampoule equipped with magnetic stirring bar. To this stirred solution was added TMA (2.54 mL, 2.0 M in heptane) dropwise. Heat and gas were evolved. The glass ampoule was sealed and the reaction contents were allowed to stir at 110°C for 12 h to yield a cloudly solution. Solvent was removed *in vacuo* to reveal the desired product as a white solid. $C_{31}H_{29}AlCl_4N_2O_2$ (630.37 g mol^{-1}) Yield: 1.28 g (40%). ^{1}H NMR (300 MHz, C_6D_6, 25°C) δ: 7.39 (d, 2H, Ar-*H*, 2.6 Hz), 7.06-7.01 (m, 6H, Ar-*H*), 6.86-6.81 (m, 4H, Ar-*H*), 6.56 (d, 2H, Ar-*H*, 2.6 Hz), 5.1 – 3.2 (br m, 4H, NC*H*$_2$C$_6$H$_4$OH), 3.26 (br s, 4H, NC*H*$_2$C$_6$H$_5$),

2.5 – 1.5 (br m, 4H, N(CH_2CH_2)N), -0.25 (s, 3H, AlCH_3). ^{13}C NMR (75 MHz, C_6D_6, 25°C) δ: 154.95, 132.23, 130.99, 129.89, 129.11, 128.71, 127.14, 126.37, 123.04, 120.79, 57.12, 56.51, 46.75, -8.19 ($AlCH_3$).

Synthesis of DPE-PLA stars under solvent-free reaction conditions

Rac or *L*-lactide (0.50 g, 3.52 mmol), DPE (1.50×10^{-2} g, 0.059 mmol) and $Sn(Oct)_2$ (4.20×10^{-2} g, 0.354 mmol) were loaded into a glass ampoule equipped with mechanical stir bar. The ampoule was sealed and heated to 120°C for the desired reaction time. The ampoule was removed from the heating bath and the contents were disolved through addition of a 10:1 v/v solution of CH_2Cl_2 and MeOH. The solution was allowed to stir at room temperature for 0.5 h, at which point it was precipitated by dropwise addition into chilled (-15°C) and stirring MeOH (100 mL). The supernatant was decanted to reveal the resulting polymer, which was dried *in vacuo* and weighed. The need for reprecipitation was determined by ^{1}H NMR or TGA.

Synthesis of DPE-PLA stars under solvent-based reaction conditions

Rac or *L*-lactide (0.50 g, 3.52 mmol), DPE (1.50×10^{-2} g, 0.059 mmol) and $Sn(Oct)_2$ (4.20×10^{-2} g, 0.354 mmol) were loaded into a glass ampoule equipped with mechanical stir bar and disolved in 5 mL of toluene. The ampoule was sealed and heated to 120°C for the desired reaction time. The ampoule was removed from the heating bath and the reaction was quenched by addition of 1 mL of MeOH. The solution was allowed to stir at room temperature for 0.5 h, at which point it was precipitated by dropwise addition into chilled (-15°C) and stirring MeOH (100 mL). The supernatant was decanted to reveal the resulting polymer, which was dried *in vacuo* and weighed. The need for reprecipitation was determined by ^{1}H NMR or TGA. ^{1}H NMR (300 MHz,

$CDCl_3$, 25°C) δ: 5.16 (m, PLA-C*H*), 4.35 (m, PLA-CH_{last}, 4.12 (dd, 6H, OCH_2CCH_2), 3.32 (s, 4H, OCH_2), 2.66 (d, O*H*), 1.55 (m, PLA-CH_3). ^{13}C NMR (75 MHz, $CDCl_3$, 25°C) δ: (169.62, 72.08, 71.72, 69.32, 66.53, 16.86).

Degradation of DPE-PLA polymer stars

Pellets of DPE-PLA stars of various tacticities were pressed under 2000 psi (d =1.3 cm, m = 200 mg). The pellets were exposed to a solution of 1,5,7-triazabicyclo[4.4.0]dec-5-ene (TBD) in methanol at a concentration of 4.34×10^{-2} M. The samples were agitated at 23°C and monitored until all PLA had dissolved in solution. The resultant solution contents were then analyzed by ^{1}H NMR spectroscopy to reveal oligomeric PLA chains.

References

1. T. Yamakawa, S. Ahmed and A.L. Kelston, *BRICs Monthly*, 2009, **7**, 15-17.

2. General Motors, Retrieved from www.gm.com on 1/30/2011.

3. M. K. Hubbert, *Spring Meeting of the Southern District, American Petroleum Institute,* 1956, 22-27.

4. R. Heinemann, *Oil Gas J.* 2006, **104**, 17-20.

5. World Coal Institute, Retrieved from www.worldcoal.org on 2/5/2011.

6. M. Margolis, *The Age of Extreme Offshore Oil is Just Beginning*, Discover Magazine, 2010, **9**, 7.

7. A. D. Chandler, *Shaping the Industrial Century: The Remarkable Story of the Evolution of the Modern Chemical and Pharmaceutical Industries.* Harvard University Press, 2005.

8. M. Braungart and W. McDonough, *Cradle to Cradle: Remaking the Way We Make Things.* North Point Press, 2002.

9. Worldwatch Institute, Retrieved from http://www.worldwatch.org/research on 2/4/2011.

10. J. M. Coe, D. B. Rogers, eds. *Marine Debris: Sources, Impacts, and Solutions.* New York: Springer-Verlag, 1996.

11. R. Rudel and L. Perovich, *Atmos. Environ.* 2008, **43**, 170-181.

12. U. Heudorf, V. Mersch-Sundermann and J. Angerer, *Int. J. Hyg. Environ. Health*, 2007, **210**, 623-634.

13. S. Sathyanarayana, C. J. Karr, P. Lozana, E. Brown, A. M. Calafat, F. Liu and S. H. Swan, *Pediatrics*, 2008, **121**, 260-268.

14. S. B. Lee, Y. H. Kim, M. S. Chong and Y. M. Lee, *Biomaterials*, 2004, **25**, 2309-2317.

15. R. D. Fields, F. Rodriguez and R. K. Finn, *J. Appl. Polym. Sci.* 1974, **18**, 3571-3579.

16. J. Yang, L. Jia, Q. Hao, Y. Li, Q. LI, Q. Fang and A. Cao, *Macromol. Biosci.* 2005, **5**, 896-903.

17. K. J. Zhu, R. W. Hendren, K. Jensen and C. G. Pitt, *Macromolecules*, 1991, **24**, 1736-1740.

18. D. Jendrossek, I. Knoke, R. B. Habibian, A. Steinbuchel and H. G. Schlegel, J. Polym. Environ. 1991, **1**, 53-63.

19. M. P. Shaver, D. J. A. Cameron, *Biomacromolecules*, 2010, **11**, 3673-3679.

20. M. P. Shaver, M. R. Perry, *Can. J. Chem*, 2011, **89**, 499-505.

21. C-W. Lou, Y-S. Chen, T-C. Hsieh, J-H. Lin and W-H. Hsing, *Text. Res. J.* 2008, **78**, 958-965.

22. A. Lafont, S. Li, H. Garreau, F. Cornhill and M. Vert, *J. Biomed, Mater. Res. B Appl. Biomater.* 2006, **77**, 349-356.

23. C. R. Chu, R. D. Coutts, M. Yoshioka, F. L. Harwood, A. Z. Monosov and D. Amiel. *J. Biomed. Mater. Res.* 1995, **29**, 1147-1154.

24. W. A. Chan, T. B. Bini, S. V. Venkatraman and F. Y. C. Boey. *J. Biomed. Mater. Res. A.* 2005, **79**, 47-52.

25. M. Denti, P. Randelli, D. Lo Vetere, M. Moioli and M. Tagliabue. J. Orthop. Traumatol. 2004, **5**, 151-155.

26. J. C. Bogaert and P. Coszach, *Macromol. Symp.* 2000, **153**, 287-303.

27. F. Rancan, D. Papakostas, S. Hadam, S. Hackbarth, T. Delair, C. Primard, B. Verrier, W. Sterry, U. Blume-Peytavi and A. Vogt. *Pharm. Res.* 2009, **26**, 2027-2036.

28. Nature Works LLC, Retrieved from http://www.natureworksllc.com/ on 1/30/2011.

29. L. Averous in *Monomers, Polymers and Composites from renewable resources,* Ed. N. Belgacem and A. Gandini, Elsevier Limited Publication, 2008, 433-450.

30. S.-H. Hyon, K. Jamshidi and Y. Ikada, *Biomaterials* 1997, **18**, 1503-1508.

31. N. Takeda and S. Inoue, *Makromol. Chem.* 1978, **179**, 1377-1381.

32. G. J. Van Hummel, S. Harkema, F. E. Kohn and J. Feijen. *Acta Crystallogr., Sect. B* 1982, **B38**, 1679-1681.

33. A. Duda and S. Penczek. *Macromolecules* 1990, **23**, 1636-1639.

34. R. E. Drumright, P. R. Gruber and D. E. Henton. *Adv. Mater.* 2000, **12**, 1841-1846.

35. R. A. Auras, L.-T. Lim, S. E. M. Selke, H. Tsuji in *Poly(lactic Acid): Synthesis, Structures, Properties, Processing, and Application*. New Jersey: John Wiley & Sons, Inc. 2010.

36. K. Numata, R. K. Srivastava, A. Finne-Wistrand, A.-C. Albertsson, Y. Doi and H. Abe, *Biomacromolecules* 2007, **8**, 3115-3125.

37. S. Matsumura, K. Mabuchi and K. Toshima, *Macromol. Rapid Commun.* 1997, **18**, 477-482.

38. H. Dong, H.-D. Wang, S.-G. Cao and J.-C. Shen. *Biotechnol. Lett.* 1998, **20**, 905-908.

39. H. R. Kricheldorf and I. Kreiser-Saunders, *Makromol. Chem.* 1990, **191**, 1057-1066.

40. J. E. Kasperczyk, *Macromolecules* 1995, **28**, 3937-3939.

41. H. R. Kricheldorf and R. Dunsing, *Makromol. Chem.* 1986, **187**, 1611-1625.

42. H. R. Kricheldorf and I. Kreiser, *Makromol. Chem.* 1987, **188**, 1861-1873.

43. X. Lou, C. Detrembleur and R. Jerome, *Macromolecules* 2002, **35**, 1190-1195.

44. Y. Shibasaki, H. Sanada, M. Yokoi, F. Sanda and T. Endo, *Macromolecules* 2000, **33**, 4316-4320.

45. D. Bourissou, B. Martin-Vaca, A. Dumitrescu, M. Graullier and F. Lacombe, *Macromolecules* 2005, **38**, 9993-9998.

46. D. A. Culkin, W. Jeong, S. Csihony, E. D. Gomez, N. P. Balsara, J. L. Hedrick and R. M. Waymouth, *Angew. Chem., Int. Ed.* 2007, **46**, 2627-2630.

47. R. C. Pratt, B. G. G. Lohmeijer, D. A. Long, R. M. Waymouth and J. L. Hedrick, *J.*

Am.Chem. Soc. 2006, **128**, 4556-4557.

48. S. Csihony, D. A. Culkin, A. C. Sentman, A. P. Dove, R. M. Waymouth and J. L. Hedrick, *J. Am. Chem. Soc.* 2005, **127**, 9079-9084.
49. A. P. Dove, H. Li, R. C. Pratt, B. G. G. Lohmeijer, D. A. Culkin, R. M. Waymouth and J. L. Hedrick, *Chem. Commun.* 2006, 2881-2883.
50. F. Nederberg, E. F. Connor, M. Moller, T. Glauser and J. L. Hedrick, *Angew. Chem. Int. Ed.* 2001, **40**, 2712-2715.
51. A. D. McNaught and A. Wilkinson, *Compendium of chemical terminoloy: IUPAC recommendations*. Blackwell Science: Oxford, 1997.
52. P. Dubois, C. Jacobs, R. Jerome and P. Teyssie, *Macromolecules* 1991, **24**, 2266-2270.
53. H. R. Kricheldorf, M. Berl and N. Scharnagl, *Macromolecules* 1988, **21**, 286-293.
54. C. Shih, *J. Control Release*, 1995, **34**, 9-15.
55. M.J. Stanford and A.P. Dove, *Macromolecules*, 2009, **42**, 141-147.
56. J. M. Berg, J. L. Tymoczko, L. Stryer, Biochemistry, 5th Ed. New York: WH Freeman, 2002.
57. E. Royte, Corn Plastic to the Rescue, *Smithsonian*, 2006.
58. I. K. Varma, A.-C. Albertsson, R. Rajkhowa and R. K. Srivastava, *Prog. Polym. Sci.* 2005, **30**, 949-981.
59. K. Masaki, N. R. Kamini, H. Ikeda and H. Iefuji, *Appl. Environ. Microbiol.* 2005, **71**, 7548-7550.
60. M. S. Reeve, S. P. McCarthy, M. J. Downey and R. A. Gross, *Macromolecules* 1994, **27**, 825-831.
61. D. E. Henton, P. Gruber, J. Lunt and J. Randall in *Natural Fibres, Biopolymers, and Biocomposites,* ed. A. K. Mohanty, M. Misra, L. T. Drzal, New York: CRC Press, 2005.

62. G. Natta, P. Pino, P. Corradini, F. Danusso, E. Mantica, G. Mazzanti and G. Moraglio, *J. Am. Chem. Soc.* 1955, **77**, 1708-1710.

63. F. A. Bovey, P. A. Mirau, *NMR of Polymers*. San Diego: Academic Press, 1996.

64. G. G. Odian, in *Principles of Polymerization, 4th Ed.* New Jersey: John Wiley & Sons, Inc. 2004, ch. 8, pp. 650-652.

65. J. A. Byers and J. E. Bercaw, *Proc. Natl. Acad. Sci. U.S.A.* 2006, **103**, 15303-15308.

66. F. Chabot, M. Vert, S. Chapelle and P. Granger, *Polymer*, 1983, **24**, 53-59.

67. S. Kang, G. Zhang, K. Aou, S. L. Hsu, H. D. Stidham and X. Yang, *J. Chem. Phys*. 2003, **118**, 3430-3437.

68. T. M. Ovitt, G. W. Coates, *J. Polym. Sci., Part A: Polym. Chem.* 2000, **38**, 4686-4692.

69. T. M. Ovitt and G. W. Coates, *J. Am. Chem. Soc.* 1999, **121**, 4072–4073.

70. M. Cheng, A. B. Attygalle, E. B. Lobkovsky, G. W. Coates, *J. Am. Chem. Soc.* 1999, **121**, 11583-11584.

71. L. Trofimoff, T. Aida, S. Inoue, *Chem. Lett.* 1987, 991-994.

72. C. P. Radano, G. L. Baker and M. R. Smith, *J. Am. Chem. Soc.* 2000, **122**, 1552-1553.

73. Z. Zhong, P. J. Dijkstra and J. Feijen, *Angew. Chem. Int. Ed.* 2002, **41**, 4510-4513.

74. T. Aida, S. Inoue, *Acc. Chem. Res.* 1996, **29**, 39-48.

75. T. M. Ovitt, G. W. Coates, *J. Am. Chem. Soc.* 2002, **124**, 1316-1326.

76. K. A. M. Thakur, R. T. Kean, E. S. Hall, J. K. Kolstad, T. A. Lindgren, M. A. Doscotch, J. I. Siepmann and E. J. Munson, *Macromolecules,* 1997, **30**, 2422-2428.

77. B. J. O'Keefe, M. A. Hillmyer and W. B. Tolman, *Dalton Trans.* 2001, 2215-2224.

78. O. Dechy-Cabaret, B. Martin-Vaca and D. Bourissou, *Chem. Rev.* 2004, **104**, 6147-6176.

79. W. Dittrich and R. C. Shulz, *Angew. Makromol. Chem.* 1971, **15**, 109.

80. H. R. Kricheldorf and D. O. Damrau, *Macromol. Chem. Phys.* 1997, **198**, 1753-1766.

81. W. M. Stevels, M. J. K. Ankone, P. J. Dijkstra and J. Feijen, *Macromolecules* 1996, **29**, 6132-6138.

82. W. M. Stevels, M. J. K. Ankone, P. J. Dijkstra and J. Feijen, *Macromolecules* 1996, **29**, 3332-3333.

83. W. M. Stevels, M. J. K. Ankone, P. J. Dijkstra and J. Feijen, *Macromol. Chem. Phys.* 1995, **196**, 1153-1161.

84. V. Simic, N. Spassky and L. G. Hubert-Pfalzgraf, *Macromolecules*, 1997, **30**, 7338-7340.

85. N. Spassky, V. Simic, L. G. Hubert-Pfalzgraf and M. S. Montaudo, *Macromol. Symp.* 1999, **144**, 257-267.

86. N. Spassky, V. Simic, M. S. Montaudo and L. G. Hubert-Pfalzgraf, *Macromol. Chem. Phys.* 2000, **201**, 2432-2440.

87. V. Simic, V. Girardon, N. Spassky, L. G. Hubert-Pfalzgraf and A. Duda, *Polym. Degrad. Stabil.* 1998, **59**, 227-229.

88. S. J. McLain, T. M. Ford and N. E. Drysdale, *Polym. Prepr.* 1992, **33**, 463-464.

89. A. Kowalski, A. Duda, S. Penczek, *Macromolecules* 2000, **33**, 7359-7370.

90. M. Moller, F. Nederberg, L. S. Lim, R. Kange, C. J. Hawker, J. L. Hedrick, Y. Gu, R. Shah and N. L. Abbott, *J. Polym. Sci. Part A. Polym. Chem.* 2001, **39**, 3529-3538.

91. M. H. Chisholm and E. E. Delbridge. *Chem. Commun*, 2001, 1308-1309.

92. A. Kowalski, J. Libiszowski, A. Duda and S. Penczek, *Macromolecules*, 2000, **33**, 1964-1971.

93. M. H. Chisholm and E. E. Delbridge, *New J. Chem*, 2003, **27**, 1177-1183.

94. K. Stridsberg, M. Ryner and A.-C. Albertsson, *Macromolecules*, 2000, **33**, 2862-2869.

95. M. Ryner, A. Finne, A. C. Albertsson, H. R. Kricheldorf, *Macromolecules* 2001, **34**, 7281-7287.

96. H. R. Kricheldorf, *Polym. Adv. Technol.* 2002, **13**, 969-974.

97. A. Finne, A.-C. Albertsson, *J. Polym. Sci, Part A: Polym. Chem.* 2003, **41**, 3074-3082.

98. Z. Zhong, P. J. Dijkstra, C. Birg, M. Westerhausen and J. Feijen, *Macromolecules* 2001, **34**, 3863-3868.

99. M. Westerhausen, S. Schneiderbauer, A. N. Kneifel, Y. Soltl, P. Mayer, H. Noth, Z. Zhong, P. J. Dijkstra and J. Feijen. *Eur. J. Inorg. Chem.* 2003, 3432-3439.

100. B. J. O'Keefe, S. M. Monnier, M. A. Hillmyer and W. B. Tolman, *J. Am. Chem. Soc.* 2001, **123**, 339-340.

101. H. R. Kricheldorf and D. O. Damrau, *Macromol. Chem. Phys.* 1997, **198**, 1767-1774.

102. D. S. McGuinness, E. L. Marshall, V. C. Gibson and J. W. Steed, *J. Polym. Sci., Part A: Polym. Chem.* 2003, **41**, 3798-3803.

103. C.-H. Huang, F.-C. Wang, B-T. Ko, T.-L. Yu and C-C. Lin, *Macromolecules*, 2001, **34**, 356-361.

104. D.J. Darensbourg and O. Karroonnirun, *Inorg. Chem.* 2010, **49**, 2360-2371.

105. N. Emig, H. Nguyen, H. Krautscheid, R. Reau, J. B. Cazaux and G. Bertrand *Organometallics* 1998, **17**, 3599-3608.

106. N. Emig, R. Reau, H. Krautscheid, D. Fenske and G. Bertrand, *J. Am. Chem. Soc.* 1996, **118**, 5822-5823.

107. A. Dumitrescu, B. Martin-Vaca, H. Gornitzka, J.-B. Cazaux, D. Bourissou and G. Bertrand, *Eur. J. Inorg. Chem.* 2002, 1948-1951.

108. J.-L. Faure, H. Gornitzka, R. Reau, D. Stalke and G. Bertrand, *Eur. J. Inorg. Chem.* 1999, 2295-2299.

109. M. H. Chisholm, N. W. Eilerts, J. C. Huffman, S. S. Iyer, M. Pacold, K. Phomphrai, *J. Am. Chem. Soc.* 2000, **122**, 11845-11854.

110. M. H. Chisholm, J. Gallucci and K. Phomphrai, *Chem. Commun.* 2003, 48-49.

111. B. Lian, C. M. Thomas, O. L. Casagrande, T. Roisnel and J.-F. Carpentier, *Polyhedron* 2007, **26**, 3817-3824.

112. M. H. Chisholm, J. Gallucci and K. Phomphrai, *Inorg. Chem.* 2004, **43**, 6717-6725.

113. B-T. Ko, C-C. Woo and C-C. Lin, *Organometallics*, 2000, **19**, 1864-1869.

114. M. H. Chisholm, D. Navarro-Llobet and W. J. Simonsick, *Macromolecules*, 2001, **34**, 6196-6201.

115. T. K. Prakasha, R. O. Day and R. R. Holmes, *J. Am. Chem. Soc.* 1993, **115**, 2690-2695.

116. Y. Takashima, Y. Nakayama, K. Watanabe, T. Itono, N. Ueyama, N. Nakamura, H. Yasuda and A. Harada, *Macromolecules*, 2002, **35**, 7538-7544.

117. H. Ma, T. P. Spaniol and J. Okuda, *Dalton Trans.* 2003, 4770-4780.

118. D. Chakraborty and E. Y-X. Chen. *Organometallics*, 2003, **22**, 769-774.

119. K. B. Aubrecht, K. Chang, M. A. Hillmyer and W. B. Tolman. *J. Polym. Sci. Part A: Polym. Chem.* 2001, **39**, 284-293.

120. K. B. Aubrecht, M. A. Hillmyer and W. B. Tolman, *Macromolecules*, 2002, **35**, 644-650.

121. B. J. O'Keefe, L. E. Breyfogle, M. A. Hillmyer and W. B. Tolman, *J. Am. Chem. Soc.* 2002, **124**, 4384-4393.

122. M. Cheng, T. M. Ovitt, P. D. Hustad and G. W. Coates. *Polym. Prepr.* 1999, **40**, 542-543.

123. B. M. Chamberlain, M. Cheng, D. R. Moore, T. M. Ovitt, E. B. Lobkovsky and G. W.

Coates, *J. Am. Chem. Soc.* 2001, **123**, 3229-3238.

124. M. H. Chisholm, J. Gallucci and K. Phomphrai, *Inorg. Chem.* 2002, **41**, 2785-2794.

125. M. H. Chisholm and K. Phomphrai, *Inorg. Chim. Acta* 2003, **350**, 121-125.

126. M. H. Chisholm, J. C. Huffman and K. Phomphrai, *Dalton Trans.* 2001, 222-224.

127. A. P. Dove, V. C. Gibson, E. L. Marshall, A. J. P. White and D. J. Williams, *Chem. Commun.* 2001, 283-284.

128. J. M. Smith, R. J. Lachicotte and P. L. Holland. *Chem. Commun.* 2001, 1542-1543.

129. V. C. Gibson, E. L. Marshall, D. Navarro-Llobet, A. J. P. White and D. J. Williams, *Dalton Trans.* 2002, 4321-4322.

130. P. H. M. Budzelaar, R. De Gelder and A. W. Gal, *Organometallics* 1998, **17**, 4121-4123

131. R. G. Cavell, R. P. Kamalesh Babu and K. Aparna, *Organomet. Chem.* 2001, **158**, 617-618.

132. A. Le Borgne, V. Vincens, M. Jouglard and N. Spassky, *Makromol. Chem. Macromol. Symp.* 1993, **73**, 37-46.

133. A. Le Borgne, M. Wisniewski and N. Spassky, *Polym. Prepr.* 1995, **36**, 217-218.

134. M. Wisniewski, A. Le Borgne and N. Spassky, *Macromol. Chem. Phys.* 1997, **198**, 1227-1238.

135. P. A. Cameron, D. Jhurry, V. C. Gibson, A. J. P. White, D. J. Williams and S. Williams, *Macromol. Rapid Commun.* 1999, **20**, 616-618.

136. A. Bhaw-Luximon, D. Jhurry and N. Spassky. *Polym. Bull.* 2000, **44**, 31-38.

137. D. Jhurry, A. Bhaw-Luximon and N. Spassky, *Macromol. Symp.* 2001, **175**, 67-76.

138. N. Nomura, R. Ishii, M. Akakura and K. Aoi, *J. Am. Chem. Soc.* 2002, **124**, 5938-5939.

139. Z. Tang, X. Chen, X. Pang, Y. Yang, X. Zhang and X. Jing, *Biomacromolecules*, 2004, **5**, 965-970.

140. Z. Zhong, P. J. Dijkstra and J. Feijen, *J. Am. Chem. Soc.* 2003, **125**, 11291-11298.

141. N. Spassky, M. Wisniewski, C. Pluta and A. Le Borgne, *Macromol. Chem. Phys.* 1996, **197**, 2627-2637.

142. T. M. Ovitt and G. W. Coates, *J. Am. Chem. Soc.* 2002, **124**, 1316-1326.

143. K. Majerska and A. Duda. *J. Am. Chem. Soc.* 2004, **126**, 1026-1027.

144. D. Agustin, G. Rima, H. Gornitzka and J. Barrau, *J. Organomet. Chem.* 1999, **1**, 592-602.

145. M. H. Chisholm, J. C. Gallucci and H. Zhen, *Inorg. Chem.* 2001, **40**, 5051-5054.

146. C. K. Williams, L. E. Breyfogle, S. K. Choi, W. Nam, V. G. Young, M. A. Hillmyer and W. B. Tolman, *J. Am. Chem. Soc.* 2003, **125**, 11350-11359.

147. P. Hormnirun, E. L. Marshall, V. C. Gibson, A. J. P. White and D. J. Williams, *J. Am. Chem. Soc.* 2004, **126**, 2688-2689.

148. Y. Kim and J. G. Verkade, *Organometallics*, 2002, **21**, 2395-2399.

149. Y. Kim, G. K. Janeshwara and J. G. Verkade, *Inorg. Chem.* 2003, **42**, 1437-1447.

150. Y. Kim, P. N. Kapoor and J. G. Verkade. *Inorg. Chem.* 2002, **41**, 4834-4838.

151. C.-X. Cai, A. Amgoune, C. W. Lehmann and J.-F. Carpentier, *Chem. Commun.* 2004, 330-331.

152. B. M. Chamberlain, Y. Sun, J. R. Hagadorn, E. W. Hemmesch, V. G. Young, M. Pink, M. A. Hillmyer and W. B. Tolman, *Macromolecules*, 1999, **32**, 2400-2402.

153. B. M. Chamberlain, B. A. Jazdzewski, M. Pink, M. A. Hillmyer and W. B. Tolman, *Macromolecules*, 2000, **33**, 3970-3977.

154. C. K. Williams, N. R. Brooks, M. A. Hillmyer and W. B. Tolman, *Chem. Commun.* 2002, 2132-2133.

155. P. Hormnirun, E. L. Marshall, V. C. Gibson, R. I. Pugh and A. J. P. White, *Proc. Natl.*

Acad. Sci. U. S. A. 2006, **103**, 15343-15348.

156. D. J. Darensbourg, and O. Karroonnirun, *Organometallics* 2010, **29**, 5627-5634.

157. H. Du, A. H. Velders, P. J. Dijkstra, J. Sun, Z. Zhong, X. Chen and J. Feijen. *Chem-Eur. J.* 2009, **15**, 9836-9845.

158. H. Du, A. H. Velders, P. J. Dijkstra, Z. Zhong, X. Chen and J. Feijen, *Macromolecules* 2009, **42**, 1058-1066.

159. N. Nomura, R. Ishii, Y. Yamamoto and T. Kondo, *Chem-Eur. J.* 2007, **13**(16), 4433-4451.

160. H. Du, X. Pang, H. Yu, X. Zhuang, X. Chen, D. Cui, X. Wang and X. Jing, *Macromolecules* 2007, **40**, 1904-1913.

161. A. J. Chmura, C. J. Chuck, M. G. Davidson, M. G. Jones, M. D., Lunn, S. D. Bull and M. F. Mahon, *Angew. Chem. Int. Ed.* 2007, **46**, 2280-2283.

162. M. Hu, M. Wang, H. Zhu, L. Zhang, H. Zhang and L. Sun, *Dalton Trans.* (2010), **39**, 4440-4446.

163. M. D. Jones, A. J. Chmura, C. J. Chuck, M. G. Davidson and M. D. Lunn, *Polymer Prepr.* (2007), **48**, 817-818.

164. J.-C. Buffet, J. Okuda and P. L. Arnold, *Inorg. Chem.* 2010, **49**, 419-426.

165. A. F. Douglas, B. O. Patrick and P. Mehrkhodavandi, *Angew. Chem. Int. Ed.* 2008, **47**, 2290-2293.

166. A. Garces, L. F. Sanchez-Barba, C. Alonso-Moreno, M. Fajardo, J. Fernandez-Baeza, A. Otero, A. Lara-Sanchez, I. Lopez-Solera and A. M. Rodriguez, *Inorg. Chem.* 2010, **49**, 2859-2871.

167. G. W. Coates and R. C. Jeske in Handbook of Green Chemistry, Volume 1: Homogenous Catalysis, Ed. R. H. Crabtree, New Jersey: John Wiley & Sons, Inc. 2009.

168. Q. Wang, L. Xiang, H. Song, and G. Zi, *J. Organomet. Chem.* 2009, **694**, 691-696.

169. P. L. Arnold, J.-C. Buffet, R. P. Blaudeck, S. Sujecki, A. J. Blake and C. Wilson, *Angew. Chem. Int. Ed.* (2008), **47**, 6033-6036.

170. H. Ma, T. P. Spaniol and J. Okuda, *Angew. Chem. Int. Ed.* **2006,** 45, 7818-7821.

171. J. R. Schaefgen and P. J. Flory, *J. Am. Chem. Soc.* 1948, **70**, 2709-2718.

172. K. Inoue, *Prog. Polym. Sci.* 2000, **25**, 453-571.

173. J. A. Simms and H. J. Spinelli, in *Macromolecular Design of Polymeric Materials*, ed. K. Hatada, T. Kitayama and O. Vogl, New York: CRC Press, 1997, ch. 22, pp. 379-392.

174. L. J. Fetters, A. D. Kiss, D. S. Pearson, G. F. Quack and F. J. Vitus, *Macromolecues* 1993, **26**, 647-654.

175. J.-C. Hsu, K. Sugiyama, Y.-C. Chiu, A. Hirao and W.-C. Chen, *Macromolecules*, 2010, **43**, 7151-7158.

176. T. Nishiura, Y. Abe and T. Kitayama, *Polym. J.* 2010, **42**, 868-874.

177. J. T. Wiltshire, and G. G. Qiao, *Aust. J. Chem.* 2007, **60**, 699-705.

178. C. M. Thomas, *Chem. Soc. Rev.* 2010, **39**, 165-173.

179. M. J. Stanford and A. P. Dove, *Chem. Soc. Rev.* 2010, **39**, 486-494.

180. K. J. Zhu, B. Song and S. Yang, *J. Polym. Sci. Polym. Chem.* 1989, **27**, 2151-2159.

181. E. S. Kim, B. C. Kim and S. H. Kim, *J. Polym. Sci. Part B: Polym. Phys.* 2004, **42**, 939-946.

182. V. C. Long, G. C. Berry and L. M. Hobbs, *Polymer* 1964, **5**, 517-524.

183. D. J. Cameron, and M. P. Shaver, *Chem. Soc. Rev.* 2011, **40**, 1761-1776.

184. S. H. Kim and Y. H. Kim, *Polymer (Korea)* 1996, **20**, 528-534.

185. S. H. Lee, S. H. Kim, Y. K. Han and Y. H. Kim, *J. Polym. Sci. Part A: Polym. Chem.* 2001,

39, 973-985.

186. H. Korhonen, A. Helminen and J. V. Seppala, *Polymer* 2001, **42**, 7541-7549.

187. T. Biela, A. Duda, K. Rode and H. Pasch, *Polymer* 2003, **44**, 1851-1860.

188. N. Kang and J. C. Leroux, *Polymer* 2004, **45**, 8967-8980.

189. W. Radke, K. Rode, A. V. Gorshkov and T. Biela, *Polymer* 2005, **46**, 5456-5465.

190. L. Wang and C. M. Dong, *J. Polym. Sci. Part A: Polym. Chem.* 2006, **44**, 2226-2236.

191. K. Numata, R. K. Srivastava, A. Finne-Wistrand, A. C. Albertsson, Y. Doi and H. Abe, *Biomacromolecules* 2007, **8**, 3115-3125.

192. M. Sobczak, E. Witkowska, E. Odedzka and W. Kolodziejski, *Molecules* 2008, **13**, 96-106.

193. H. R. Kricheldorf, K. Ahrensdorf and S. Rost, *Macromol. Chem. Phys.* 2004, **205**, 1031-1038.

194. K. A. George, T. V. Chirila and E. Wentrup-Byrne, *Polymer* 2010, **51**, 1670-1678.

195. J. S. Lee, D. J. Choo, S. H. Kim and Y. H. Kim, *Polymer (Korea)* 1998, **22**, 880-889.

196. L. Wang, C. Cai and C. M. Dong, *Chin. J. Polym. Sci.* 2008, **26**, 161-168.

197. T. Biela. A. Duda. H. Pasch and K. Rode, *J. Polym. Sci. Part A: Polym. Chem.* 2005, **43**, 6116-6133.

198. M. Danko, J. Libiszowski, T. Biela, M. Wolszczak and A. Duda, *J. Polym. Sci. Part A: Polym. Chem.* 2005, **43**, 4586-4599.

199. Q. Hao, F. Li, Q. Li, Y. Li, L. Jia, J. Yang, A. Fang and A. Cao, *Biomacromolecules* 2005, **6**, 2236-2247.

200. S. Y. Park, B. R. Han, K. M. Na, D. K. Han and S. C. Kim, *Macromolecules* 2003, **36**, 4115-4124.

201. J. Xu and J. Song *Proc. Nat. Acad. Sci.* 2010, **107**, 7652-7657.

202. D. Astruc, E. Boisselier and C. Ornelas, *Chem. Rev.* 2010, **110**, 1857-1959.

203. K. Odelius, A. Finne and A. C. Albertsson, *J. Polym. Sci. Part A: Polym. Chem.* 2006, **44**, 596-605.

204. A. Finne and A. C. Albertsson, *Biomacromolecules* 2002, **3**, 684-690.

205. A. Finne and A. C. Albertsson, *J. Polym. Sci. Part A: Polym. Chem.* 2003, **41**, 1296-1305.

206. R. M. Johnson and C. L. Fraser, *Biomacromolecules* 2004, **5**, 580-588.

207. C. Hiemstra, Z. Zhong, L. Li, P. J. Dijkstra and J. Feijan, *Biomacromolecules* 2006, **7**, 2790-2795.

208. C. Hiemstra, W. Zhou, Z. Zhong, M. Wouters and J. Feijen, *J. Am. Chem. Soc.* 2007, **129**, 9918-9926.

209. K. A. George, F. Schue, T. V. Chirila and E. Wentrup-Byrne, *J. Polym. Sci. Part A: Polym. Chem.* 2009, **47**, 4736-4748.

210. M. J. Stanford and A. P. Dove, *Macromolecules* 2009, **42**, 141-147.

211. T. Zou, S. L. Li, S. X. Cheng, X. Z. Zhang and R. X. Zhuo, *J. Bio. Mater. Res. Part A.* 2007, **83**, 696-702.

212. H. L. Fu, S. X. Cheng, X. Z. Zhang and R. X. Zhuo, *J. Controlled Release* 2007, **124**, 181-188.

213. Q. Zhang, D. Zhao, X. Z. Zhang, S. X. Cheng and R. X. Zhuo, *J. Biomed. Mater. Res. Part B: Appl. Biomater.* 2009, **91B**, 172-180.

214. Q. Zhang, S. X. Cheng, X. Z. Zhang and R. X. Zhuo, *Macromol. Biosci.* 2009, **9**, 1262-1271.

215. Y. Q. Li, F. Li, X. Z. Zhang, S. X. Cheng and R. X. Zhuo, *J. Mater. Chem.* 2009, **19**, 6733-6739.

216. Z. Y. Wang, H. J. Zhao, Q. F. Wang, R. R. Ye and D. E. Finlow, *J. Appl. Polym. Sci.* 2010, **117**, 1405-1415.

217. M. Adeli, Z. Zarnegar and R. Kabiri, *Eur. Polym. J.* 2008, **44**, 1921-1930.

218. X. Yu, X. Tang and C. Pan, *Polymer* 2005, **46**, 11149-11156.

219. H. A. Klok, S. Becker, F. Schuch, T. Pakula and K. Mullen, *Macromol. Biosci.* 2003, **3**, 729-741.

220. L. Gorczynski, J. Chen and C. L. Fraser, *J. Am. Chem. Soc.* 2005, **127**, 14956-14957.

221. L. Bender, P. S. Corbin, C. L. Fraser, D. H. Metcalf, F. S. Richardson, E. L. Thomas and A. M. Urbas, *J. Am. Chem. Soc.* 2002, **124**, 8526-8527.

222. R. Szymanski, *Macromolecules*, 2002, **35**, 8239-8242.

223. K. Matyjaszewski, *Polym. Int.* 2003, **52**, 1559-1565.

224. F.D. Kopinke, M. Remmler, K. Mackenzie, M. Moder and O. Wachsen, *Polym. Degrad. Stabil.* 1996, **53**, 329-342.

225. H. Nishida, T. Mori, S. Hoshihara, Y. Fan, Y. Shirai and T. Endo, *Polym. Degrad. Stabil.* 2003, **81**, 515-523.

226. S. Inkinen, M. Hakkarainen, A. C. Albertsson and A. Sodergard, Biomacromolecules, 2011, DOI:10.1021/bm101302t.

227. M. Noda, *Prep. Biochem. Biotechnol.* 1999, **29**, 333-338.

228. E. Petinakis, X. Liu, L. Yu, C. Way, P. Sangwan, K. Dean, S. Bateman and G. Edward, *Polym. Degrad. Stabil.* 2010, **95**, 1704-1707.

229. I. C. McNeill and H. A. Leiper, *Polym. Degrad. Stabil.* 1985, **11**, 309-326.

230. M. P. Sepe, *Thermal Analysis of Polymers.* Rapra Review Reports, 1997, **8**, 13-18.

231. P. R. Gruber, J. J. Kolstad, D. R. Witzke, M. H. Hartmann and A. L. Brosch, Viscosity-

Modified Lactide Polymer Composition and Process for Their Manufacture, U.S. Patent 5,594,095, 1997.

232. E. L. Marshall, V. C. Gibson, H. S. Rzepa, *J. Am. Chem. Soc.* 2005, **127**(16), 6048-6051.

233. D. Cohn, H. Younes and G. Marom, *Polymer* 1987, **28**, 2018-2022.

234. C. Migliaresi, A. De Lollis, L. Fambria and D. Cohn, *Clin. Mater.* 1991, **8**, 111-118.

235. W. Hoogsteen, A. R. Postema, A. J. Pennings, G. Ten Brinke and P. Zugenmaier, *Macromolecules* 1990, **23**, 634-642.

236. R. Masirek, E. Piorkowska, A. Galeski and M. Mucha, *J. Appl. Polym. Sci.* 2007, **105**, 282-290.

237. D. M. Bigg, *Society of Plastics Engineers—Annual Polymers*, 1996, **54**(2), 2028–2039.

238. M. R. Mucalo, N. B. Milestone and I. W. M. Brown, *J. Mater. Sci.* 1997, **32**(9) 2433-2444.

239. R. Giere and P. Stille Eds. Energy, Waste and the Environment: a Geochemical Perspective, The Geological Society Publishing House, Bath, UK, 2004.

240. A. Patterson, Phys. Rev. 1939, **56**, 978-982.

241. S. J. de Jong, E. R. Arias, D. T. S. Rijkers, C. F. van Nostrum, J. J. Kettenes-van den Bosch and W. E. Hennink, *Polymer*, 2001, **42**, 2795-2802.

242. E. W. Fischer, H. J. Sterzel and G. Wegner, *Kolloid Z. Z. Polym.* 1973, **251**, 980-990.

243. M. Vert, J. Mauduit and S. Li, *Biomaterials,* 1994, **15**, 1209-1213.

244. M. H. Stenzel-Rosenbaum, T. P. Davis, V. Chen and A. G. Fane, *Macromolecules,* 1991, **34**, 5433-5438.

245. P. G. Hayes, G. C. Welch, D. J. H. Emslie, C. L. Noack, W. E. Piers and M. Parvez, *Organometallics*, 2003, **22**, 1577-1579.

246. X. Liu, W. Gao, Y. Mu, G.-H. Li, L. Ye, H. Xia, Y. Ren and S.-H. Feng, *Organometallics*,

2005, **24**, 1614-1619.

247. X. Shang, X. Liu and D. Cui, *J. Polym. Sci. Part A: Polym. Chem.* 2007, **45**, 5662-5672.

248. W. Gao, D. Cui, X. Liu, Y. Zhang and Y. Mu, *Organometallics*, 2008, **27**, 5889-5893.

249. Y.-H. Tsai, C.-H. Lin, C.-C. Lin and B.-T. Ko, *J. Polym. Sci. Part A: Polym. Chem.* 2009, **47**, 4927-4936.

250. Y.-C. Liu, C.-H. Lin, B.-T. Ko and R.-M. Ho, *J. Polym. Sci. Part A: Polym. Chem.* 2010, **48**, 5339-5347.

251. D. J. Doyle, V. C. Gibson and A. J. P. White, *Dalton Trans.* 2007, 358-368.

252. W. Yao, Y. Mu, A. Gao, W. Gao and L. Ye, *Dalton Trans.* 2008, 3202-3206.

253. B. Y. Lee, H. Y. Kwon, S. Y. Lee, S. J. Na, S. Han, H. Yun, H. Lee and Y.-W. Park, *J. Am. Chem. Soc.* 2005, **127**, 3031-3037.

254. Y. Xiao, Z. Wang and K. Ding, *Macromolecules*, 2006, **39**, 128-137.

255. Y. Xiao, Z. Wang and K. Ding, *Chem. Eur. J.* 2005, **11**, 3668-3678.

256. T. Bok, H. Yun and B. Y. Lee, *Inorg. Chem.* 2006, **45**, 4228-4237.

257. M. Cheng, E. B. Lobkovsky and G. W. Coates, *J. Am. Chem. Soc.* 1998, **120**, 11018-11019.

258. C. N. Wall, *Phys. Rev.* 1930, **36**, 1243-1250.

259.A. P. Dove, V. C. Gibson, E. L. Marshall, H. S. Rzepa, A. J. P. White and D. J. Williams, *J. Am. Chem. Soc.* 2006, **128**, 9834-9843.

260. S. J. Moravek, J. M. Messman and R. F. Storey, *J. Polym. Sci. Part A: Polym. Chem.* 2008, **47**, 797-803.

Appendix 1

Crystallographic Data for structures (14) and (16)

Table A.1. Crystal data and structure refinement for (14).

Identification code	MS091022	
Empirical formula	C42 H55 Al N4	
Formula weight	642.88	
Temperature	173(1) K	
Wavelength	0.71073 Å	
Diffractometer used	Bruker AXS P4/SMART 1000	
Detector distance	5 cm	
Monochromator used	Graphite	
Crystal size	0.50 x 0.30 x 0.30 mm^3	
Colour and habit	Yellow, irregular	
Crystal system	Monoclinic	
Space group	P2(1)/c	
Unit cell dimensions	a = 13.496(2) Å	$\alpha = 90°$
	b = 13.913(3) Å	$\beta = 99.431(2)°$
	c = 20.820(5) Å	$\gamma = 90°$
Volume	3856.7(13) $Å^3$	
Z	4	
Density (calculated)	1.107 Mg/m^3	

Absorption coefficient	0.086 mm^{-1}
F(000)	1392
Theta range for data collection	1.53 to 27.50°
Completeness to theta = 25.00°	99.9 %
Scan type	ω and ϕ
Scan range	0.3°
Exposure time	30s
Index ranges	$-17 \leq h \leq 17$, $-17 \leq k \leq 18$, $-25 \leq l \leq 26$
Standard reflections	50 frames at beginning and end of data collection
Crystal stability	no decay
Reflections collected	25597
Independent reflections	8584 [R(int) = 0.0602]
Solution	Direct methods
Hydrogen atoms	Calculated positions, riding model
Absorption correction	SADABS
Max. and min. transmission	0.9748 and 0.9585
Refinement method	Full-matrix least-squares on F^2
Data / restraints / parameters	8584 / 0 / 437
Goodness-of-fit on F^2	1.052
Final R indices [I>2sigma(I)]	R1 = 0.0581, wR2 = 0.1368
R indices (all data)	R1 = 0.1010, wR2 = 0.1701

Largest/mean shift/esd 0.001/0.000

Largest diff. peak and hole 0.459 and -0.221 e.Å^{-3}

$wR2 = (\Sigma[w(F_o^2-F_c^2)^2]/\Sigma[wF_o^4])^{1/2}$

$R1 = \Sigma\,||F_o|-|F_c||/\Sigma\,|F_o|$

$Weight = 1 / [\sigma^2(F_o^2) + (0.0808 * P)^2 + (0.8917 * P)]$

where $P = (\max(F_o^2, 0) + 2 * F_c^2)/3$

Table A.2. Atomic coordinates (x 10^4) and equivalent isotropic displacement parameters (Å^{2}x 10^3) for (14). U(eq) is defined as one third of the trace of the orthogonalized U^{ij} tensor.

	x	y	z	U(eq)
Al(1)	2078(1)	2809(1)	389(1)	36(1)
N(1)	3081(1)	1857(1)	702(1)	36(1)
N(2)	1359(1)	2642(1)	1087(1)	31(1)
N(3)	3460(30)	-240(20)	202(17)	32(3)
N(3')	3550(30)	-70(20)	284(17)	32(3)
N(4)	3664(1)	-1184(1)	1352(1)	35(1)
C(1)	1353(2)	2439(2)	-468(1)	57(1)
C(2)	2849(2)	4005(2)	366(1)	56(1)
C(3)	366(1)	3068(2)	993(1)	32(1)
C(4)	244(2)	4033(2)	1160(1)	37(1)
C(5)	-716(2)	4438(2)	1022(1)	44(1)
C(6)	-1524(2)	3906(2)	728(1)	46(1)

C(7)	-1394(2)	2956(2)	578(1)	44(1)
C(8)	-460(2)	2512(2)	702(1)	38(1)
C(9)	1102(2)	4650(2)	1503(1)	44(1)
C(10)	958(2)	4847(2)	2211(1)	53(1)
C(11)	1208(2)	5599(2)	1145(2)	61(1)
C(12)	-370(2)	1450(2)	552(1)	46(1)
C(13)	-906(2)	1191(2)	-135(1)	61(1)
C(14)	-787(2)	834(2)	1061(1)	62(1)
C(15)	1688(1)	2195(1)	1668(1)	31(1)
C(16)	2624(2)	1686(1)	1781(1)	34(1)
C(17)	2956(2)	1266(2)	2399(1)	42(1)
C(18)	2402(2)	1313(2)	2891(1)	46(1)
C(19)	1478(2)	1784(2)	2777(1)	44(1)
C(20)	1126(2)	2204(2)	2188(1)	37(1)
C(21)	3240(2)	1535(2)	1294(1)	36(1)
C(22)	3776(2)	1574(2)	262(1)	49(1)
C(23)	3407(2)	717(2)	-151(1)	54(1)
C(24)	3683(2)	-948(2)	-25(1)	38(1)
C(25)	3920(2)	-1153(2)	2045(1)	34(1)
C(26)	3202(2)	-1432(2)	2427(1)	39(1)
C(27)	3480(2)	-1398(2)	3103(1)	52(1)

C(28)	4433(2)	-1112(2)	3380(1)	60(1)
C(29)	5127(2)	-846(2)	2997(1)	52(1)
C(30)	4884(2)	-850(2)	2320(1)	38(1)
C(31)	2154(2)	-1742(2)	2113(1)	45(1)
C(32)	1477(2)	-871(2)	1938(2)	66(1)
C(33)	1670(2)	-2446(2)	2532(1)	62(1)
C(34)	5669(2)	-541(2)	1914(1)	41(1)
C(35)	6106(2)	446(2)	2111(1)	56(1)
C(36)	6496(2)	-1299(2)	1946(1)	58(1)
C(37)	3886(1)	-1960(2)	990(1)	34(1)
C(38)	3852(1)	-1862(2)	310(1)	33(1)
C(39)	4036(2)	-2680(2)	-50(1)	42(1)
C(40)	4263(2)	-3556(2)	236(1)	53(1)
C(41)	4322(2)	-3633(2)	905(1)	56(1)
C(42)	4140(2)	-2854(2)	1277(1)	47(1)

Table A.3. Bond lengths [Å] for (14).

Al(1)-N(2)	1.8881(18)	Al(1)-N(1)	1.9292(18)
Al(1)-C(1)	1.958(3)	Al(1)-C(2)	1.967(3)
N(1)-C(21)	1.295(3)	N(1)-C(22)	1.468(3)
N(2)-C(15)	1.369(3)	N(2)-C(3)	1.449(2)
N(3)-C(24)	1.15(3)	N(3)-C(23)	1.52(4)

N(3')-C(24)	1.40(3)	N(3')-C(23)	1.41(4)
N(4)-C(37)	1.378(3)	N(4)-C(25)	1.430(3)
N(4)-H(4)	0.8800	C(1)-H(1A)	0.9800
C(1)-H(1B)	0.9800	C(1)-H(1C)	0.9800
C(2)-H(2A)	0.9800	C(2)-H(2B)	0.9800
C(2)-H(2C)	0.9800	C(3)-C(4)	1.404(3)
C(3)-C(8)	1.410(3)	C(4)-C(5)	1.399(3)
C(4)-C(9)	1.521(3)	C(5)-C(6)	.376(3)
C(5)-H(5)	0.9500	C(6)-C(7)	1.376(4)
C(6)-H(6)	0.9500	C(7)-C(8)	1.390(3)
C(7)-H(7)	0.9500	C(8)-C(12)	1.518(3)
C(9)-C(11)	1.534(4)	C(9)-C(10)	1.542(4)
C(9)-H(9)	1.0000	C(10)-H(10A)	0.9800
C(10)-H(10B)	0.9800	C(10)-H(10C)	0.9800
C(11)-H(11A)	0.9800	C(11)-H(11B)	0.9800
C(11)-H(11C)	0.9800	C(12)-C(13)	1.535(3)
C(12)-C(14)	1.540(4)	C(12)-H(12)	1.0000
C(13)-H(13A)	0.9800	C(13)-H(13B)	0.9800
C(13)-H(13C)	0.9800	C(14)-H(14A)	0.9800
C(14)-H(14B)	0.9800	C(14)-H(14C)	0.9800
C(15)-C(20)	1.421(3)	C(15)-C(16)	1.433(3)

C(16)-C(17)	1.416(3)	C(16)-C(21)	1.429(3)
C(17)-C(18)	1.366(3)	C(17)-H(17)	0.9500
C(18)-C(19)	1.393(3)	C(18)-H(18)	0.9500
C(19)-C(20)	1.370(3)	C(19)-H(19)	0.9500
C(20)-H(20)	0.9500	C(21)-H(21)	0.9500
C(22)-C(23)	1.506(4)	C(22)-H(22A)	0.9900
C(22)-H(22B)	0.9900	C(23)-H(23A)	0.9900
C(23)-H(23B)	0.9900	C(24)-C(38)	1.452(3)
C(24)-H(24)	0.9500	C(25)-C(30)	1.399(3)
C(25)-C(26)	1.404(3)	C(26)-C(27)	1.396(3)
C(26)-C(31)	1.520(3)	C(27)-C(28)	1.379(4)
C(27)-H(27)	0.9500	C(28)-C(29)	1.376(4)
C(28)-H(28)	0.9500	C(29)-C(30)	1.394(3)
C(29)-H(29)	0.9500	C(30)-C(34)	1.521(3)
C(31)-C(32)	1.526(4)	C(31)-C(33)	1.528(3)
C(31)-H(31)	1.0000	C(32)-H(32A)	0.9800
C(32)-H(32B)	0.9800	C(32)-H(32C)	0.9800
C(33)-H(33A)	0.9800	C(33)-H(33B)	0.9800
C(33)-H(33C)	0.9800	C(34)-C(35)	1.524(4)
C(34)-C(36)	1.529(3)	C(34)-H(34)	1.0000
C(35)-H(35A)	0.9800	C(35)-H(35B)	0.9800

C(35)-H(35C)	0.9800	C(36)-H(36A)	0.9800
C(36)-H(36B)	0.9800	C(36)-H(36C)	0.9800
C(37)-C(42)	1.398(3)	C(37)-C(38)	1.414(3)
C(38)-C(39)	1.406(3)	C(39)-C(40)	1.369(4)
C(39)-H(39)	0.9500	C(40)-C(41)	1.385(4)
C(40)-H(40)	0.9500	C(41)-C(42)	1.378(3)
C(41)-H(41)	0.9500	C(42)-H(42)	0.9500

Table A.4. Bong angles (°) for (14)

N(2)-Al(1)-N(1)	94.38(8)	N(2)-Al(1)-C(1)	115.16(10)
N(1)-Al(1)-C(1)	110.23(11)	N(2)-Al(1)-C(2)	117.58(10)
N(1)-Al(1)-C(2)	104.12(10)	C(1)-Al(1)-C(2)	112.82(13)
C(21)-N(1)-C(22)	118.50(18)	C(21)-N(1)-Al(1)	123.84(15)
C(22)-N(1)-Al(1)	117.25(14)	C(15)-N(2)-C(3)	117.65(16)
C(15)-N(2)-Al(1)	127.07(13)	C(3)-N(2)-Al(1)	115.25(12)
C(24)-N(3)-C(23)	123(3)	C(24)-N(3')-C(23)	113(2)
C(37)-N(4)-C(25)	122.54(17)	C(37)-N(4)-H(4)	118.7
C(25)-N(4)-H(4)	118.7	Al(1)-C(1)-H(1A)	109.5
Al(1)-C(1)-H(1B)	109.5	H(1A)-C(1)-H(1B)	109.5
Al(1)-C(1)-H(1C)	109.5	H(1A)-C(1)-H(1C)	109.5
H(1B)-C(1)-H(1C)	109.5	Al(1)-C(2)-H(2A)	109.5
Al(1)-C(2)-H(2B)	109.5	H(2A)-C(2)-H(2B)	109.5

Al(1)-C(2)-H(2C)	109.5	H(2A)-C(2)-H(2C)	109.5
H(2B)-C(2)-H(2C)	109.5	C(4)-C(3)-C(8)	121.04(18)
C(4)-C(3)-N(2)	120.07(17)	C(8)-C(3)-N(2)	118.82(18)
C(5)-C(4)-C(3)	118.5(2)	C(5)-C(4)-C(9)	118.5(2)
C(3)-C(4)-C(9)	123.03(18)	C(6)-C(5)-C(4)	120.9(2)
C(6)-C(5)-H(5)	119.5	C(4)-C(5)-H(5)	119.5
C(7)-C(6)-C(5)	119.8(2)	C(7)-C(6)-H(6)	120.1
C(5)-C(6)-H(6)	120.1	C(6)-C(7)-C(8)	122.1(2)
C(6)-C(7)-H(7)	119.0	C(8)-C(7)-H(7)	119.0
C(7)-C(8)-C(3)	117.7(2)	C(7)-C(8)-C(12)	119.7(2)
C(3)-C(8)-C(12)	122.58(19)	C(4)-C(9)-C(11)	112.5(2)
C(4)-C(9)-C(10)	110.1(2)	C(11)-C(9)-C(10)	110.4(2)
C(4)-C(9)-H(9)	107.9	C(11)-C(9)-H(9)	107.9
C(10)-C(9)-H(9)	107.9	C(9)-C(10)-H(10A)	109.5
C(9)-C(10)-H(10B)	109.5	H(10A)-C(10)-H(10B)	109.5
C(9)-C(10)-H(10C)	109.5	H(10A)-C(10)-H(10C)	109.5
H(10B)-C(10)-H(10C)	109.5	C(9)-C(11)-H(11A)	109.5
C(9)-C(11)-H(11B)	109.5	H(11A)-C(11)-H(11B)	109.5
C(9)-C(11)-H(11C)	109.5	H(11A)-C(11)-H(11C)	109.5
H(11B)-C(11)-H(11C)	109.5	C(8)-C(12)-C(13)	112.2(2)
C(8)-C(12)-C(14)	110.4(2)	C(13)-C(12)-C(14)	109.9(2)

C(8)-C(12)-H(12)	108.0	C(13)-C(12)-H(12)	108.0
C(14)-C(12)-H(12)	108.0	C(12)-C(13)-H(13A)	109.5
C(12)-C(13)-H(13B)	109.5	H(13A)-C(13)-H(13B)	109.5
C(12)-C(13)-H(13C)	109.5	H(13A)-C(13)-H(13C)	109.5
H(13B)-C(13)-H(13C)	109.5	C(12)-C(14)-H(14A)	109.5
C(12)-C(14)-H(14B)	109.5	H(14A)-C(14)-H(14B)	109.5
C(12)-C(14)-H(14C)	109.5	H(14A)-C(14)-H(14C)	109.5
H(14B)-C(14)-H(14C)	109.5	N(2)-C(15)-C(20)	122.26(18)
N(2)-C(15)-C(16)	121.31(18)	C(20)-C(15)-C(16)	116.42(18)
C(17)-C(16)-C(21)	116.67(19)	C(17)-C(16)-C(15)	119.5(2)
C(21)-C(16)-C(15)	123.75(19)	C(18)-C(17)-C(16)	122.0(2)
C(18)-C(17)-H(17)	119.0	C(16)-C(17)-H(17)	119.0
C(17)-C(18)-C(19)	118.6(2)	C(17)-C(18)-H(18)	120.7
C(19)-C(18)-H(18)	120.7	C(20)-C(19)-C(18)	121.5(2)
C(20)-C(19)-H(19)	119.2	C(18)-C(19)-H(19)	119.2
C(19)-C(20)-C(15)	121.8(2)	C(19)-C(20)-H(20)	119.1
C(15)-C(20)-H(20)	119.1	N(1)-C(21)-C(16)	126.80(19)
N(1)-C(21)-H(21)	116.6	C(16)-C(21)-H(21)	116.6
N(1)-C(22)-C(23)	112.6(2)	N(1)-C(22)-H(22A)	109.1
C(23)-C(22)-H(22A)	109.1	N(1)-C(22)-H(22B)	109.1
C(23)-C(22)-H(22B)	109.1	H(22A)-C(22)-H(22B)	107.8

N(3')-C(23)-C(22)	104.4(9)	N(3')-C(23)-N(3)	11.4(17)
C(22)-C(23)-N(3)	115.8(9)	N(3')-C(23)-H(23A)	113.0
C(22)-C(23)-H(23A)	108.3	N(3)-C(23)-H(23A)	108.3
N(3')-C(23)-H(23B)	115.0	C(22)-C(23)-H(23B)	108.3
N(3)-C(23)-H(23B)	108.3	H(23A)-C(23)-H(23B)	107.4
N(3)-C(24)-N(3')	108(3)	N(3)-C(24)-C(38)	125(2)
N(3')-C(24)-C(38)	124.3(17)	N(3)-C(24)-H(24)	117.3
N(3')-C(24)-H(24)	117.8	C(38)-C(24)-H(24)	117.3
C(30)-C(25)-C(26)	122.26(19)	C(30)-C(25)-N(4)	118.49(18)
C(26)-C(25)-N(4)	119.24(18)	C(27)-C(26)-C(25)	117.7(2)
C(27)-C(26)-C(31)	121.4(2)	C(25)-C(26)-C(31)	120.95(19)
C(28)-C(27)-C(26)	120.6(2)	C(28)-C(27)-H(27)	119.7
C(26)-C(27)-H(27)	119.7	C(29)-C(28)-C(27)	120.8(2)
C(29)-C(28)-H(28)	119.6	C(27)-C(28)-H(28)	119.6
C(28)-C(29)-C(30)	121.0(2)	C(28)-C(29)-H(29)	119.5
C(30)-C(29)-H(29)	119.5	C(29)-C(30)-C(25)	117.6(2)
C(29)-C(30)-C(34)	119.4(2)	C(25)-C(30)-C(34)	122.94(18)
C(26)-C(31)-C(32)	110.9(2)	C(26)-C(31)-C(33)	113.1(2)
C(32)-C(31)-C(33)	110.5(2)	C(26)-C(31)-H(31)	107.4
C(32)-C(31)-H(31)	107.4	C(33)-C(31)-H(31)	107.4
C(31)-C(32)-H(32A)	109.5	C(31)-C(32)-H(32B)	109.5

H(32A)-C(32)-H(32B)	109.5	C(31)-C(32)-H(32C)	109.5
H(32A)-C(32)-H(32C)	109.5	H(32B)-C(32)-H(32C)	109.5
C(31)-C(33)-H(33A)	109.5	C(31)-C(33)-H(33B)	109.5
H(33A)-C(33)-H(33B)	109.5	C(31)-C(33)-H(33C)	109.5
H(33A)-C(33)-H(33C)	109.5	H(33B)-C(33)-H(33C)	109.5
C(30)-C(34)-C(35)	112.3(2)	C(30)-C(34)-C(36)	110.51(19)
C(35)-C(34)-C(36)	111.2(2)	C(30)-C(34)-H(34)	107.5
C(35)-C(34)-H(34)	107.5	C(36)-C(34)-H(34)	107.5
C(34)-C(35)-H(35A)	109.5	C(34)-C(35)-H(35B)	109.5
H(35A)-C(35)-H(35B)	109.5	C(34)-C(35)-H(35C)	109.5
H(35A)-C(35)-H(35C)	109.5	H(35B)-C(35)-H(35C)	109.5
C(34)-C(36)-H(36A)	109.5	C(34)-C(36)-H(36B)	109.5
H(36A)-C(36)-H(36B)	109.5	C(34)-C(36)-H(36C)	109.5
H(36A)-C(36)-H(36C)	109.5	H(36B)-C(36)-H(36C)	109.5
N(4)-C(37)-C(42)	121.51(19)	N(4)-C(37)-C(38)	119.83(19)
C(42)-C(37)-C(38)	118.7(2)	C(39)-C(38)-C(37)	118.4(2)
C(39)-C(38)-C(24)	118.7(2)	C(37)-C(38)-C(24)	122.82(19)
C(40)-C(39)-C(38)	122.3(2)	C(40)-C(39)-H(39)	118.8
C(38)-C(39)-H(39)	118.8	C(39)-C(40)-C(41)	118.5(2)
C(39)-C(40)-H(40)	120.8	C(41)-C(40)-H(40)	120.8
C(42)-C(41)-C(40)	121.3(2)	C(42)-C(41)-H(41)	119.4

C(40)-C(41)-H(41)	119.4	C(41)-C(42)-C(37)	120.8(2)
C(41)-C(42)-H(42)	119.6	C(37)-C(42)-H(42)	119.6

Table A.5. Anisotropic displacement parameters ($Å^2 x\ 10^3$) for DC-ethylcat. The anisotropic displacement factor exponent takes the form: $-2\pi^2[\ h^2\ a^{*2}U^{11} + ... + 2\ h\ k\ a^*\ b^*\ U^{12}\ ]$

	U^{11}	U^{22}	U^{33}	U^{23}	U^{13}	U^{12}
Al(1)	34(1)	38(1)	36(1)	5(1)	7(1)	4(1)
N(1)	32(1)	35(1)	43(1)	5(1)	10(1)	2(1)
N(2)	27(1)	33(1)	32(1)	0(1)	3(1)	2(1)
N(3)	43(6)	31(9)	23(7)	-7(5)	4(5)	3(6)
N(3')	43(6)	31(9)	23(7)	-7(5)	4(5)	3(6)
N(4)	42(1)	34(1)	28(1)	-3(1)	5(1)	3(1)
C(1)	47(1)	88(2)	37(1)	5(1)	5(1)	9(1)
C(2)	60(2)	43(2)	69(2)	11(1)	23(1)	2(1)
C(3)	30(1)	37(1)	29(1)	2(1)	6(1)	3(1)
C(4)	35(1)	39(1)	38(1)	2(1)	8(1)	3(1)
C(5)	41(1)	42(1)	50(1)	3(1)	9(1)	12(1)
C(6)	33(1)	59(2)	47(1)	10(1)	6(1)	13(1)
C(7)	31(1)	60(2)	41(1)	-1(1)	1(1)	-1(1)
C(8)	32(1)	48(1)	33(1)	-2(1)	6(1)	0(1)
C(9)	40(1)	35(1)	57(2)	-7(1)	8(1)	3(1)
C(10)	53(1)	46(2)	57(2)	-10(1)	2(1)	-2(1)

C(11)	66(2)	42(2)	79(2)	-7(1)	20(1)	-5(1)
C(12)	37(1)	48(1)	52(1)	-12(1)	4(1)	-4(1)
C(13)	48(1)	71(2)	62(2)	-26(2)	5(1)	-9(1)
C(14)	67(2)	48(2)	71(2)	-3(1)	7(1)	-8(1)
C(15)	32(1)	26(1)	34(1)	-4(1)	3(1)	-3(1)
C(16)	36(1)	28(1)	36(1)	-2(1)	2(1)	0(1)
C(17)	46(1)	36(1)	40(1)	0(1)	-2(1)	5(1)
C(18)	65(2)	41(1)	31(1)	2(1)	-1(1)	0(1)
C(19)	58(1)	42(1)	34(1)	-4(1)	11(1)	-5(1)
C(20)	39(1)	36(1)	37(1)	-4(1)	7(1)	-1(1)
C(21)	31(1)	30(1)	46(1)	2(1)	1(1)	4(1)
C(22)	45(1)	48(2)	60(2)	21(1)	26(1)	14(1)
C(23)	72(2)	60(2)	34(1)	12(1)	22(1)	29(1)
C(24)	31(1)	56(2)	28(1)	-4(1)	5(1)	6(1)
C(25)	43(1)	29(1)	29(1)	0(1)	7(1)	1(1)
C(26)	49(1)	34(1)	37(1)	-5(1)	12(1)	-6(1)
C(27)	65(2)	59(2)	35(1)	-1(1)	19(1)	-17(1)
C(28)	78(2)	74(2)	29(1)	1(1)	8(1)	-20(2)
C(29)	56(2)	64(2)	33(1)	2(1)	3(1)	-14(1)
C(30)	46(1)	37(1)	31(1)	3(1)	6(1)	0(1)
C(31)	49(1)	47(1)	43(1)	-11(1)	15(1)	-11(1)

C(32)	56(2)	62(2)	74(2)	-9(2)	-3(1)	-6(1)
C(33)	61(2)	58(2)	72(2)	-6(1)	25(1)	-21(1)
C(34)	38(1)	49(1)	36(1)	5(1)	4(1)	0(1)
C(35)	45(1)	58(2)	64(2)	8(1)	8(1)	-10(1)
C(36)	55(2)	65(2)	56(2)	9(1)	13(1)	13(1)
C(37)	30(1)	36(1)	36(1)	-7(1)	8(1)	-6(1)
C(38)	26(1)	40(1)	34(1)	-8(1)	4(1)	-3(1)
C(39)	37(1)	51(2)	38(1)	-14(1)	9(1)	-6(1)
C(40)	62(2)	41(2)	58(2)	-18(1)	19(1)	-7(1)
C(41)	77(2)	33(1)	64(2)	-2(1)	26(1)	-2(1)
C(42)	65(2)	35(1)	44(1)	-2(1)	17(1)	-3(1)

Table A.6. Hydrogen coordinates (x 10^4) and isotropic displacement parameters ($Å^2$x 10^3) for (14).

	x	y	z	U(eq)
H(4)	3352	-688	1148	42
H(1A)	1118	1774	-452	86
H(1B)	1802	2491	-791	86
H(1C)	775	2866	-589	86
H(2A)	2391	4532	210	84
H(2B)	3341	3924	72	84
H(2C)	3200	4154	805	84
H(5)	-812	5090	1133	53
H(6)	-2170	4193	629	56
H(7)	-1961	2593	383	53
H(9)	1739	4280	1516	53
H(10A)	332	5204	2211	79
H(10B)	1525	5227	2431	79
H(10C)	926	4235	2440	79
H(11A)	1236	5466	686	92
H(11B)	1827	5924	1344	92

H(11C)	630	6012	1176	92
H(12)	359	1295	578	55
H(13A)	-1633	1263	-156	92
H(13B)	-752	525	-234	92
H(13C)	-676	1621	-453	92
H(14A)	-410	971	1495	93
H(14B)	-718	152	960	93
H(14C)	-1498	987	1052	93
H(17)	3584	941	2473	50
H(18)	2640	1031	3303	56
H(19)	1084	1815	3115	53
H(20)	488	2509	2126	45
H(21)	3828	1159	1417	43
H(22A)	4438	1421	523	59
H(22B)	3868	2122	-26	59
H(23A)	3807	667	-508	65
H(23B)	2701	835	-352	65
H(24)	3765	-929	-469	46
H(27)	3008	-1573	3374	62
H(28)	4612	-1099	3841	72
H(29)	5782	-656	3198	62

H(31)	2218	-2078	1697	54
H(32A)	1408	-517	2336	98
H(32B)	813	-1086	1723	98
H(32C)	1774	-449	1644	98
H(33A)	2131	-2981	2662	93
H(33B)	1044	-2694	2281	93
H(33C)	1523	-2115	2921	93
H(34)	5328	-498	1451	49
H(35A)	5561	917	2084	84
H(35B)	6569	636	1816	84
H(35C)	6470	419	2558	84
H(36A)	6826	-1378	2399	87
H(36B)	6991	-1092	1679	87
H(36C)	6200	-1913	1782	87
H(39)	4003	-2622	-507	50
H(40)	4377	-4099	-18	63
H(41)	4491	-4234	1110	68
H(42)	4187	-2925	1735	56

Table A.7. Crystal data and structure refinement for (16).

Identification code	MS090595	
Empirical formula	C45 H62 Al2 N4	
Formula weight	712.95	
Temperature	173(1) K	
Wavelength	0.71073 Å	
Diffractometer used	Bruker AXS P4/SMART 1000	
Detector distance	5 cm	
Monochromator used	Graphite	
Crystal size	0.55 x 0.45 x 0.30 mm^3	
Colour and habit	Yellow, irregular	
Crystal system	Orthorhombic	
Space group	Pbcn	
Unit cell dimensions	a = 15.7648(16) Å	$\alpha = 90°$
	b = 17.2749(17) Å	$\beta = 90°$
	c = 15.2425(15) Å	$\gamma = 90°$
Volume	4151.1(7) $Å^3$	
Z	4	
Density (calculated)	1.141 Mg/m^3	
Absorption coefficient	0.105 mm^{-1}	
F(000)	1544	

Theta range for data collection	1.75 to 27.50°
Completeness to theta = 25.00°	100.0 %
Scan type	ω and ϕ
Scan range	0.3°
Exposure time	10s
Index ranges	$-20 \leq h \leq 20$, $-20 \leq k \leq 22$, $-18 \leq l \leq 19$
Standard reflections	50 frames at beginning and end of data collection
Crystal stability	no decay
Reflections collected	27336
Independent reflections	4742 [R(int) = 0.0316]
Solution	Direct methods
Hydrogen atoms	Found, refined isotropically
Absorption correction	SADABS
Max. and min. transmission	0.9691 and 0.9444
Refinement method	Full-matrix least-squares on F^2
Data / restraints / parameters	4742 / 0 / 355
Goodness-of-fit on F^2	1.123
Final R indices [I>2sigma(I)]	R1 = 0.0435, wR2 = 0.1081
R indices (all data)	R1 = 0.0676, wR2 = 0.1339
Largest/mean shift/esd	0.000/0.000
Largest diff. peak and hole	0.361 and -0.234 e.$Å^{-3}$

$wR2 = (\Sigma[w(F_o^2-F_c^2)^2]/\Sigma[wF_o^4])^{1/2}$

$R1 = \Sigma| |F_o|- |F_c| |/ \Sigma |F_o|$

$Weight = 1 / [\sigma^2(F_o^2) + (0.0563 * P)^2 + (2.0533 * P)]$

where $P = (\max (F_o^2, 0) +2 * F_c^2)/3$

Table A.8. Atomic coordinates (x 10^4) and equivalent isotropic displacement parameters ($Å^2$x 10^3)for (16). U(eq) is defined as one third of the trace of the orthogonalized U^{ij} tensor.

	x	y	z	U(eq)
Al(1)	1849(1)	1273(1)	1184(1)	29(1)
N(1)	2205(1)	1983(1)	314(1)	26(1)
N(2)	1201(1)	2029(1)	1856(1)	30(1)
C(1)	1141(2)	423(1)	742(2)	44(1)
C(2)	2740(2)	915(1)	1989(1)	42(1)
C(3)	2773(1)	1654(1)	-330(1)	26(1)
C(4)	3652(1)	1643(1)	-155(1)	32(1)
C(5)	4182(1)	1248(1)	-737(1)	38(1)
C(6)	3867(1)	890(1)	-1476(1)	36(1)
C(7)	3012(1)	934(1)	-1664(1)	33(1)
C(8)	2448(1)	1312(1)	-1104(1)	27(1)

C(9)	4044(1)	2061(1)	624(1)	41(1)
C(10)	4723(2)	1578(2)	1089(2)	59(1)
C(11)	4421(2)	2839(2)	333(2)	57(1)
C(12)	1520(1)	1372(1)	-1363(1)	34(1)
C(13)	1133(1)	592(2)	-1623(2)	47(1)
C(14)	1419(2)	1946(2)	-2125(2)	53(1)
C(15)	2033(1)	2756(1)	268(1)	26(1)
C(16)	1554(1)	3141(1)	934(1)	28(1)
C(17)	1425(1)	3949(1)	883(1)	35(1)
C(18)	1718(1)	4381(1)	196(1)	40(1)
C(19)	2162(1)	4004(1)	-470(1)	41(1)
C(20)	2322(1)	3226(1)	-438(1)	34(1)
C(21)	1185(1)	2760(1)	1679(1)	30(1)
C(22)	791(1)	1763(1)	2677(1)	44(1)
C(23)	0	1292(2)	2500	55(1)

Table A.9. Bond lengths [Å] for (16).

Al(1)-N(1)	1.8918(14)	C(8)-C(12)	1.518(2)
Al(1)-N(2)	1.9482(15)	C(9)-C(10)	1.530(3)
Al(1)-C(1)	1.963(2)	C(9)-C(11)	1.536(3)
Al(1)-C(2)	1.965(2)	C(9)-H(9)	0.93(2)
N(1)-C(15)	1.365(2)	C(10)-H(10A)	0.99(3)

N(1)-C(3)	1.445(2)	C(10)-H(10B)	1.04(3)
N(2)-C(21)	1.293(2)	C(10)-H(10C)	0.97(3)
N(2)-C(22)	1.481(2)	C(11)-H(11A)	1.04(3)
C(1)-H(1A)	1.00(3)	C(11)-H(11B)	0.98(3)
C(1)-H(1B)	1.02(3)	C(11)-H(11C)	0.99(3)
C(1)-H(1C)	0.96(3)	C(12)-C(13)	1.532(3)
C(2)-H(2A)	0.99(3)	C(12)-C(14)	1.535(3)
C(2)-H(2B)	1.04(3)	C(12)-H(12)	0.96(2)
C(2)-H(2C)	0.98(3)	C(13)-H(13A)	0.97(3)
C(3)-C(4)	1.410(2)	C(13)-H(13B)	0.93(3)
C(3)-C(8)	1.415(2)	C(13)-H(13C)	0.99(3)
C(4)-C(5)	1.396(3)	C(14)-H(14A)	1.02(3)
C(4)-C(9)	1.521(3)	C(14)-H(14B)	1.03(3)
C(5)-C(6)	1.377(3)	C(14)-H(14C)	1.00(3)
C(5)-H(5)	0.95(2)	C(15)-C(20)	1.423(2)
C(6)-C(7)	1.380(3)	C(15)-C(16)	1.429(2)
C(6)-H(6)	0.96(2)	C(16)-C(17)	1.413(3)
C(7)-C(8)	1.394(2)	C(16)-C(21)	1.436(2)
C(7)-H(7)	0.94(2)	C(17)-C(18)	1.366(3)
C(17)-H(17)	0.997(19)	C(21)-H(21)	0.95(2)
C(18)-C(19)	1.396(3)	C(22)-C(23)	1.512(3)
C(18)-H(18)	0.95(2)	C(22)-H(22A)	0.96(3)
C(19)-C(20)	1.368(3)	C(22)-H(22B)	0.97(2)
C(19)-H(19)	0.96(2)	C(23)-C(22)#1	1.512(3)
C(20)-H(20)	0.92(2)	C(23)-H(23)	0.96(3)

Table A.10. Bond Angles (°) for (16)

N(1)-Al(1)-N(2)	95.15(6)	C(4)-C(3)-C(8)	120.51(15)
N(1)-Al(1)-C(1)	114.35(8)	C(4)-C(3)-N(1)	119.08(15)
N(2)-Al(1)-C(1)	112.55(9)	C(8)-C(3)-N(1)	120.33(14)
N(1)-Al(1)-C(2)	115.45(8)	C(5)-C(4)-C(3)	118.29(16)
N(2)-Al(1)-C(2)	104.90(8)	C(5)-C(4)-C(9)	118.96(16)
C(1)-Al(1)-C(2)	112.70(11)	C(3)-C(4)-C(9)	122.73(16)
C(15)-N(1)-C(3)	118.30(13)	C(6)-C(5)-C(4)	121.53(18)
C(15)-N(1)-Al(1)	127.65(11)	C(6)-C(5)-H(5)	119.9(13)
C(3)-N(1)-Al(1)	113.89(11)	C(4)-C(5)-H(5)	118.5(13)
C(21)-N(2)-C(22)	118.03(16)	C(5)-C(6)-C(7)	119.80(17)
C(21)-N(2)-Al(1)	123.78(12)	C(5)-C(6)-H(6)	119.3(13)
C(22)-N(2)-Al(1)	117.76(13)	C(7)-C(6)-H(6)	120.9(13)
Al(1)-C(1)-H(1A)	110.3(16)	C(6)-C(7)-C(8)	121.42(17)
Al(1)-C(1)-H(1B)	111.7(16)	C(6)-C(7)-H(7)	120.4(12)
H(1A)-C(1)-H(1B)	105(2)	C(8)-C(7)-H(7)	118.2(12)
Al(1)-C(1)-H(1C)	113.5(15)	C(7)-C(8)-C(3)	118.34(16)
H(1A)-C(1)-H(1C)	110(2)	C(7)-C(8)-C(12)	119.14(16)
H(1B)-C(1)-H(1C)	106(2)	C(3)-C(8)-C(12)	122.47(15)
Al(1)-C(2)-H(2A)	107.7(15)	C(4)-C(9)-C(10)	112.81(19)
Al(1)-C(2)-H(2B)	114.8(16)	C(4)-C(9)-C(11)	110.33(18)
H(2A)-C(2)-H(2B)	107(2)	C(10)-C(9)-(11)	109.9(2)
Al(1)-C(2)-H(2C)	117.5(19)	C(4)-C(9)-H(9)	106.6(13)

H(2A)-C(2)-H(2C)	107(2)	C(10)-C(9)-H(9)	107.4(13)
H(2B)-C(2)-H(2C)	102(2)	C(11)-C(9)-H(9)	109.7(13)
C(9)-C(10)-H(10A)	110.5(16)	C(12)-C(14)-H(14C)	110.0(16)
C(9)-C(10)-H(10B)	113.3(14)	H(14A)-C(14)-H(14C)	107(2)
H(10A)-C(10)-H(10B)	110(2)	H(14B)-C(14)-H(14C)	106(2)
C(9)-C(10)-H(10C)	109.8(17)	N(1)-C(15)-C(20)	122.15(15)
H(10A)-C(10)-H(10C)	106(2)	N(1)-C(15)-C(16)	121.66(15)
H(10B)-C(10)-H(10C)	107(2)	C(20)-C(15)-C(16)	116.18(16)
C(9)-C(11)-H(11A)	111.9(15)	C(17)-C(16)-C(15)	119.80(16)
C(9)-C(11)-H(11B)	109.3(17)	C(17)-C(16)-C(21)	115.99(16)
H(11A)-C(11)-H(11B)	107(2)	C(15)-C(16)-C(21)	124.21(16)
C(9)-C(11)-H(11C)	110.4(14)	C(18)-C(17)-C(16)	122.22(18)
H(11A)-C(11)-H(11C)	109(2)	C(18)-C(17)-H(17)	122.0(11)
H(11B)-C(11)-H(11C)	109(2)	C(16)-C(17)-H(17)	115.8(11)
C(8)-C(12)-C(13)	112.98(16)	C(17)-C(18)-C(19)	118.18(18)
C(8)-C(12)-C(14)	109.93(17)	C(17)-C(18)-H(18)	122.0(13)
C(13)-C(12)-C(14)	109.33(18)	C(19)-C(18)-H(18)	119.8(13)
C(8)-C(12)-H(12)	108.7(12)	C(20)-C(19)-C(18)	121.68(19)
C(13)-C(12)-H(12)	107.3(12)	C(20)-C(19)-H(19)	118.8(13)
C(14)-C(12)-H(12)	108.5(12)	C(18)-C(19)-H(19)	119.5(13)
C(12)-C(13)-H(13A)	110.6(15)	C(19)-C(20)-C(15)	121.88(18)
C(12)-C(13)-H(13B)	108.2(16)	C(19)-C(20)-H(20)	120.4(12)
H(13A)-C(13)-H(13B)	109(2)	C(15)-C(20)-H(20)	117.7(12)
C(12)-C(13)-H(13C)	112.1(15)	N(2)-C(21)-C(16)	127.24(16)
H(13A)-C(13)-H(13C)	111(2)	N(2)-C(21)-H(21)	118.4(12)

H(13B)-C(13)-H(13C)	106(2)	C(16)-C(21)-H(21)	114.4(12)
C(12)-C(14)-H(14A)	112.9(17)	N(2)-C(22)-C(23)	112.10(15)
C(12)-C(14)-H(14B)	107.1(14)	N(2)-C(22)-H(22A)	108.2(16)
H(14A)-C(14)-H(14B)	113(2)	C(23)-C(22)-H(22A)	108.7(16)

Table A.1.1. Anisotropic displacement parameters ($Å^2$x 10^3)for (16). The anisotropic displacement factor exponent takes the form: $-2\pi^2[h^2a^{*2}U^{11} + ... + 2 h k a^* b^* U^{12}]$

	U^{11}	U^{22}	U^{33}	U^{23}	U^{13}	U^{12}
Al(1)	33(1)	29(1)	26(1)	0(1)	7(1)	-2(1)
N(1)	28(1)	27(1)	24(1)	-1(1)	5(1)	-2(1)
N(2)	29(1)	36(1)	25(1)	-1(1)	6(1)	-1(1)
C(1)	50(1)	41(1)	42(1)	-6(1)	12(1)	-12(1)
C(2)	49(1)	41(1)	36(1)	6(1)	1(1)	5(1)
C(3)	28(1)	27(1)	23(1)	2(1)	6(1)	-1(1)
C(4)	29(1)	39(1)	28(1)	0(1)	4(1)	-4(1)
C(5)	27(1)	49(1)	37(1)	0(1)	6(1)	1(1)
C(6)	36(1)	40(1)	33(1)	-3(1)	12(1)	4(1)
C(7)	40(1)	34(1)	26(1)	-4(1)	5(1)	-2(1)
C(8)	28(1)	26(1)	25(1)	1(1)	4(1)	-2(1)
C(9)	30(1)	61(1)	33(1)	-9(1)	2(1)	-6(1)
C(10)	41(1)	94(2)	42(1)	-8(1)	-8(1)	2(1)

C(11)	46(1)	65(2)	59(2)	-14(1)	-2(1)	-20(1)
C(12)	31(1)	42(1)	30(1)	-6(1)	-1(1)	2(1)
C(13)	37(1)	55(1)	47(1)	-10(1)	-5(1)	-9(1)
C(14)	53(1)	56(2)	50(1)	9(1)	-14(1)	5(1)
C(15)	26(1)	28(1)	25(1)	-2(1)	-1(1)	-5(1)
C(16)	27(1)	29(1)	27(1)	-4(1)	-1(1)	-3(1)
C(17)	35(1)	32(1)	36(1)	-7(1)	-4(1)	0(1)
C(18)	49(1)	26(1)	44(1)	-1(1)	-5(1)	-2(1)
C(19)	53(1)	34(1)	36(1)	6(1)	1(1)	-9(1)
C(20)	40(1)	32(1)	29(1)	0(1)	5(1)	-4(1)
C(21)	28(1)	36(1)	26(1)	-8(1)	1(1)	1(1)
C(22)	49(1)	50(1)	32(1)	7(1)	17(1)	12(1)
C(23)	63(2)	34(2)	69(2)	0	46(2)	0

Table A.12. Hydrogen coordinates (x 10^4) and isotropic displacement parameters ($Å^2$x 10^3) for (16).

	x	y	z	U(eq)
H(1A)	972(18)	72(17)	1234(19)	79(9)
H(1B)	1467(18)	78(17)	315(19)	77(8)
H(1C)	645(17)	596(14)	437(16)	58(7)
H(2A)	2462(17)	616(15)	2464(18)	71(8)
H(2B)	3085(19)	1353(17)	2290(20)	83(9)
H(2C)	3190(20)	587(19)	1740(20)	95(10)
H(5)	4773(15)	1220(12)	-607(14)	43(6)
H(6)	4243(14)	596(12)	-1841(14)	45(6)
H(7)	2793(12)	707(12)	-2179(13)	37(5)
H(9)	3609(14)	2145(12)	1023(13)	37(5)
H(10A)	5237(18)	1540(15)	724(18)	71(8)
H(10B)	4512(17)	1028(15)	1270(16)	59(7)
H(10C)	4900(19)	1839(16)	1620(20)	77(9)
H(11A)	3973(18)	3184(17)	18(18)	74(8)
H(11B)	4880(20)	2746(16)	-90(20)	80(9)
H(11C)	4654(16)	3124(14)	846(17)	60(7)

H(12)	1202(13)	1564(12)	-868(14)	36(5)
H(13A)	1376(16)	409(14)	-2173(17)	61(7)
H(13B)	553(17)	660(14)	-1701(16)	60(7)
H(13C)	1197(16)	199(15)	-1155(17)	59(7)
H(14A)	1625(19)	2492(18)	-1970(20)	84(9)
H(14B)	1727(15)	1710(14)	-2660(17)	57(7)
H(14C)	805(19)	1989(15)	-2294(18)	76(8)
H(17)	1114(11)	4187(11)	1386(13)	29(5)
H(18)	1626(13)	4923(15)	162(14)	45(6)
H(19)	2363(14)	4296(13)	-967(15)	46(6)
H(20)	2623(12)	2987(11)	-882(13)	30(5)
H(21)	905(12)	3098(11)	2080(13)	33(5)
H(22A)	1187(17)	1448(15)	2989(17)	63(7)
H(22B)	670(14)	2202(13)	3051(14)	42(6)
H(23)	99(18)	990(15)	1981(18)	77(8)